Bioinspired Materials Science and Engineering

Bioinspired Materials Science and Engineering

Edited by

Guang Yang, Lin Xiao, and Lallepak Lamboni

Huazhong University of Science and Technology, Wuhan, China

WILEY

This edition first published 2018

Registered Offices
John Wiley & Sons, Inc., 111 River Street, Hoboken, NJ 07030, USA

Editorial Office
111 River Street, Hoboken, NJ 07030, USA

For details of our global editorial offices, customer services, and more information about Wiley products visit us at www.wiley.com.

Wiley also publishes its books in a variety of electronic formats and by print-on-demand. Some content that appears in standard print versions of this book may not be available in other formats.

Library of Congress Cataloging-in-Publication Data

Names: Yang, Guang, 1968 April 18– editor. | Xiao, Lin, 1986– editor. | Lamboni, Lallepak, 1988– editor.
Title: Bioinspired materials science and engineering / edited by Guang Yang, Lin Xiao, Lallepak Lamboni.
Description: First edition. | Hoboken, NJ : John Wiley & Sons, 2018. | Includes bibliographical references and index. |
Identifiers: LCCN 2018002997 (print) | LCCN 2018009868 (ebook) | ISBN 9781119390336 (pdf) | ISBN 9781119390343 (epub) | ISBN 9781119390329 (cloth)
Subjects: LCSH: Biomimetics. | Materials–Biotechnology. | Materials science. | Engineering.
Classification: LCC QP517.B56 (ebook) | LCC QP517.B56 B4796 2018 (print) | DDC 610.28–dc23
LC record available at https://lccn.loc.gov/2018002997

Cover Design: Wiley
Cover Images: © SergeOstroverhoff/Getty Images; © TonyBaggett/Getty Images; ©vitstudio/Shutterstock; © me4o/Getty Images; Shamrock logo courtesy of Guang Yang

Set in 10/12pt Warnock by SPi Global, Pondicherry, India

Printed in the United States of America

10 9 8 7 6 5 4 3 2 1

Contents

Sehrish Manan
Huazhong Agricultural University
Wuhan, China

Lin Mao
Huazhong University of Science and Technology
Wuhan, China

Tom Masselter
University of Freiburg
Freiburg, Germany

Michiya Matsusaki
Osaka University
Osaka, Japan

Frank A. Müller
Friedrich Schiller University Jena
Jena, Germany

Akihiro Nishiguchi
Osaka University
Osaka, Japan

Daniel Van Opdenbosch
Technische Universität München
Munchen, Germany

Zhenchao Qian
Beijing National Laboratory for Molecular Sciences
Beijing, China

Amarachi Rosemary Osi
Ningbo Institute of Material Technology and Engineering
Ningbo, China

Takahiro Sato
Osaka University
Osaka, Japan

Heng Shen
Beijing National Laboratory for Molecular Sciences
Beijing, China

Zhijun Shi
Huazhong University of Science and Technology
Wuhan, China

Tiatou Souho
University of Kara
Kara, Togo
Huazhong University of Science and Technology
Wuhan, China

Olga Speck
University of Freiburg
Freiburg, Germany

Thomas Speck
University of Freiburg
Freiburg, Germany

Lixue Tang
National Center for NanoScience and Technology
Beijing, China

Ken Terao
Osaka University
Osaka, Japan

Marc Thielen
Freiburg Materials Research Centre
Freiburg, Germany

Francisco Vilaplana
KTH Royal Institute of Technology
Stockholm, Sweden

Muhammad Wajid Ullah
Huazhong University of Science and Technology
Wuhan, China

Li Wang
Huazhong University of Science and Technology
Wuhan, China

Ruili Wang
Donghua University
Shanghai, China

Shutao Wang
Technical Institute of Physics and Chemistry
Beijing, China

Xiao-Wei Wang
Peking University
Beijing, China

Yazi Wang
Donghua University
Shanghai, China

Lin Xiao
Huazhong University of Science and Technology
Wuhan, China

Table I.1 Typical biological materials with function integration.

Biological materials	Functions	Ref.
Butterfly wing	Superhydrophobicity, directional adhesion, structural color, self-cleaning, chemical sensing capability, fluorescence emission functions	[3–7]
Brittlestar	Mechanical and optical functions	[8]
Cicada wing	Anti-reflection, superhydrophobicity	[9]
Fish scale	Drag reduction, superoleophilicity in air, superoleophobicity in water	[10]
Gecko foot	Reversible adhesive, superhydrophobicity, self-cleaning	[11]
Lotus leaf	Superhydrophobicity, low adhesion, self-cleaning	[12]
Mosquito compound eye	Superhydrophobicity, anti-reflection, anti-fogging	[13]
Nacre	Mechanical property, structural color	[14, 15]
Peacock feather	Structural color, superhydrophobicity	[16]
Polar bear fur	Optical property, thermal insulation	[17]
Rice leaf	Superhydrophobicity, anisotropic wettability	[12]
Rose petal	Superhydrophobicity, structural color, high adhesion	[18–20]
Shark skin	Drag reduction, anti-biofouling	[21]
Spicule	Mechanical and fiber-optical properties	[22–24]
Spider capture silk	Water collection ability, mechanical property, elasticity, stickiness	[25–27]
Spider dragline silk	Mechanical property, supercontraction, torsional shape memory	[28–35]
Water strider leg	Durable and robust superhydrophobicity	[36]

Source: Reproduced from [2] with permission from Elsevier.

the design principles which can lead to subsequent designing of bioinspired complements. For example, mechanical modeling of biological materials based on natural materials has attracted immense attention owing to their diverse applications in medicine and engineering. This can be attributed to the structurally hierarchical biomaterials which possess a highly desirable structure-properties relationship and can serve as templates for the fabrication of bioinspired materials. Several approaches, such as single- and multi-scale, micro-structural and phenomenological, and continuum and discrete, etc. have been developed for the mechanical modeling of biological and bioinspired materials [37]. However, further extensive research is required to fabricate bioinspired materials due to their greater flexibility in design variables, such as the selection of material components, the varying degree of constraints among the different available components, the variable boundary conditions, and the novel architectural conformations.

I.3 Biofabrication

Biofabrication is the combination of two words: "bio" means living and "fabrication" means to synthesize or design using templates etc., thus biofabrication refers to the synthesis of living structures using some standard templates or models. Precisely, biofabrication refers to the application principle of engineering and information science to produce an automated robotic assembly of living cells, tissues, and organs, etc. [38]. Further narrowing down the concept, biofabrication refers to the biomedical applications of rapid prototyping or computer-aided additive technologies. It is closely related to tissue engineering and is considered an integral part of it and uses engineering approaches in the assembly of complex tissues and organs. Despite extensive developments in the field of tissue engineering, the transformation of this labor-intensive technology into an automated industry still requires further innovative and creative strategies.

I.3.1 Summary of Part I Biofabrication

In Part I, "Biofabrication," we discuss various biotemplating principles and recent advances in the one-dimensional and two-dimensional biotemplated formation of inorganic functional materials using natural templates. The chapters in Part I (Chapters 2–6) also discuss microbial-mediated material manufacturing techniques for the fabrication of a variety of functional materials. Recently developed tubular structures are discussed, which serve as templates for *in vitro* recapitulating of highly complex tissues such as blood vessels, etc. and microfluidics-based cell manipulation and development of tubular tissues. This Part also illustrates the fabrication of three-dimensional (3D) tissues with capillary networks by controlling the cell microenvironment with emphasis on 3D-tumor invasion models with blood- and lymph-capillary networks. Furthermore, biofabrication of ordered cellulose scaffolds (nematic ordered) to mediate 3D cell culturing and biomineralization is discussed. As an example of bioinspiration, the preparation and application of biomimetic materials inspired by muscle adhesive proteins are overviewed in detail. Finally, the self-assembly of poly(lactic acid)-based amphiphilic diblock copolymers and their applications in biomedical field are presented.

Table I.2 Comparison of four types of bioprinting techniques.

Parameters	Inkjet	Laser-assisted	Extrusion	Stereolithography	Reference
Cost	Low	High	Moderate	Low	[62–65]
Cell viability	>85%	>95%	40%–80%	>85%	[66, 67]
Print speed	Fast	Medium	Slow	Fast	[68–70]
Supported viscosities	3.5–12 mPa/s	1–300 mPa/s	30 mPa/s to above 6×10^7 mPa/s	No limitation	[70–72]
Resolution	High	High	Moderate	High	[63]
Quality of vertical structure	Poor	Fair	Good	Good	[73]
Cell density	Low $<10^6$ cells/mL	Medium $< 10^8$ cells/mL	High (cell spheroids)	Medium $<10^8$ cells/mL	[70]
Representative materials for bioinks	Alginate, PEGDMA, Collagen	Collagen, Matrigel	Alginate, GelMA, Collagen	GelMA, GelMA-PEGDA hybrid hydrogel	[65, 73–77]
Reported applications	Tissue engineering (blood vessel, bone, cartilage, and neuron)	Tissue engineering (blood vessel, bone, skin, and adipose)	Tissue engineering (blood vessel, bone, cartilage, neuron, muscle, tumor) Controlled release of biomacromolecules Organ-on-a-chip	Tissue engineering (blood vessel and cartilage) Organ-on-a-chip	[78–81]

Source: Reproduced from [147] with permission from Elsevier.

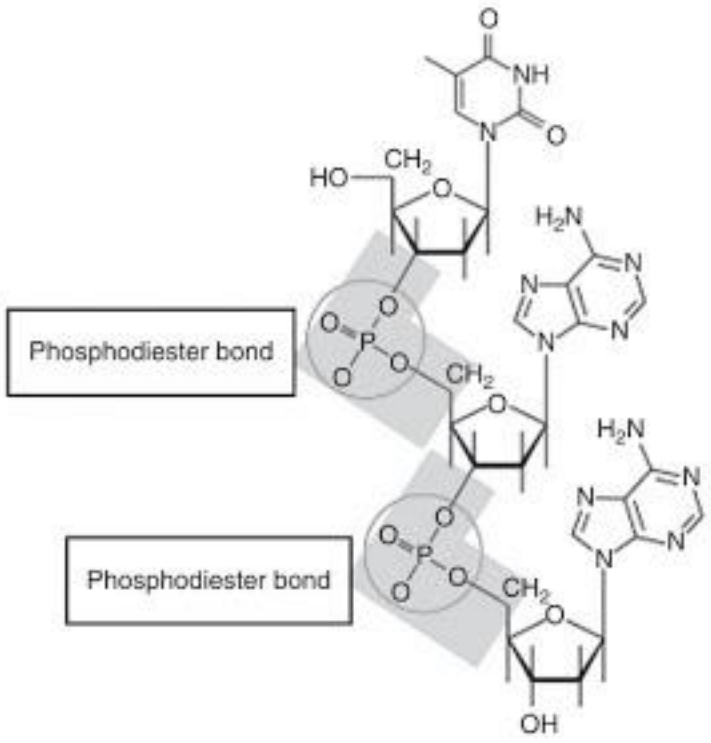

Figure I.4 Chemistry of phosphodiester bond formation in nucleic acids.

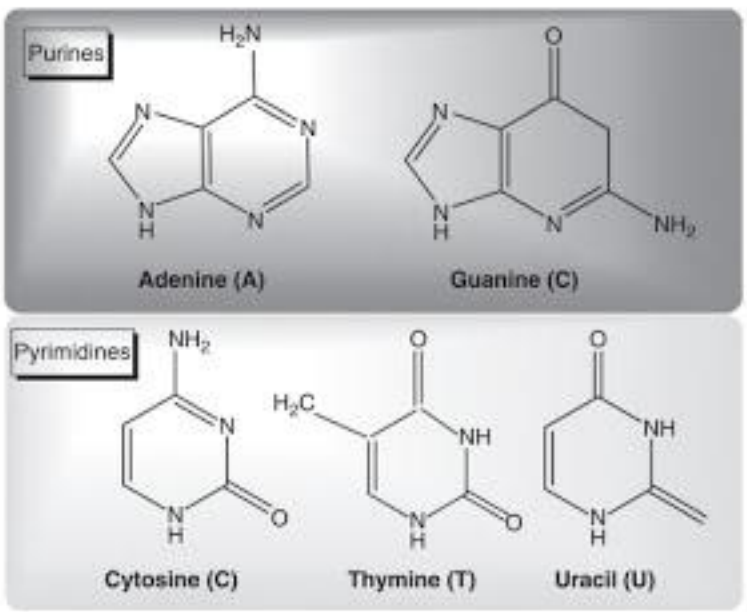

Figure I.5 Illustration of chemical structures of various nitrogenous bases in nucleic acids.

(i.e. protein), molecular assemblies, cellular and sub-cellular structures, organs, and organisms, etc.

I.5.4.1 DNA

Deoxyribonucleic acid (DNA) carries the genetic information of a cell and is referred to as a "genome." A genome is the structural and functional organization of a cell. It contains all the information for the growth, shape, size, pattern, development, and functionality, etc. of a cell, tissue, organ, and organism. Typically, the DNA molecule is present in the nucleus of eukaryotes and forms a complex with histone proteins, referred to as a chromosome. In prokaryotes, the chromosomes are suspended in the cytoplasm. A DNA molecule is typically comprised of two polynucleotide strings which form a double-helical structure. These strands run in opposite directions to each other. The nucleotides on two separate strands in DNA are bonded to each other through hydrogen bonding. Typically, a double hydrogen bond is formed between A of first strand and T of another strand while a triple hydrogen bond is formed between G of one strand and C of another strand. The DNA backbone is flexible enough to resist any cleavage. Under some specialized conditions, the DNA molecule is twisted like a rope through a process called DNA supercoiling. In a relaxed state, one strand in DNA molecule encircles the axis of the double helix once after every 10.4 base pairs (bp) on average, however, in a twisted state, the strands become tighter or are loosely arranged [119]. Supercoiling can be either positive (twisting in the direction of the strand) or negative (twisting in the opposite direction of the strand). Most DNA molecules in nature exist as negatively supercoiled, which is caused by an enzyme topoisomerase. DNA molecules can exist in different conformations such as A-DNA, B-DNA, and Z-DNA, however, only B-DNA and Z-DNA are known to be identified in functional organisms [120]. Both DNA strands contain the same biological information which is replaced when two strands separate from each other during mitotic cell division. The strand of DNA which is the same as the mRNA formed as a result of transcription is termed the sense-strand, while the complementary strand is called the anti-sense strand. However, both sense and anti-sense sequences can co-exist on the same DNA strand. To date, the function of the anti-sense sequences is unknown [121]. It has been suggested that anti-sense RNAs might be involved in regulating gene expression through RNA-RNA base pairing [122]. It is worth mentioning here that about 98% of the total DNA in humans does not code for any protein and is referred to as non-coding or junk DNA.

DNA forms temperature, pH, enzymes, and UV light-responsive hydrogels through physical entanglement or chemical cross-linking upon extraction from the nucleus (eukaryotes) or pooling out from cytoplasm (prokaryotes). For example, it forms hydrogels with cationic polyelectrolytes [123] or metal ions, such as silver [124] for their applications in cell culture and differentiation studies [125] and 3D bioprinting [126].

I.5.4.2 RNA

Ribonucleic acid (RNA) is typically a single-stranded molecule, however, it forms an intra-strand double helix through complementary base pairing. Similar to DNA, it is also comprised of nucleotides linked via phosphodiester bonds, except it contains uracil (U) nitrogenous base

and represents a typical example of how knowledge is acquired from nature, and how in turn this information contributes to biological sciences, with an accent on biomedical applications. This book is devised both for novice readers and experts in the field who will find it valuable as it presents recent advances in topics of current interest, such as biotemplating, microfluidics, self-assembly, mussel-inspired surface modification, and several others. Furthermore, its different Parts, each of which is a multidisciplinary research area, will appeal not only to chemists, but also to biologists, physicists, and engineers, etc.

Acknowledgments

This work was supported by the National Natural Science Foundation of China (21574050, 31270150, 51603079), the China Postdoctoral Science Foundation (2016M602291, 2015M572132), Fundamental Research Funds for the Central Universities, Open Research Fund of State Key Laboratory of Polymer Physics and Chemistry, Changchun Institute of Applied Chemistry, Chinese Academy of Sciences.

References

1 McKittrick, J., Chen, P.Y., Tombolato, L. et al. (2010) *Mat. Sci. Eng. C.*, **30**, 331–342.
2 Liu, K., Jiang, L. (2011) *Nano Today*, **6**, 155–175.
3 Zheng, Y.M., Gao, X.F., Jiang, L. (2007) *Soft Matter*, **3**, 178–182.
4 Vukusic, P., Sambles, J.R. (2003) *Nat.*, **424**, 852–855.
5 Potyrailo, R.A., Ghiradella, H. Vertiatchikh, A. et al. (2007) *Nat. Photon.*, **1**, 123–128.
6 Vukusic, P., Hooper, I. (2005) *Sci.*, **310**, 1151–1155.
7 Sato, O., Kubo, S., Gu, Z.Z. (2009) *Acc. Chem. Res.*, **42**, 1–10.
8 Aizenberg, J., Tkachenko, A., Weiner, S. et al. (2001) *Nat.*, **412**, 819–822.
9 Sun, T.L., Feng, L., Gao, X.F., Jiang, L. (2005) *Acc. Chem. Res.*, **38**, 644–652.
10 Liu, M.J., Wang, S.T., Wei, Z.X. et al. (2009) *Adv. Mater,*. **21**, 665–669.
11 Hansen, W.R., Autumn, K. (2005) *Proc. Natl. Acad. Sci. U.S.A.*, **102**, 385–389.
12 Feng, L., Li, S.H. Li, Y.S. et al. (2002) *Adv. Mater.*, **14**, 1857–1860.
13 Gao, X.F., Yan, X., Yao, X. et al. (2007) *Adv. Mater.*, **19**, 2213–2217.
14 Mayer, G. (2005) *Science*, **310**, 1144–1147.
15 Tan, T.L., Wong, D., Lee, P. (2004) *Opt. Express*, **12**, 4847–4854.
16 Zi, J., Yu, X.D., Li, Y.Z. et al. (2003) *Proc. Natl. Acad. Sci. U.S.A.*, **100**, 12576–12578.
17 Stegmaier, T., Linke, M., Planck, H. (2009) *Philos. Trans. R. Soc. A*, **367**, 1749–1758.
18 Feng, L., Zhang, Y.A., Xi, J.M. et al. (2008) *Langmuir*, **24**, 4114–4119.
19 L. Feng, Y.A. Zhang, M.Z. Li, et al. (2010) *Langmuir*, **26**, 14885–14888.
20 Bhushan, B., Her, E.K. (2010) *Langmuir* **26**, 8207–8217.
21 Ball, P. (1999) *Nature* **400**, 507–509.
22 Sundar, V.C., Yablon, A.D., Grazul, J.L. et al. (2003) *Nature*, **424**, 899–900.
23 Aizenberg, J., Sundar, V.C., Yablon, A.D. et al. (2004) *Proc. Natl. Acad. Sci. U.S.A.*, **101**, 3358–3363.
24 Aizenberg, J., Weaver, J.C., Thanawala, M.S. et al. (2005) *Science*, **309**, 275–278.
25 Zheng, Y.M., Bai, B., Huang, Z.B. et al. (2010) *Nature*, **463**, 640–643.
26 Becker, N., Oroudjev, E., Mutz, S. et al. (2003) *Nat. Mater.*, **2**, 278–283.
27 Swanson, B.O., Blackledge, T.A., Hayash, C.Y. (2007) *J. Exp. Zool.*, **307A**, 654–666.
28 Vollrath, F., Knight, D.P. (2001) *Nature*, **410**, 541–548.
29 Work, R.W. (1985) *J. Exp. Biol.*, **118**, 379–404.
30 Shao, Z.Z., Vollrath, F. (1999) *Polymer*, **40**, 1799–1806.
31 Shao, Z., Vollrath, F., Sirichaisit, J., Young, R.J. (1999) *Polymer*, **40**, 2493–2500.
32 Perez-Rigueiro, J., Elices, M., Guinea, G.V. (2003) *Polymer*, **44**, 3733–3736.
33 Liu, Y., Shao, Z.Z., Vollrath, F. (2005) *Nat. Mater.*, **4**, 901–905.
34 Bell, F.I., McEwen, I.J., Viney, C. (2002) *Nature*, **416**, 37–137.
35 Emile, O., Le Floch, A., Vollrath, F. (2006) *Nature*, **440**, 621–1621.
36 Gao, X.F., Jiang, L. (2004) *Nature*, **432**, 36–136.
37 Wu, M.S. (2011) *Mat. Sci. Eng. C.*, **31**, 1209–1220.
38 Mironov, V., Kasyanov, V., Markwald, R.R. (2011) *Curr. Opin. Biotechnol.*, **22**, 667–673.
39 Annabi, N., Nichol, J.W., Zhong, X. et al. (2010) *Tissue Eng. Part B Rev.*, **16**, 371–383.
40 Khan, S., Ul-Islam, M., Khattak, W.A. et al. (2015) *Cellulose*, **22**, 565–579.
41 Madihally, S.V., Matthew, H.W.T. (1999) *Biomat.*, **20**, 1133–1142.
42 Kang, H.W., Tabata, Y., Ikada, Y. (1999) *Biomat.*, **20**, 1339–1344.
43 Mooney, D.J., Baldwin, D.F., Suh, N.P. et al. (1996) *Biomat.*, **17**, 1417–1422.

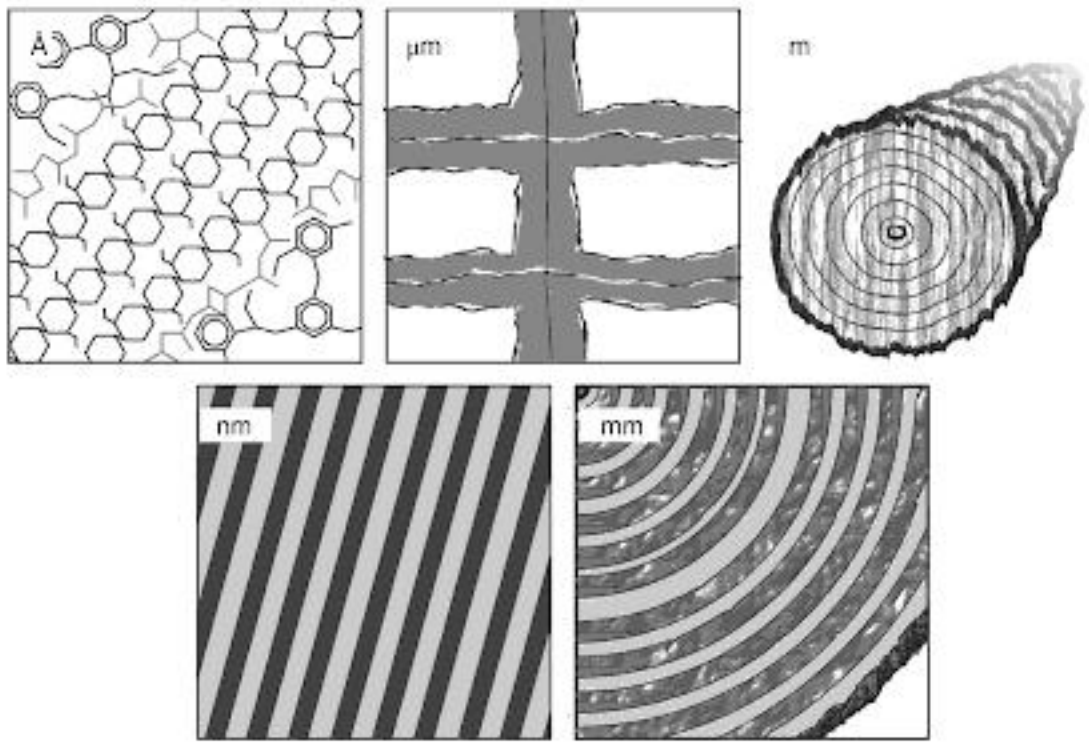

Figure 1.1 Scheme of the deposition of inorganic phases (red) in a biological material (black, adaptation of the wood structure) on several levels of hierarchy. The shown levels of hierarchy may themselves contain sublevels. For example, in the actual wood structure, the nm scale contains the hierarchical levels of the cellulose micro- and elementary fibrils.

structures, on the other hand, are created by molecule-assisted low-energy bottom-up assembly, resulting in complexly structured organic phases, often in composite with inorganic phases [14]. Another aspect of natural materials is their multifunctionality. Arthropod cuticle "produced by a single layer of epithelial cells, is called upon to provide a large number of functions, such as shape, structure, hinges, barrier, filter and similar functions" [15]. Another example is wood, which provides mechanical support, fluid transport [16] and even actuation [17–19]. Straddling the borders of biotemplating is the use of structures made from shaped biological materials, such as corrugated fiberboards [20, 21] or preceramic papers [22].

As further detailed in this chapter, the biotemplating approach has already enabled casting such materials as compact, fibrous ceramics with a non-catastrophic fracturing behavior, photonic reflectors with an internal continuous Schwartz surface, or quasicrystalline structuring on the $n{\cdot}100$ nm scale.[1]

In the following we will first outline the discovery and description of the naturally occurring paragon for biotemplating, namely, fossilization. This will be followed by its human adaptation, and the transition from a purely academic interest toward its use for the manufacturing of novel functional materials. The characteristics and properties of biotemplated materials will be explored, highlighting prominent examples. Finally, we will discuss the challenges and limitations of this technique, while sketching directions of further development and instances of usage. Since research in this field is currently strong, and continues to produce exciting results, this chapter not only presents well-established general findings. It also endeavors to point out the most recent findings in order to show the complete history, the present, and the future of biotemplating.

1.2 Mineralization in Nature

1.2.1 Biomineralization

Biomineralization denotes the precipitation of mineral phases by living organisms, typically aided by biomacromolecules.[2] Examples include the silica deposition in various species of grass, the formation of nacre in aquatic animals, or tooth enamel in vertebrates. Due to the abundance of exhaustive and detailed literature on the subject [23–29], biomineralization, or its immediate [30, 31] or abstracted [32] application for materials synthesis will not be detailed here.

However, there are important lessons to be learned and adapted from biomineralization. Jerominidis wrote:

> an engineer is not very good at extracting maximum benefit from *structural shapes* with indifferent materials. In Nature it is the other way round, yet the properties of shapes manufactured from materials possessing poor attributes [are] truly staggering ...[33]

petrified wood was being widely used as whetstones in Bohemia. He also names many places where petrified wood was found, such as the Elbogen ("Elboganum") fig tree, several trees in Meissen ("Misena") near Chemnitz or the petrified oak of Hildesheim.

1.4 Structural Description and Emulation

1.4.1 Antiquity

From the observation of the locations in which petrified organic substances can be found, it is conclusive that minerals dissolved in waters are responsible for their formation. Theophrastus of Eresos (third and fourth centuries BC) is reported to have written a two-volume treaty on petrifactions [109].[3] Pliny the Elder (first century AD) wrote of various bodies of water with the ability to petrify embedded organic substances, or induce stone growth. A river near the Cicones (a tribe, i.e. in Thrace) and a river in Colchis (the southern Caucasus) named Sirius, lead to embedded organic substances being covered by a skin of stone. Further, he writes that the Sele River near Sorrento (and Salerno) bears potable, yet petrifying water, while the marshlands of the Rieti plain induce the growth of embedded stones.[4] Considering that these observations were only briefly noted in an encyclopedia, one can assume that they were preceded by more systematic research. Even without mining operations, petrified remains of archaeoplantae can be found. Prominent examples likely to have been known to writers of antiquity[5] are the Lybian and Lesbian petrified forests, readily presenting petrified wood above ground [111].

1.4.2 Modern Age: Advent of the Light Microscope

It first required the development of the light microscope to analyze microstructures and identify and name petrified biological materials, which in return led to staggering micrographs. The first analyses of the micrometer structures – and functions – of biological materials were made by Anton van Leeuwenhoek [112]. Robert Hooke, who expanded on Leeuwenhoek's work, imaged fossilized wood in side illumination geometry as well [113]. His engravings thereof show tracheae, tracheids, and an annual growth ring. Hooke also correctly hypothesized about the general pathway of petrifaction, namely,

> by precipitation, cohesion, or coagulation, abundance of stony particles from that permeating water; which stony particles, having by means of the fluid vehicle, conveyed themselves not only into the microscopical pores, and perfectly stoped [*sic*] up them, but also into the pores, which may perhaps be even in that part of the wood, which through the microscope appears most solid, do thereby so augment the weight of the wood… [114]

As discussed in Section 1.2.2, one only has to take "stony particles" to mean colloidal oligomers of silica, or any other mineral, to find that this is the correct description of the mechanism of both natural and artificial mineralization.

The first step toward imaging smaller levels of structural hierarchy in wood, both native and petrified, was Nicol's preparation of thin sections for transmitted light microscopy [115]. These showed the layered cell wall structures, as well as the pit holes (alternatively termed areolae or discs). In the latter, the typical birefringence patterns were observed, whose "beautiful appearance" and "minute assemblages of prismatic colors as seen in the microscope, cannot be represented either by the pencil or the tool of the engraver."[6] Since this birefringence is due to the tangential alignment of the cellulose crystals around the pit hole, the resulting images illustrate three hierarchical levels of hierarchy in wood. Another important finding by William Nicol was that siliceous fossil pit holes do not display birefringence. We will see later, that this indicates not only a loss of the cellulose crystallinity, but also of the nanometer structuring of the fibrillar arrangements of these crystals. Conversely, it was noted that crystallization of calcium carbonate during fossilization occurs

> in divergent prisms, and has thus given rise to a kind of cellular appearance, very readily distinguishable from the true, but which a novice may easily interpret into the regular structure of a cellular or agamic plant; while the siliceous or chalcedonic has arranged itself in parallel undulations or series of curves. [66]

We will discover that such crystallization is a major issue in synthetic mineralization as well.

Nowadays, the confocal light or scanning electron microscopes are arguably the most versatile microanalysis tools, because they afford good depth resolution and therefore allow one to image the often curved contours of biological materials or their fossil forms. An alternative, or additional, method of preparing samples for light microscopy involves increasing the surface structuring by etching with a suitable acid such as hydrochloric or hydrofluoric acid. Then, a thin film of cellulose acetate is placed, or a carbon film evaporated, on the sample [116]. Selmeier noted, among other practical notes on the preparation of microscopic sections, that

deposited material [196, 197]. In particular, the relaxation times, dielectric constants, and dispersion parameters of the entire material allow one to assess whether the wood hydroxyl groups are still freely oscillating in the electric field, or bound by reactions. The incentives for creating covalent bonds between the wood structure and embedded phases for wood protection purposes are: (1) creating a stable link, thereby preventing the opening of micropores through mechanical actuation; and (2) preventing the hydroxyl ligands from forming hydrogen bonds with water molecules. For biotemplating purposes, the latter aspect is arguably less important, since the ultimate step of the processing is to remove the template.

The removal of the organic phase is complicated by the fact that it comprises a significant proportion of the mineralized structure, typically more than 50% [198–201]. This necessitates an approach, which does not induce large stresses on the mineral phase in order to avoid cracking. This could, as happens in nature, be achieved through biological removal [202, 203]. However, the mineralization of natural structural materials is known to lead to a decrease in its susceptibility to biological decrease [204–206]. One finds organic residuals, even in millennia-old petrified materials [207–210]. Therefore, and due to the long time frame required for a thorough organics removal, this approach has not been used in biotemplating approaches. Instead, Ryan Drum used chromic acid, a strong oxidant and highly toxic compound, to selectively remove the wood from his artificially mineralized composites [116]. The most common approach, however, is using thermal oxidation of the organic phase [96, 211]. This approach allows fine control of the degradation velocity of the organic phase by matching the temperature profile to the existing thermal analysis data, a typical example being shown in Figure 1.4. The regions of high mass loss should be traversed slowly, either by holding at a set temperature, or via a slow heating rate. For each mineral phase, there is a maximum temperature, after which it will undergo sintering, destroying the finer structural details of the template [96, 97, 212].

1.5 Characteristic Parameters

1.5.1 Hierarchical Structuring

All materials are structured on more than one length scale. Even monolithic and monocrystalline or amorphous materials possess an outer shape, with dimensions of, for example, several millimeters, as well as the crystal structure, or the structure of the amorphous building blocks, at the sub-nanometer level. Therefore, the *number* of hierarchical levels is what sets biological materials apart from their technological counterparts.

The number of hierarchical levels may be defined in two different ways. One is to look at the dimensions of all structural features present in the sample and sort them into categories, e.g. the decimal metric scale. We are using this approach in the following. The other way is to determine which composite *functional* units are present.

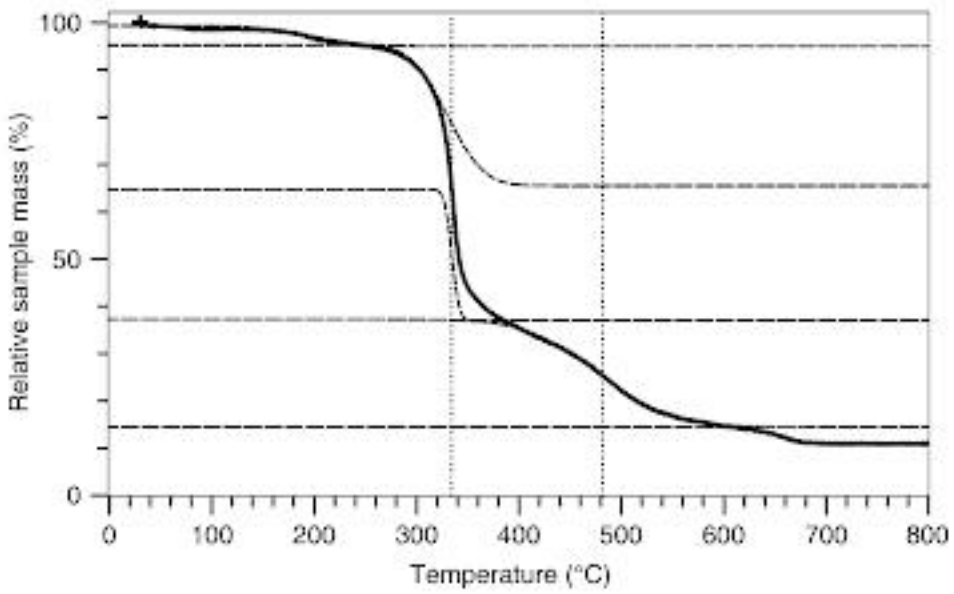

Figure 1.4 Deconvolution of a thermal analysis curve (in air, solid line) of an artificially mineralized biological template (phenylated silicon dioxide on wood) [213] by Gaussian cumulative distribution functions (dashed lines) to give a fit of the curve with a goodness $R^2 = 0.9999$. The mass losses associated with the proposed processes are (low temperature to high): 4.4 Ma% loss of absorbed moisture, 29.8 Ma% and 27.7 Ma% stepwise devolatilization of the wood structure,[1] 22.7 Ma% combustion of the carbonized material, 3.6 Ma% combustion of the temperature-resistant phenyl substituents, 11.9 Ma% ash. The vertical dotted lines mark appropriate holding temperatures for a gentle template removal.
Source: Van Opdenbosch (2013) [213].
Note:[1] The widely accepted sequence is the carbonization of the hemicelluloses followed by the more crystalline cellulose, both of which have an initial endothermic and a subsequent exothermic phase [214–216].

uniform photonic lattices also determines the visual impression provided by natural reflectors. Mixing the colors reflected from domains in the direction of an observer leads to an observed range of wavelengths and a mixed optical impression [258, 259]. This also means that a uniform overall coloring over a large angular range is observed. Such a strategy to create a uniform coloring from anisotropic photonic reflecting domains is not only found in animal reflectors but also in plants [260]. There is also a combination of pixilated coloring and polarization dependence that might be described as ingenious if it were man-made. It is based on geometries of the reflecting multilayers that selectively reflect light of different polarization by means of trapezoid cavities [258]. The afore-mentioned examples provide not only inspiration for bioinspired materials but also for biotemplated materials obtained from the structures themselves [261, 262]. In Section 1.6, we will discuss how these properties can be transferred to engineering materials.

Nature not only uses hierarchical structuring to create functionalities, it also uses low-energy pathways to create these materials. The complex structure presented in Figure 1.5 is grown underwater in a cool and dark, low-energy environment by an immobile sponge. The body of *Euplectella sp.*, was found to have a layered structuring not unlike a man-made glass fiber, as seen in Figure 1.5. It was proposed that it fulfills a similar light-guiding function [219]. Man-made glass fibers on the other hand are drawn from a melt at about 1200 °C. With vitreous silica having a heat capacity of 700 J·kg^{-1}·K^{-1}, making an 'artificial Euplectella' that weighs the same as the original, around 18 g, from drawn glass fibers would require an energy of 15 kJ for the melting step alone, enough to bring 36 g of water to the boil.

1.5.2 Specific Surface Areas

A measure of the replication detail is the specific surface of the resulting materials. However, it is elusive for two reasons. First, materials with the same specific surface areas may have different pore hierarchies. An aerogel with uniform pore sizes may have the same specific area as a hierarchically structured material with a smaller minimal pore size. Second, biotemplated materials may have high specific surface areas due to retention of the smallest structural details. However, this is not a guarantee that these details have been retained, since the finest pores may become closed, or crystallites may precipitate that provide a large surface area but do not reflect the nanoscale structure of the template. Therefore, most studies combine a nitrogen sorption analysis with transmission electron microscopy or Small-angle X-ray scattering (SAXS) to determine all pore sizes that are present in the sample, and whether they relate to the structuring of the template [263–265].

1.5.3 Pore Structures

The actual pore structures are, therefore, a more suitable measure of the structure retention during biotemplating processes. There are ample descriptions and depictions of geologically petrified wood sections fossilized in their entirety, while retaining their original structuring from the meter to the micrometer level, i.e. the stem cross-section, bark, wood, and pith, as well as the pores [66]. Such a replication of hierarchical structures requires that there are available pores on all levels of hierarchy.

In plants, the smallest pore volumes are partially filled by extractives, such as terpenes, fats, and low molecular extractives [146]. Also, fresh plants may contain a significant amount of water. Its thermal removal would greatly alter the pore structure. Instead, as exemplified by work on plant leaf templating [266], chemical dehydration, i.e. the exchange of water for an organic solvent, is usually necessary. Further, the selective removal of cell wall components, as happens in nature by white- or brown rot, opens up volumes in plant cell walls into which minerals can be deposited [267]. The field of wood modification [267–269] can give important insight into the accessibility of wood cell walls, since wood cell wall mineralization for protective purposes is only one step – the template removal – away from biotemplating.

A property that can be achieved by replicating biological materials is a chiral porosity at the 10 nm or 100 nm scale. As comprehensively reviewed by Sotiropoulou et al., many biological structures, among them lipids and DNA, show chiral structuring by self-assembly [270]. It is possible to artificially create chiral structures by self-assembly of nematic cellulose with the same methods also employed in biotemplating [271, 272]. The resulting material was very similar to chiral protein stacks found in the cuticles of beetles, as discussed in Section 1.6.4.

As further discussed in Section 1.6.4, chiral structures on the 100 nm scale are responsible for the polarization-dependent optical response of photonic biological materials. These structures, containing rotation-translational symmetry axes describing corkscrewing planes running through the material, are thought to be assembled from cytoplasmic membranes in beetles [273]. However, the exact process – if there is a unifying route – of the structure formation is, to our best knowledge and due to lack of observations *in vivo*, unknown. It requires systematic analysis to correctly identify a chiral motif in such lattice works, since the helical pitch is not apparent when viewed from any fixed direction in the microscope [274]. Correspondingly, Stavenga et al. describe how the internal structuring of *Callophrys rubi* was successively identified as simple cubic, face-centered cubic, as inverted face-centered cubic opals and finally, the gyroid structure [273]. The gyroid is described as a net of points centered between and normal to adjacent surfaces with a space

porous, spongy structures, such as wood, citrus peels, sea urchins [326], or sponges [327]. Suitable target phases include aluminum oxide [328], silicon nitride [327], or yttria-stabilized zirconia [329]. The processing includes the infiltration of organometallic alkoxide precursors. The resulting materials are characterized by large porosities and a large variation of pore sizes [330], providing a large surface area. All of these are intended and suitable for filters [327], sensors, catalyst carriers, thermal insulators or electrolyte materials for solid oxide fuel cells [329], or burner applications [331].

1.6.4 Photovoltaic and Sensing Materials

Photonic materials, by definition, guide the propagation of light. The guidance is based on the allowed electromagnetic resonant frequencies, as defined by the dimensions of the alternating optical densities of the constituent phases of the materials [332]. In the simplest case, the alternation is one-dimensional and leads to a strongly directional reflection of wavelengths that correspond to the lengths of the repeating units in the material. One-dimensional materials are very commonly found in the carapaces of beetles [253]. However, as already discussed in Section 1.5.1, such structures are not the only ones found in nature. On the contrary, structures in nature are often more complexly structured and may even contain areas of deliberate disorder [333–335]. Straddling the border between order and disorder is the crystallographic motif that was only recently discovered in man-made materials, the quasicrystalline lattice. It has been synthesized by nature for millennia in the shape of photonic crystals, for example, in *Eupholus magnificus* [336]. It has further been shown that such quasi-ordered structures can be transformed into engineering materials by the biotemplating approach, enabling the synthesis of structures whose existence has only just been shown [337].

Importantly, biotemplating is a processing method that is often required instead of alternative bottom-up manufacturing techniques [338]. While intricate structures mimicking natural photonic crystals can be manufactured, this is often only possible through elaborate combined bottom-up and top-down approaches [339]. These have the advantage that the obtained structure may be more freely tuned and altered. Biotemplating only allows for a certain degree of control over the dimensions of the final structure through controlling the shrinkage during processing [340]. On the other hand, it allows for a rapid replication even of complex three-dimensional biological structures in a comparatively simple and rapid manner.

The exact procedure to biotemplate photonic materials differs from the processing routes used to create mechanoceramics, filters, and substrates in several ways. The resulting material should be transparent to allow the propagation of light through the structure. This means that the material should have no energy transitions in the visible range. The filling factor, i.e. the fraction of solid material, is an important factor to determine the optical response of a material [341]. In natural photonic materials, it is carefully tuned to provide the maximum band gap width of the material, and should therefore be retained [342]. Further, the target material should have an index of refraction of at least 3 in order to achieve a complete band gap [343]. As discussed in Section 1.5.1, the second phase is most commonly air, but may also be actively or passively filled with a fluid, thereby reducing the dielectric contrast.

Suitable material precursors are metal alkoxide precursors that have been prehydrolized. They provide a strong pore volume filling as well as a large dielectric contrast when condensed to a metal oxide such as titanium oxide [337], or aluminum oxide [344]. Some structures require a double-infiltration approach during which the structure is first inverted by an intermediate phase [337]. Structures that require double infiltration are all structures whose inverts are not identical to their originals. As noted earlier, structures in nature are optimized for a maximum band gap width, while their inverts are typically not. Further, most structures, such as densely packed opals, cannot readily achieve complete band gaps [345]. Therefore, many structures found in nature require a double inversion process to yield a positive copy of the original material [346]. Templating routes using a two-step double inverse replication yielded materials with high dielectric contrasts such as alumina or titania [347, 348]. A prominent example of this is the gyroid structure, which produces a circularly polarized reflectance and transmittance, and is found in nature [349–351]. It is therefore a highly interesting optical material, with potential applications as circular polarization-dependent beamsplitters or dichroic mirrors [352]. However, manufacturing "full" gyroid structures [353], as found in nature, poses a manufacturing challenge due to the complex three-dimensional structuring, which is currently only achievable with bottom-up assembly using low-dielectric contrast materials [354, 355]. Therefore, several studies have undertaken to assess routes to either biotemplate, or template from self-assembled, polymer phase, gyroid-structured materials [356, 357]. Further suitable precursors are silicone melts, which provide a trade-off between a smooth resulting structure, albeit with a lower dielectric contrast to air [340]. Thermal template removal has been used in all known studies, which can be traced to chitin's relative resistance to chemical degradation [358, 359]. Photonic crystals can be designed and tailored to a variety of applications including anti-reflective [360, 361] and highly

If even higher temperatures are involved, crystal growth may lead to fibrous particle growth inward from the cell walls, as shown by Luo et al. during the templating of wood with silicon nitride [419]. Even if the initially deposited phase is an amorphous intermediate, temperature treatment will result in a phase transformation and crystal growth to particle sizes on the size order of 100 nm [420]. A further processing detail that has consistently been found to aid the good replication of biological structures was drying the sample in the replication liquid [96, 211].

1.7.2 Comparison with Alternating Processing Principles

When comparing biotemplating to other processing principles, one can draw up a list of definitive differences. We will use two materials that are challenging to manufacture for our comparisons, namely, ceramic gradient foams and D-surface structured photonic crystals. These stand proxy for other sought-after structures and illustrate the relative ease, as well as the problemd, by which such materials can be made via biotemplating approaches.

Gradient foams in technology can be obtained by mixing and firing alumina with carbon powder [421]. Routes to obtain hierarchical silica materials include sintering of graded particles, pulsed electric current sintering, pressure filtration of mixed particles, infiltration of compression-molded sponge, multiple and differentiated impregnation, multiple tape casting and lamination, solid free form fabrication, centrifugation of a suspension and freeze drying, introduction of a graded biodegradable phase, electrospraying into a template, freeze casting, microspheres for scaffolds, templating of emulsions, polymer foams, colloidal spheres settled by sedimentation or ice and phase separation, as reviewed by Miao et al. and Triantafillidis et al. [422, 423]. For example, gradient ceramic foams find application in implantable biomaterials for tissue regeneration, strengthening, or drug delivery. Gradient foams in nature, on the other hand, are abundant and appear as cellular soft tissue with many outer dimensions and gradient pore structures, for example, in citrus peels, sponges or grasses [293, 424]. Due to their accessible pore structure, they provide suitable biotemplates, as has been shown with the examples of the pomelo peel [425], sponges [426, 427], and the *Luffa*, among many others [428–430].

There are also several non-biotemplating routes to obtain three-dimensional photonic materials with complete band gaps. Spherically projected thin film reflectors prepared by coating polyethylene terephtalate with dichromated gelatin and alternating refractive indices produced directionally uniform reflections [431]. Titania woodpile structures, fabricated by two-photon polymerization and then twice replicated by zinc oxide and then titania showed complete directional band gaps, a first in entirely man-made materials [432]. Photonic structures found in nature do not typically possess complete band gaps, owing to the low refractive index of chitin [273]. However, certain biological photonic structures attain a complete band gap when replicated with a material with a higher refractive index. Galusha et al. used scales of the beetle *Lamphrocyphus augustus* as templates for a double replication process, as outlined in Section 1.6.4 [337]. The result was a titania structure possessing a lattice with diamond symmetry and a complete band gap in the visible range. The routes utilized by Frölich et al. and Galusha et al. are very similar, the main difference being the starting template. It can be argued that, since structures from nature are highly adapted, artificially manufactured templates can at best achieve the same quality and "adaptability" of structuring. However, biotemplates do not provide the possibility for targeted tailoring, e.g. the inclusion of waveguiding defects.

Assessing the complexity of a manufacturing process would require an in-depth study of its economic viability, which has to our best knowledge not been performed for biotemplating processes. However, we have compiled in Table 1.3 a comparative list of two materials together with the steps to obtain them via a biotemplating and an alternative route.

1.7.3 Availability

The biotemplating process relies on templates found in nature. However, we have outlined many examples of structures that are highly complex and adapted. As pointed out by Philip Ball, geometries that were determined, forgotten, or overlooked and then rediscovered by man were ultimately found to already exist in nature [433]. To obtain the best structuring for a given task requires a good knowledge of structures that exist in the different classes of animals. Since similar living objects may contain similarly structured materials with minute, but important differences (Figure 1.8), it may also require a comprehensive analysis of specimens beforehand.

The best starting point is, however, the ever-growing body of literature, of which we could only present a minute fraction in this chapter. In the literature, it has been shown that biotemplating approaches are consistently able to replicate even the most delicate of structures, including rattan [434], pomelo peel [425], even leaves [426]. Bhushan presented an overview of natural structural materials with widely differing structures and properties, as well as derivatives created by bioinspired, i.e. abstracted approaches [435]. Fan reviewed the state of biotemplating in a 118-page review in 2009 [436]. He discussed many topics outlined

47 Addadi, L., Weiner, S. (1992) *Angew. Chem. Int. Ed. English*, **31**, 153.
48 Massey, F.P., Ennos, A.R., Hartley, S.E. (2006) *J. Anim. Ecol.*, **75**, 595.
49 Jackson, P., Vincent, J.F.V., Turner, R.M. (1988) *Proc. R. Soc. B*, **234**, 415–440.
50 Raabe, D., Romano, P., Sachs, C. et al. (2006) *Mat. Sci. Eng.: A*, **421**(1–2), 143–153.
51 Burgert, I. Fratzl, P. (2009) *Integr. Comp. Biol.*, **49**(1), 69–79.
52 Harrington, M.J., Razghandi, K., Ditsch, F. et al. (2011) *Nat. Comm.*, **2**, 337.
53 Siau, J. (1984) *Transport Processes in Wood*, Springer, Berlin, Germany, p. 245.
54 Van den Honert, T. (1948) *Disc. Faraday Soc.*, **3**(146), 146.
55 Gosline, J.M., DeMont, M.E., Denny, M.W. (1986) *Endeavour*, **10**(1), 37.
56 Lin, L.H., Edmonds, D.T., Vollrath, F. (1995) *Nature*, **373**(6510), 146–148.
57 Gao, X., Jiang, L., (2004) *Nature*, **432**(7013), 36.
58 Gao, H., Wang, X., Yao, H., Gorb, S., Arzt, E. (2005) *Mech. of Mat.*, **37**(2–3), 275–285.
59 Galusha, J.W., Richey, L.R., Gardner, J.S. et al. (2008) *Phys. Rev.*, **77**(5), 2.
60 Srinivasarao, M. (1999) *Chem. Rev*, **99**(7), 1935.
61 Vukusic, P., Sambles, J. R. (2004) *Nature*, **424**, 852.
62 Vignolini, S., Rudall, P.J., Rowland, A.V. et al. (2012) *Proc. Nat. Acad. Sci. U.S.A.*, 1–4.
63 Land, M.F. (1972) *Prog. Biophys. Mol. Bio.*, **24**, 75.
64 Simon, R., Holderied, M.W., Koch, C.U., Von Helversen, O. (2011) *Science*, **333**(6042), 631.
65 Murlis, J., Elkinton, J.S., Cardé, R.T., Carde, R. (1992) *Ann. Rev. Entomol.*, **37**(1), 505.
66 Witham, H. (1831) *Observations on Fossil Vegetables, Accompanied by Representations of Their Internal Structure as Seen Through the Microscope*, Blackwood, Edinburgh, pp. 28–30.
67 Nowak, J., Florek, M., Kwiatek, W. et al. (2005) *Mater. Sci. Eng. C*, **25**, 119.
68 Buurman, P. (1972) *Scr. Geol.*, **12**, 1.
69 Kuczumow, A., Pikus, S., Un-Ro, C. et al. (2001) *Spectrochim. Acta B*, **56**(4) 339.
70 Kuczumow, A., Vekemans, B., Schalm, O. et. al. (1999) *J. Anal. Atom. Spectrom.*, **14**(3), 435.
71 Kuczumow, A. et. al. (2000) *Atom. Spectrosc.*, **55**(10), 1623.
72 Martyn, J. (1747) *The Philosophical Transactions (From the Year 1743, to the Year 1750)*, Vol. 10 (Ed: J. Martyn), Royal Society: London, Chap. III, p. 590–671.
73 Agricola, G. (1546) *De Natura Eorum Quae Effluunt Ex Terra*, Hieronymus Froben and Nicolaus Episcopius, Basel, Switzerland, Book 2.
74 Stankiewicz, A., Briggs, D.D.E.G., Evershed, R.P. et al. (1997) *Science*, **276**(5318), 1541.
75 Mustoe, G.E. (2008) *Geol. Soc. Am. Spec. Paper*, **435**, 127.
76 St. John, R.N. (1927) *Econ. Geol.*, **22**(7), 729.
77 Sigleo, C. (1978) *Geochim. Cosmochim. Ac.*, **42**, 1397.
78 Petersen, D., Link, R., Carll, C., Highley, T. (1999) *J. Test. Eval.*, **27**(2), 150.
79 Kim, Y.S., Singh, A.P. (2000) *IAWA J.*, **21**(2), 135.
80 Renaut, R.W., Jones, B., Sciences, A., Tiercelin, J. (1998) *Sedimentology*, **45**, 1083.
81 Channing, A., Edwards, D. (2009) *Plant Ecol. Divers.*, **2**, 111.
82 Ferris, F.G., Fyfe, W.S., Beveridge, T.J. (1988) *Geology*, **16**(2), 149.
83 Zhang, F.-Q., Chen, H.-L., Batt, G.E. et al. (2014) *Palaios*, **29**, 325.
84 Dernbach, U., Glas, M., Hochleitner, R. (1994) *Versteinertes Holz: aus Holz wird Stein - die Mineralogie der Holzversteinerung*, Christian Weise, Munich, Germany, pp. 49–54.
85 Kuczumow, A., Pikus, S., Un-Ro, C. et al. (2001) *Spectrochim. Acta B*, **56**(4), 339.
86 Crook, T. (1922) *Nature*, **110**, 253.
87 Correns, C.W. (1940) *Die Naturwissenschaften*, **28**(24), 369.
88 Leo, E., Barghoorn, E.S. (1976) *Bot. Mus. Leaf. Harv. Univ.*, **25**, 1.
89 Dernbach, U., Glas, M., Hochleitner, R. (1994) *Versteinertes Holz: aus Holz wird Stein - die Mineralogie der Holzversteinerung*, Christian Weise, Munich, p. 50.
90 Scurfield, G., Segnit, E.R. (1984) *Sediment. Geol.*, **39**, 149.
91 Buurman, P. (1972) *Scr. Geol.*, **12**, 1.
92 Dernbach, U., Glas, M. & Hochleitner. R. (1994) *Versteinertes Holz: aus Holz wird Stein - die Mineralogie der Holzversteinerung*, Christian Weise Munich, Germany, p. 63.
93 Harder, H. (1993) *Der Aufschluss*, **44**, 23–31.
94 Siever, R. (1959) *Soc, Econ. Paleontol. Miner.*, **7**, 55.
95 Leo, R.E., Barghoorn, E.S. (1976) *Bot. Mus. Leaf. Harv. Univ.*, **25**, 1.
96 Van Opdenbosch, D., Fritz-Popovski, G., Paris, O., Zollfrank, C. (2011) *J. Mater. Res.*, **26**(10), 1193.
97 Fritz-Popovski, G., Van Opdenbosch, D., Zollfrank, C. et al. (2013) *Adv. Funct. Mater.*, **23**, 1265.
98 Scurfield, G., Segnit, E.R. (1984) *Sediment. Geol.*, **39**, 149.
99 Alexander, G.B., Heston, W., Iler, R.K. (1954) *J. Phys. Chem.*, **58**, 453.
100 Correns, W. (1940) *Die Naturwissenschaften*, **28**(24), 369.
101 Humar, M., Petri, M., Pohleven, F. (2001) *Holz als Roh- und Werkstoff*, **59**(4), 288.
102 Reinsch, S., Unger, B., Bu, M. et al., (2012) *Wood Sci. Technol.*, **47**, 83.

262 Barrows, F.P., Bartl, M.H. (2014) *Nanomater. Nanotechnol.*, **4**(1), 1.
263 Shin, Y., Liu, J., Chang, J.H. et al. (2001) *Adv,. Mat.*, **13**(10), 728.
264 Persson, P.V., Fogden, A., Daniel, G. et al. (2004) *Biomacromolecules*, **5**(3), 1097.
265 Deshpande A.S., Burgert I., Paris, O. (2006) *Small*, **2**(8–9), 994.
266 Zimmerman, A.B., Nelson, A.M., Gillan, E.G. (2012) *Chem. Mater.*, **24**, 4301.
267 Allan, G.G., Carroll, J.P., Negri, A.R. et al. (1992) *Tappi J.*, **75**, 175.
268 Donath, S., Militz, H., Mai, C. (2004) *Wood Sci. Technol.*, **38**, 555.
269 Xie, Y., Hill, C.A.S., Xiao, Z. et al. (2010) *Compos. A Appl. Sci. Manuf.*, **41**, 806.
270 Sotiropoulou, S., Sierra-Sastre, Y., Mark, S.S., Batt, C.A. (2008) *Chem. Mater.*, **20**(3), 821.
271 Dujardin, E., Blaseby, M., Mann, S. (2003) *J. Mater. Chem.*, **13**, 696.
272 Shopsowitz, K.E., Qi, H., Hamad, W.Y., MacLachlan, M.J. (2010) *Nature*, **468**, 422.
273 Michielsen, K., Stavenga, D.G. (2008) *J. R. Soc. Interf.*, **5**(18), 85.
274 Schröder-Turk, G.E., Wickham, S., Averdunk, H. et al. (2011) *J. Struct. Biol.*, **174**(2), 290.
275 Wohlgemuth, M., Yufa, N., Hoffman, J., Thomas, E.L. (2001) *Macromolecules*, **34**(17), 6083.
276 Fratzl, P., Jakob, H.F., Rinnerthaler, S. et al. (1997) *J. Appl. Crystallogr.*, **30**(5, Pt. 2), 765.
277 Glatter, O. (1977) *J. Appl. Crystallogr.*, **10**, 415.
278 Glatter, O. (1980) *J. Appl. Crystallogr.*, **13**, 7.
279 Donaldson, L., Xu, P. (2005) *Trees*, **19**(6), 644.
280 Salmen, L., Burgert, I., Salmén, L. (2009) *Holzforschung*, **63**(2), 121.
281 Fritz-Popovski, G. (2015) *J. Appl. Crystallogr.*, **48**, 44.
282 Feigin, L.A., Svergun, D.I. (1987) *Structure Analysis by Small-Angle X-Ray and Neutron Scattering*, Plenum Press, New York, pp. 219–273.
283 Ota, T., Takahashi, M., Hibi, T. et al. (1995) *J. Am. Ceram. Soc.*, **78**, 3409.
284 Ota, T., Imaeda, M., Takase, H. et al. (2000) *J. Am. Ceram. Soc.*, **83**(6), 1521.
285 Sun, B.H., Fan, T.X., Zhang, D., Okabe, T. (2004) *Carbon*, **42**, 177.
286 Wood, L.L., Messina, P., Frisch, K.C. (1974) US Patent 3,833,386A.
287 Peng, H.X., Fan, Z., Evans, J.R.G., Busfield, J.J.C. (2000) *J. Eur, Ceram. Soc.*, **20**, 807.
288 Byrne, C.E., Nagle, D.C. (1997) *Mat. Res. Innovat*, **1**(3), 137.
289 Chakrabarti, O., Weisensel, L., Sieber, H. (2005) *J. Am. Ceram. Soc.*, **88**, 1792.
290 Greil, P., Lifka, T., Kaindl, A. (1998) *J. Eur. Ceram. Soc*, **18**, 1974.
291 Vogli, E., Zollfrank, C., Sieber, H. et al. (2002) *Ceram. Transact.*, **129**, 33.
292 Zollfrank, C., Kladny, R., Sieber, H., Greil, P. (2001) In *Verbundwerkstoffe und Werkstoffverbunde* (Eds: B. Wielage, G. Leonhardt), Wiley-VCH, Weinheim, Germany, pp. 274–278.
293 Brandt, B., Zollfrank, C., Franke, O. et al. (2010) *Acta BioMater.*, **6**, 4345.
294 Paris, O., Zollfrank, C., Zickler, G.A. (2005) *Carbon*, **43**, 53.
295 Greil, P., Lifka, T., Kaindl, A. (1998) *J. Eur. Ceram. Soc.*, **18**(14), 1975.
296 Xu, Y., Cheng, L., Zhang, L. (1999) *Carbon*, **37**, 1179.
297 Singh, M., Martınez-Fernández, J., de Arellano-López, A.R. (2003) *Curr. Opin. Solid State Mater. Sci.*, **7**, 247.
298 Weiner, S. Addadi, L. (1997) *J. Mater. Chem.*, **7**, 689.
299 Zhang, X., Yu, M., Liu, J., Li, S. (2012) *Langmuir*, **28**, 3690.
300 Fritz-Popovski, G., Morak, R., Schöberl, T. et al. (2014) *Bioinspired, Biomim. Nanobiomater.*, **3**, 160.
301 Wang, J. He, S., Xie, S. et al. (2007) *Mater. Lett.*, **61**, 917.
302 Zhang, X., Yu, M., Liu, J., Li, S. (2012) *Langmuir*, **28**, 3690.
303 Götze, J., Möckel, R., Langhof, N. et al. (2008) *Ceram. Silikáty*, **52**, 268.
304 Wang, T.-C., Fan, T-X., Zhang, D., Zhang, G.-D. (2006) *Mater. Lett.*, **60**, 2695.
305 Wang, T.-C., Fan, T-X., Zhang, D., Zhang, G.-D. (2006) *Carbon N, Y.*, **44**, 900.
306 Haas, D., Fey, T., Greil, P. (2007) *Adv. Eng. Mater.*, **9**(10), 892.
307 Wang, T.-C., Fan, T-X., Zhang, D. et al. (2007) *Mater. Lett.*, **61**, 1849.
308 Arellano-López, A.R., Martínez-Fernandez, J., González, P. et al. (2004) *Int. J. Appl. Ceram. Technol.*, **67**, 56.
309 Beck-Candanedo, S., Roman, M., Gray, D.G. (2005) *Biomacromolecules*, **6**, 1048.
310 Padalkar, S., Capadona, J.R., Rowan, S.J. et al. (2010) *Langmuir*, **226**, 8497.
311 Zhang, T., Wang, W., Zhang, D. et al. (2010) *Adv, Funct. Mater.*, **20**, 1152.
312 Gruber, S., Klupp Taylor, R.N., Scheel, H. et al. (2011) *Mater. Chem Phys.*, **129**, 19.
313 Gruber, S., Zollfrank, C. (2012) *Bioinspired, Biomim. Nanobiomater.*, **1**(2), 95.
314 Scheel, H., Zollfrank, C., Greil, P. (2009) *J. Mater. Res.*, **24**, 1709.
315 Nogi, B.M., Yano, H., Nogi, M. (2008) *Adv. Mater.*, **20**, 1849.
316 Olsson, R.T., Azizi Samir, M.A.S., Salazar-Alvarez, G. et al. (2010) *Nat. Nanotechnol.*, **5**, 584.
317 Korhonen, J.T., Hiekkataipale, P., Malm, J. et al. (2011) *ACS Nano.*, **5**, 1967.

To realize the cell patterning, most mammalian cells must first of all attach themselves to a surface though cell-surface interactions in order to survive, proliferate, and function. To enhance the cell adhesion, necessary surface modification techniques such as SAMs formation, Langmuir-Blodgett deposition, and layer by-layer assembly have been employed to fabricate a thin layer of composites whose properties are similar to an extracellular matrix (ECM), which provides structural integrity and a suitable chemical environment for the cells. Among these modification methods, SAMs are widely implemented because the nature and density of functional groups can easily be tuned on SAMs to tune cell adhesion [16].

The cell-surface interactions can be divided into two categories: nonspecific and specific interactions. Nonspecific interactions are mediated by physical attachments, including electrostatic force, van der Waals interaction, and hydrophobic forces. By employing nonspecific interactions, Lee et al. used dopamine self-polymerization to form thin, surface-adherent polydopamine films on a wide range of inorganic and organic materials [16]. Jiang et al. reported that polydopamine is a versatile nonspecific adhesive material for cell adhesion [17].

Specific cell-surface interactions refer to the involvement of specific receptor-ligand bonding formations in cell adhesion. The RGD (Arg-Gly-Asp) sequence is an excellent mediator to promote the specific attachment of cells on surfaces. Its ability to bind a variety of cells through ligand-receptor interactions makes RGD an exceptionally useful sequence for cell patterning [18]. The surface density of RGD peptides has been demonstrated to elicit different cellular responses and a minimum RGD density of 10 fmol/cm^2 is needed for cell adhesion [19]. The clustering of RGD peptides at the nanoscale level can significantly reduce the average ligand density and cell adhesion [20].

The physical properties such as topographical and stiffness of the surface, the temperature, light can also influence the cell adhesion. Topographical cues generated by the ECM, independent of biochemistry, have direct effects on cell behavior such as adhesion, migration, cytoskeletal arrangements, and differentiation [21–24]. Teruo Okano et al. introduced the Poly(N-isopropylacrylamide) (PIPAAm) onto the surface of polystyrene cell culture dishes to control the cell adhesion by adjusting the temperature of the polymer [25]. Cells attached on PIPAAm-grafted surfaces at 37 °C, and detached from the surfaces at 20 °C without the usual damage associated with trypsinization. The cell sheets fabricated using this strategy have been widely used in the tissue engineering field [26, 27]. Light also has been used to dynamically control cell adhesion on substrates. However, existing techniques have mostly relied on irreversible control, that is, once the original structure for controlling cell adhesion on the surface is altered, it cannot be regenerated for further use [28–31]. Jiang et al. reported a photochemical method to reversibly control cell adhesion using azobenzene-embedded self-assembled monolayers. In this method, reversible cell adhesion was realized depending on the conformational transition of the azobenzene group embedded in the SAMs, which were elicited by different wavelengths of lights (Figure 2.3a) [32].

Patterning cells in 3D to simultaneously realize the combination of ordered cells arrangement and functions still remains challenging. Jiang et al. reported an on-chip method to construct a kind of long-term 3D neuronal network with ordered somata patterns and guided neurite connections as well as recordable neuronal activities in functions [33]. In this strategy, gravity-driven, the microchamber-assisted assembly of borosilicate glass microspheres is employed to fabricate scaffolds onto which dissociated neurons develop 3D neuronal networks (Figure 2.3b). Compared with the existing strategies which can just realize either ordered pattern of neuronal somata [34, 35] or controllable guidance of neurites [36, 37], this strategy is more promising for applications in the fields of fundamental neuroscience, tissue engineering, and brain-machine interfaces.

2.3.2.2 Cell Mechanics

Mechanics play key role in tissue development, tissue repair, and microenvironment maintenance. The mechanical cues, typically including stretching, shear stress, and matrix rigidity, drastically affect cell proliferation, differentiation, and functions, and consequently influence the process of tissue regeneration. Compressive loads have been shown to increase cell differentiation and extracellular matrix synthesis [38]. Dynamic fluid perfusion can induce higher cell proliferation and differentiation than static cultures [39]. Shear stress has been reported to influence cell adhesion, cytoskeletal alignment, as well as gene expressions [40]. Tensile forces can stimulate cell proliferation and vascular remodeling in living skin [41]. The rigidity of the substrate can also influence the behavior of the cells. Chen et al. observed cells prefer to migrate to stiffer regions of substrate [42]. LeDuc et al. employed microfluidic channels to pattern alternative rigidities on substrate. Their results show that localized rigidity would restrict the outgrowth and orientation of neurite in differentiating neuroblasts [40]. All these discoveries imply that mechanical stimuli is a very important component in the field of tissue engineering.

Microfluidics provides unique tools for mimicking various mechanical environments to investigate cells behavior *in vitro*. Douville et al. developed a microsystem

network of scaffolds provides channels for cell migration, signaling molecule diffusion, nutrient delivery, and waste removal. Scaffolds can also be divided into two types, one has a good biological stability which provides long-term support in the human body; the other is made of biodegradable materials whose degradation rate equals that of tissue regeneration. Scaffolds of both types can be made from synthetic biomaterials or be naturally occurring.

Synthetic materials have great potential in terms of being vascular scaffolds because they are widely available, and their cost and performance are controllable. However, the biocompatibility of the synthetic materials influences their performance in vascular tissue engineering. Zella et al. lined ePTFE grafts with functional autologous endothelium to overcome the problems associated with acute thrombosis [85]. However, this approach introduces a potential risk to the body due to the permanent presence of a synthetic scaffold. In 1999, Niklason et al. fabricated tissue engineering blood vessels with biodegradable polyglycolic acid (PGA). SMCs were seeded into the tubular PGA scaffolds and cultured in a bioreactor under conditions of pulsatile radial stress for eight weeks, and finally endothelial cells were lined in the luminal surface. Their vessels had high patent and burst pressure with contractile responses to pharmacological agents [78]. However, problems, such as the long period of construction time and the complex fabrication process, limited this method. With advances in technology, some materials with excellent performance are being developed, and the acellular tissue engineering scaffolds are attracting increasing attention. Wang et al. developed a cell-free scaffold from poly (glycerol sebacate) (PGS), a biodegradable material that has an appropriate degradation time [86]. The inner layer of the scaffold is porous PGS for host cell infiltration, and over 99.99% of the pores are interconnected. In the luminal surface, heparin is coated to reduce the platelet adhesion to prevent thrombosis. To enhance the mechanical strength and prevent blood cell loss, the grafts were enclosed in a dense, nonwoven poly (ε-caprolactone) PCL sheath. The entire scaffold was directly connected to rat abdominal aorta and exposed to the hemodynamic environment without seeding any cells *in vitro*. Under the interaction of the scaffold degradation and host remolding, new arteries, which were almost free of foreign materials, were yielded after three months.

There are also some non-mainstream methods for vascular remolding. Some researchers inserted silastic, polypropylene or polyglycolic acid tube into the peritoneal cavity, in which macrophage-derived granulation tissue will form on the surface of the tube, the vessel yielded after the tube was removed. This living vessel, though with good patency and mechanical strength, is still risky in clinical trials owing to the invasive requirement of inserting foreign materials into the human body [87, 88].

2.4.2.2 Rapid Prototyping of 3D Tubular Structures

Tissues with tubular structures, such as blood vessels, lymph vessels, trachea, and intestines are abundant in the bodies of higher-order animals. Tubular tissues have two distinguishing features: (1) they have specific 3D shapes; and (2) they have different types of cells at specific locations. Mimicking both of these features is a prerequisite in fabricating functional tubular tissues. Furthermore, most of the present methods used on 3D tubular structure fabrication need several months of *in vitro* culture before implantation, a rapid 3D tubular structure fabrication method is desirable. Jiang and colleagues provide three efficient and facile strategies to fabricate tubular structures. Briefly, based on the stress-induced rolling membrane (SIRM) technique, combined with the microfluidic and cell patterning technology, tissue-engineered blood vessels with highly controllable distribution and orientation of vascular cells were fabricated.

The first strategy, based on the SIRM technique, provided a self-assembly method to fabricate a series of complex 3D structures, such as tubular structures, tubes-in-a-tube structures, spirals, and tubes with wrinkled walls [89]. Using the SIRM techniques to fabricate the tubular structure, the SIRM is fabricated by binding two elastic membranes together. The top membrane of the two binding elastic membranes is a piece of cured PDMS which is stretched by a mechanical stretcher to produce stress, and the bottom membrane is relaxed and semi-cured PDMS. After the two layers of membranes bond together, the SIRM is obtained. if the top and the bottom membrane were released at the same time, the bi-layer membrane will roll up and turn into a tubular structure because of the internal stress. By using this technique, the tubes-in-a-tube structure, which refers to the structure where several small tubes are embedded in a big tube, could be fabricated with only two steps (Figure 2.4a): first, a rectangular array was cut in the middle part of the SIRM with a scalpel, with one side of each rectangle left uncut. The rectangular array will roll up to form the tubular array. Next, one end of the entire SIRM was cut off along one side of the tubular array, then the entire SIRM is rolled toward another end to form a big tube. The two ends of the big tube were cut to generate the tubes-in-a-tube structure. In addition, spiral structures could be formed using the SIRM technique. It is known that closing the gaps of the spiral ribbons can lead to the formation of rigid and straight tubes [90]. Conversely, if a rectangular strip were cut with a certain angle (?° from

segments of trachea in rats. In further experiments, an attempt was made to seed the inner surface with tracheal epithelial cells. Moreover, a decellularized human donor trachea, colonized by the recipient's epithelial cells and chondrogenic mesenchymal stem cells (MSC), was implanted into a patient with end-stage airway disease [119]. More than one year after the tissue-engineered tracheal transplantation, the function parameters of the implanted tracheal are all within the normal range. This provides compelling evidence that tissue engineering with a well-designed strategy is an ideal way to treat large tracheal lesions.

2.5 Conclusion

In this review, we first introduced the main natural tubular structures in the human body: the blood vessel, the lymphatic vessel, the vessels in the digestive system, and the vessels in the respiratory system and their key structural features such as 3D tubular shapes and multi-layered structure. This knowledge may help us to understand the importance of the structural and functional mimicking in the construction of tissue engineering scaffold.

Microfluidics, an emerging set of technologies for manipulating cells, cell-cell interactions, and cell-material interactions, are powerful tools for tubular structure tissue engineering. By bonding and stretching bi-layer membrane with different Young modulus, a two-dimensional membrane could become a three-dimensional tubular structure with multi-layers. By microfluidic printing (μ CP) different cell types with different microchannels on the two-dimensional membrane, the corresponding three-dimensional tubular structure could be a multi-layered construction where different types of cells are distributed at specific locations. This three-dimensional rapid prototyping technology is a promising method for the construction of advanced, complex, tubular structures.

Although tubular tissue engineering has achieved exciting progress, there are still many problems that need to be addressed. For example, the elasticity, stiffness, and degradation rate of the scaffold materials still cannot fully match the requirement of the operations, the mechanical properties of the original tissues, and the tissue repair processes. The source of the pre-loaded cells in the scaffold is also limited at present. To solve these problems, we may focus on the improvement of biomaterials and the utilization of stem cells.

Acknowledgments

Financial support was provided by the Ministry of Science and Technology of China (2011CB933201, 2012AA030308), the National Science Foundation of China (31170905, 81361140345, 31470911, 51373043, and 21222502), the CAS (XDA09030305, XDA09030307), and the CAS/SAFEA International Partnership Program for Creative Research Teams.

References

1 Papka, R.E. (1995) *Encyclopedia of Neuroscience.*
2 Pepper, M.S., Skobe, M. (2003) *J. Cell Biol,.* **163**, 209–213.
3 Shayan, R., Achen, M.G., Stacker, S.A. (2006) *Carcinogenesis*, **27**, 1729–1738.
4 Nerem, R.M., Seliktar, D. (2001) *Annu. Rev. Biomed. Eng.*, **3**, 225–243.
5 Whitesides, G.M. (2006) *Nat.*, **442**, 368–373.
6 Terry, S.C., Jerman, J.H., Angell, J.B. (1979) *IEEE Trans. Electron. Dev.*, **26**, 1880–1886.
7 Manz, A., Miyahara, Y., Miura, J. et al. (1990) *Sensor Actuator B: Chem.*, **1**, 249–255.
8 Harrison, D.J., Fluri, K., Seiler, K. et al. (1993) *Sci.*, **261**, 895–895.
9 El-Ali, J., Sorger, P.K., Jensen, K.F. (2006) *Nat.*, **442**, 403–411.
10 Meyvantsson, I., Beebe, D.J. (2008) *Annu. Rev. Anal. Chem,.* **1**, 423–449.
11 Khademhosseini, A., Langer, R., Borenstein, J., Vacanti, J.P. (2006) *Proc. Natl. Acad. Sci. U.S.A.*, **103**, 2480–2487.
12 Weibel, D.B., DiLuzio, W.R., Whitesides, G.M. (2007) *Nat. Rev. Microbiol.*, **5**, 209–218.
13 Whitesides, G.M., Ostuni, E., Takayama, S. et al. (2001) *Annu. Rev. Biomed. Eng.*, **3**, 335–373.
14 Kane, R.S., Takayama, S., Ostuni, E. et al. (1999) *Biomat.*, **20**, 2363–2376.
15 Mrksich, M. (2009) *Acta Biomaterialia*, **5**, 832–841.
16 Lee, H., Dellatore, S.M., Miller, W.M., Messersmith, P.B. (2007) *Sci.* **318**, 426–430.
17 Sun, K., Song, L., Xie, Y. et al. (2011) *Langmuir*, **27**, 5709–5712.
18 Humphries, J.D., Byron, A., Humphries, M.J. (2006) *J. Cell Sci.*, **119**, 3901–3903.
19 Massia, S.P., Hubbell, J.A. (1991) *J. Cell Biol.*, **114**, 1089–1100.

the cells are surrounded by a lot of ECMs. In such a situation, the cell distance in the tissues is of a micrometer-sized level. Although the LbL FN-G coating methodology provide possibilities to construct functionalized 3D-tissue models in one day, the fabricated films on the cell surfaces are only nanometer-sized, so it is hard to obtain thick films in a short time. Hence, we developed another novel approach called the "collagen coating method" and the "multiple coating method" to achieve the aim of construction of 3D-tissue models with lower cell density [46]. This chapter gives an overview of our attempts to construct artificial 3D-tissue models possessing similar structures and functions as a natural tissue in the body by using nano- and micro-coating technologies (Figure 3.1).

3.2 Fabrication of Nanometer- and Micrometer-Sized ECM Layers on Cell Surfaces

Tissues and organs consist of various cell types and densities, for example, heart tissues and muscle tissues are composed of higher cell densities, and skin tissues and cartilage tissues are composed of lower or gradient cell densities with aging or even injury. To develop a 3D-tissue model similar to natural tissues, direct fabrication on cell surfaces of nanometer- and micrometer-sized ECM fibrous scaffolds onto a cell membrane is crucial, as insufficient ECMs are secreted during the early cell culture to form 3D-tissue models. In this study, we focus on the fabrication of ECMs films on a cell membrane, based on specific interactions between ECMs and the integrin receptor on the cell membranes. There are many different types of ECM in the body, for example, collagen, laminin, hyaluronic acid, fibronectin, elastin, and gelatin, etc. Selection of the appropriate natural ECM components is important when fabricating ECM films onto cell surfaces without cytotoxicity. A typical ECM has specific cell-adhesive moieties like RGD (arginine-glycine-aspartic acid) [47].

The cell membrane is a biological membrane which is selectively favorable to ions or organic molecules in and out of cells, which consist of a phospholipid bi-layer with various kinds of embedded proteins. Proteins on cell membranes play an important role as they are responsible for various biological activities. Among these proteins, integrin receptors are one of the most important proteins on cell membranes. Integrin receptors consist of 18 types of α subunits and 8 types of β subunits. The combination of α and β subunits determines the specificity for extracellular ligands as well as intracellular signaling processes [48, 49]. In these different kinds of integrin receptors, α5β1 integrin receptor [50] and other integrin receptors can recognize FN since it contains an RGD sequence. Binding of the RGD motif to initiate fibril formation to integrin receptors may be the initial event which triggers the subsequent reactions. In the case of G, this is a mixture of peptides and proteins produced from partial hydrolysis of collagen extracted from the skin, bones, and connective tissues. FN and G can interact with each other because FN has a collagen-binding domain, indicating these two proteins may connect to each other similar to a nanometer-sized film on cell surfaces. Thus, the FN-G nanofilms are expected to provide a suitable cell-adhesive surface similar to the natural ECMs for multilayered structures without any cytotoxicity. As shown in Figure 3.1, a 3D multilayer composed of cells and FN-G nano films was fabricated onto cell surfaces by using an LbL assembly based on the their specific interactions.

3.2.1 Control of Cell Surface by FN Nanofilms

In order to fabricate micrometer-sized films onto cell surfaces, another natural molecule is needed. Collagen is the most abundant structural protein found in the human body and is the major and most abundant component of animal connective tissues. Among different types of collagen, type I is the most widely used material in biomedical and tissue engineering fields, because it is easily denatured by environment temperatures and pH [51, 52]. Different from α5β1 integrin receptor used for the recognition of FN on cell membranes [47], another integrin receptor called the α2β1 integrin receptor can recognize collagen molecules with an association constant of $6.7 \times 10^4 M^{-1}$ [53]. The fabrication of micrometer-sized layers on cell membranes was performed according to the process shown in Figure 3.1. Recently, we published a new coating method called "collagen coating method" and "multiple coating method" to fabricate micrometer-sized films onto cell surfaces based on specific recognition abilities between the α2β1 integrin receptors and collagen fibers.

In order to discover the thickness of the ECM films coated onto cell surfaces, in the case of FN-G assembly films, the film thickness was analyzed quantitatively by a quartz crystal microbalance (QCM) as the assembly substrate, and with a phospholipid bi-layer membrane as a model cell membrane (Figure 3.2). A phospholipid bi-layer was prepared by 1, 2-dipalmitoyl-*sn*-glycero-3-phosphatidylcholine (DPPC) and 1, 2-dipalmitoyl-*sn*-glycero-3-phosphate (DPPA) on a base layer constructed by LbL assembly of poly(diallyldimethyl-ammonium chloride) (PDDA) and poly(sodium styrenesulfate) (PSS) as stated in Krishna's report [54]. About 2.3, 6.2,

and 21.1 nm-thick FN-G nanofilms were fabricated on the substrates after 1, 7, and 23 assembly steps. By using the fluorescently labeled method, deposition of rhodamine-labeled FN (Rh-FN) on cell surfaces was observed by using a confocal laser scanning microscope (CLSM). The thickness of FN increased after 7-step-assembled Rh-FN-G procedures (Figure 3.2b) and also can be calculated by detecting changes in the fluorescence intensity. By using the fluorescent labeling method, the coating results of Rh-FN and FITC-G nanofilms on the floating (Figure 3.2a) and the adhered (Figure 3.2c) cell surfaces also can be visualized by CLSM.

Other compounds such as sodium dextran sulfate (DS) were also applied to coat a nanometer-sized films with the combination of FN on the cell surfaces, although FN and DS have a negative charge under physiological conditions [55]. Furthermore, we also successfully applied PE films, for example, FN-ε-Lys and ε-Lys-PSS onto the cell surfaces based on their common electrostatic interactions between the positive and negative components. To evaluate the effect of LbL nanometer-sized films on cell functions, mouse L929 cells with and without different kinds of LbL films were used for proliferation experiments. Figure 3.3a shows the morphologies of cells after 24 h of incubation with and without different LbL films on the cell surfaces. From the results, the FN-G and FN-DS nanofilms-coated mouse L929 fibroblasts revealed almost the same morphologies as shown in the control group. Proliferation curves of FN-G and FN-DS groups were also evaluated. The results shown in Figure 3.3b indicate that proliferation curves of FN nanofilm groups agreed well with the control group (without coating) during 72 h of incubation, suggesting no cytotoxicity to cell functions. To understand the details of the FN nanofilms coating, mouse L929 fibroblasts with FN nanofilms coating were also observed by fluorescence microscopy and scanning electron microscopy (SEM). As shown in Figures 3.3a, b, the results of nanometer-sized meshwork structures of the FN films spread on culture dishes and the cell surfaces were observed after 24 h of incubation, which are similar to natural ECMs in the human body.

Similarly, proliferation experiments of polyelectrolyte (PE) nanofilms-coated cells (FN-ε-Lys and ε-Lys-PSS) were also evaluated during 72 h of incubation. The results show that the coating affects the cell adhesion morphology (Figure 3.4a) and their proliferation (Figure 3.4b). This might be due to the strong non-specific adsorption of cationic polymers onto the cell surfaces. The results showed that the FN nanofilms did not affect the cell functions, and can form a nano-meshwork on the cell surfaces, which increases cell adhesion on culture dishes.

3.2.2 Control of Cell Surface by Collagen Microfilms

Apart from the FN nanofilm coating methodology, we also developed a microfilm coating approach called the "collagen coating method" as mentioned in Section 3.2.1 [46]. Based on the specific interactions between collagen fibers and α2β1 integrin receptors on the cell membranes, we successfully coated collagen microfilms on the cell surfaces. To modulate cell density precisely, we tried to control the thickness of the collagen microfilms on the cell surfaces by multiple coating approach as shown in Figure 3.2d, NHDFs were coated with collagen molecules once, twice, and three times. To visualize the thickness changing of each layer, fluorescein isothiocyanate (FITC)-labeled collagen was applied to distinguish each time the coating of the collagen microlayer on the cell surfaces, and rhodamine (Rh)-labeled FN was added to the collagen solution to clarify the second layer. Figure 3.2e clearly presents the green fluorescent collagen microfilms on the cell surfaces by CLSM. When the second coating solution contains Rh-FN, red fluorescence corresponding to Rh-FN was also clearly observed. We also tried to fabricate a third layer using a FITC-collagen solution without Rh-FN. CLSM images clearly revealed three distinct layers consisting of collagen fibers and FN. The average thicknesses of these three layers are about 3, 15, and 30 μm, respectively. The line scanning results shown in Figure 3.2f also indicate each coated layer after different coating procedures. The results demonstrated the fabrication of collagen microfilms on the cell surfaces.

To confirm the collagen microfilm coating results under wet conditions, we used a low-voltage SEM instrument (LVSEM, Miniscope Tm3030, Hitachi). A high density of meshwork structures was observed on surfaces with collagen coating in Figure 3.3d, whereas no fiber structure was coated on the cell surfaces (Figure 3.3c) [56]. The meshwork structures coated on the cell surfaces are similar to natural ECMs. Other detail measurements such as FTIR and XRD were also applied to evaluate the coating effect on the structures of collagen and cells.

To evaluate the effects of cells on the functional groups of collagen molecules, FTIR spectra analyses of cells and collagen micro-coated cells were measured. From previous reported studies [57, 58], the amide I band of collagen molecules, which exhibits a high sensitivity to conformational changes, is a frequently used spectral region for IR spectroscopic analysis of protein secondary structure. This band of $\nu_{C=O}$ is centered in the range 1650–1660 cm^{-1}. The amide II band is located at ~1540–1550 cm^{-1}, which represents the complex nature comprising both the N-H bending vibration (δ^{NH}) [59], whereas the stretching

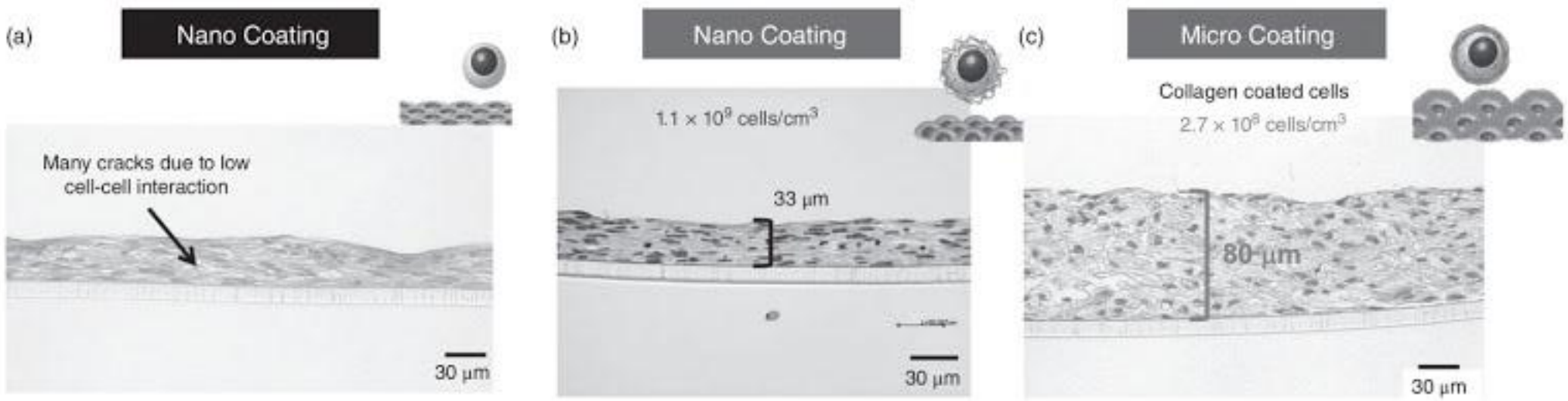

Figure 3.5 Histological staining images and schematic illustration of cell densities inside 3D tissues constructed by (a) cells without coating, (b) FN-G coated cells, and (c) collagen-coated cells (coated once), using the cell accumulation technique. *Source:* Reprinted with permission from [46].

expression of cardiac myoblasts in the 3D iPS-CM tissues. Protein staining such as actin staining identified the cytoskeleton, which contributes to muscle contraction, troponin T staining proved the modulation of strained muscle, connexin staining marked the typical gap junction at virtually every interface between the cultured cardiomyocytes in the tissues, and Azan staining was applied to distinguish the collagen matrix inside the tissues [65]. These results suggested that collagen microfilm coating method can be applied to various types of cells for different purposes.

3.5 Conclusion

We have successfully developed nanofilm and microfilm coating method to coat different sizes of cells to construct 3D-tissue models for different purposes. Both coating methods showed no obvious effect on cell functions. A bottom-up approach is valuable to develop 3D-tissue architectures using various types of cells with controlled location, functions, and cell densities. These two approaches could be the solutions to construct functional 3D-tissue models similar to natural tissues. We would like to apply these methods to contribute to the development of tissue engineering and pharmaceutical fields.

Acknowledgments

This chapter was supported by the NEXT Program (LR026), a Grant-in-Aid for Scientific Research (S), a Grant-in-Aid for Scientific Research on Innovative Areas (26106717), and a Grant-in-Aid for Scientific Research (B) (26282138) from MEXT of Japan, and JST-PRESTO (10825).

References

1 Takao, H., Hasegawa, H. (2004) *Mater. Trans.*, **45**, 747–753.
2 Guzman, L., Miotello, A., Voltolini, E., Adami, M. (2000) *Thin Solid Films*, **377–378**, 760–765.
3 Shulz, U. Munzert, P., Kaiser N. (2001) *Surf. Coat. Technol.*, **45**, 507–511.
4 Nakamori, T., Adachi, Y., Arai, M., Shibuya, A. (1995) *ISIJ Int.*, **35**, 1494–1501.
5 Nikravesh, B., Ramezanzadeh, B., Sarabi, A.A., Kasiriha, S.M. (2011) *Corros. Sci.*, **53**, 1592–1603.
6 Kalenda, P., Kalendová, A. (1995) *Dye. Pigment.*, **27**, 305–312.
7 Da Silva Sobrinho, A. (1998) *J. Vac. Sci. Technol.*, **16**, 3190.
8 Quinto, D.T., Wolfe, G.J., Jindal, P.C. (1987) *Thin Solid Films*, **153**, 19–36.
9 Sproul, W.D. (1996) *Surf. Coatings Technol.*, **81**, 1–7.
10 Chen, H., Ding, C.X. (2002) *Surf. Coatings Technol.*, **150**, 31–36.
11 Li, C. J., Li, W.Y. (2003) *Surf. Coatings Technol.*, **167**, 278–283.
12 Bakshi, S.R., Singh, V., Balani, K. et al. (2008) *Surf. Coatings Technol.*, **202**, 5162–5169.
13 Søndergaard, R., Hösel, M., Angmo, D. et al. (2012) *Mater. Today*, **15**, 36–49.
14 Krebs, F.C. (2009) *Sol. Energy Mater. Sol. Cells*, **93**, 465–475.
15 Pierschbacher M.D. (1987) *J. Biol. Chem.*, **262**, 17294–17298.
16 Recknor, J. B., Sakaguchi, D.S., Mallapragada, S.K. (2006) *Biomaterials*, **27**, 4098–4108.
17 Chang, P.-C., Liu, B.-Y., Liu, C.-M. et al. (2007) *J. Biomed. Mater. Res. A*, **81**, 771–780.
18 Liss, M., Petersen, B., Wolf, H., Prohaska, E. (2002) *Anal. Chem.*, **74**, 4488–4495.
19 Decher, G. (1997) *Science*, **277**, 1232–1237.
20 Decher, G., Hong, J. (1991) *J. Makromol. Chem., Macromol. Symp.*, **46**, 321–327.
21 Roberts, A.B., McCune, B.K., Sporn, M.B. (1992) *Kidney Int.*, **41**, 557–559.
22 Vukicevic, S., Kleinman, H.K., Luyten, F.P. et al. (1992) *Exp. Cell Res.*, **202**, 1–8.
23 Gumbiner, B.M. (1996) *Cell*, **84**, 345–357.
24 Werb, Z. (1997) *Cell*, **91**, 439–442.
25 Cursio, R., Mari, B., Louis, K. et al. (2002) *FASEB J.*, **16**, 93–95.
26 Wolf, K., te Lindert, M., Krause, M. et al. (2013) *P. J. Cell Biol.*, **201**, 1069–1084.
27 Sasagawa, T., Shimizu, T., Sekiya, S. et al. (2010) *Biomaterials*, **31**, 1646–1654.
28 Sekine, H., Shimizu, T., Sakaguchi, K. et al. (2013) *Nat. Comm.*, **4**, 1399.
29 Yang, J., Yamato, M., Kohno, C. et al. (2005) *Biomaterials*, **26**, 6415–6422.
30 Uygun, B.E., Soto-Gutierrez, A., Yagi, H. et al. (2010) *Nat. Med.*, **16**, 814–820.
31 Themistocleous, G. S., Katopodis, H., Sourla, A. et al. (2004) *In Vivo*, **18**, 687–696.
32 Cheema, U., Brown, R.A. (2013) *Adv. Wound Care*, **2**, 176–184.
33 Choi, N.W., Cabodi, M., Held, B. et al. (2007) *Nat. Mater.*, **6**, 908–915.

derivatives blends were also employed for the bacterial cultures. Furthermore, the autonomous bottom-up fabrication of three-dimensional honeycomb cellulose structures was established [8] using *G. xylinus* as a bacterial nanoengine, on cellulose honeycomb templates prepared [9] by casting water-in-oil emulsions on glass substrates.

As an extended concept for the NOC, attempts are discussed to propose a sort of biomimic mineralization of calcium phosphate using modified NOC templates. This process was initially mediated by the modified NOC template in the roles of the ion supply sources and scaffolds for 3D-ordering architecture of the calcium phosphate as a biomineral [10]. In addition, the NOC template successfully established a three-dimensional, hierarchical structure of epidermal cells by cell attachment and subsequent culture [11].

In this way, this chapter will provide results on the unique surface properties of NOC templates in patterning the bacterial movement and deposition of their secreted cellulose nanofibers, on the patterned deposition of biominerals and the induction of the formation of three-dimensional, hierarchical structures of epidermal cells. Then, the regulated fabrication could lead to the design of 3D architecture from the nano to the micro scales of functional bio-based materials with the desired patterned nanostructures, which also opens the door to the preparation of potentially versatile organic-inorganic as well as organic-organic 3D order-patterned composites with less energy consumption.

4.2 What Is Nematic Ordered Cellulose (NOC)?

4.2.1 Nematic Ordered Cellulose

Before we discuss NOC, it is necessary to know the characteristic features of a cellulose molecule (Figure 4.1). Cellulose has an extended structure with a 2_1 screw axis composed by the β-1,4 glucosidic linkages between anhydroglucose units. Thus, it would be natural to accept the dimer called "cellobiose" as a repeating unit. The present three kinds of hydroxyl groups within an anhydroglucose unit exhibit different polarities, which contribute to the formation of various kinds of inter- and intramolecular hydrogen bonds among secondary OH at the C-2, secondary OH at the C-3 and primary OH at the C-6 positions. In addition, all the hydroxyl groups are bonded to a glucopyranose ring equatorially. This causes the appearance of a hydrophilic site parallel to the ring plane. On the contrary, the CH groups are bonded to a glucopyranose ring axially, causing a hydrophobic site perpendicular to the ring as shown in the upper image of Figure 4.1. These effects lead to the formation of hydrogen bonds in parallel direction to a glucopyranose ring, and to Van der Waals interaction perpendicular to the ring.

Another important feature for the hydroxyl groups is the type of hydroxymethyl conformation at the C-6 position, because the conformation of C(5)–C(6) and the resulting interactions, including inter- and intramolecular hydrogen bonds in the present cellulose structure, may differ from that in crystallites and also it is assumed to make up the extent of crystallization, as well as the final morphology of cellulose. In the noncrystalline regions, the rotational position of hydroxymethyl groups at the C-6 position may be considered indeterminate or totally non-oriented, which are not identical to those in the crystallites. Therefore, it was important to confirm the type of O(6) rotational position with respect to the O(5) and C(4) in a β-glucan chain, by employing CP/MAS^{13} and C NMR [12]. The types of hydroxymethyl conformations are gauche-trans (*gt*), trans-gauche (*tg*) or gauche-gauche (*gg*) at the C-6 positions in carbohydrates. As for the noncrystalline states, they are considered the *gg* conformation (see Figure 4.2).

Now, NOC is prepared by uniaxial stretching of water-swollen cellulose from the N, N-dimethylacetamide (DMAc)/LiCl solution at the draw ratio of 2.0 to provide highly oriented β-1,4-glucan molecular chains of cellulose toward the stretching axis [13].When the dissolved cellulose molecules in DMAc/LiCl system are self-aggregated in water vapor to form a gel, presumably by a minimum amount of restricted engagement between the hydrophobic sites of the ring above described, it is stretched to reach NOC. It is noted that the drawability requires entanglements such as cross-linking, but they are supposed to be minimized. In the present DMAc/LiCl system for NOC preparation, however, the slower coagulation using water vapor yielded the stable noncrystalline cellulose. The key to maintaining the amorphous or noncrystalline state should be the formation of small amounts of the three-dimensional cross-linking network. When the cellulose solution spread on the Petri dish is exposed by a saturated water vapor, it turns to a gel state with shrinking. The shrinkage is probably due to the interchain hydrogen bonds forming during its coagulation process of cellulose molecules into a sort of network structure. After the solvent was exchanged into water, a transparent water-swollen fixed gel of cellulose (WSC) was obtained. The WSC is composed of approximately 93 wt% water and 7 wt% cellulose. During the drawing of the WSC, the water retained inside of the WSC appeared to bleed out from its surface. The expulsion of the excess water from the drawn WSC gel may be attributed to the cellulose chains linking between the

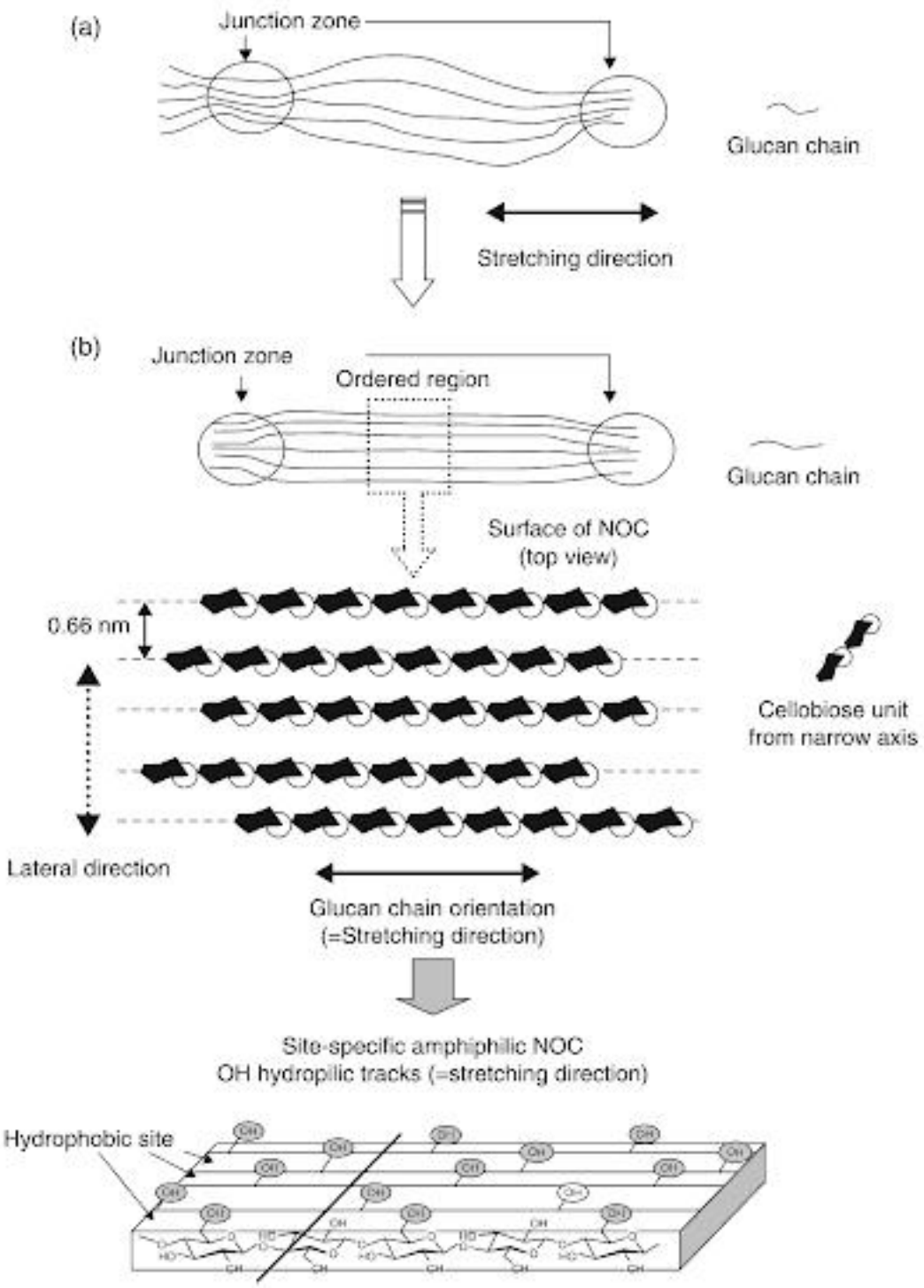

Figure 4.3 Schematic images of NOC: (a) the initial state before stretching; (b) after stretching; the inserted view is the arrangement of cellulose molecules on the NOC surface.

width over 60%, when compared with the starting sizes of WSC. The NOC films thus obtained exhibited almost perfect transparency like the coagulated cellulose solution under water vapor atmosphere. This transparency suggests that the NOC consists of noncrystalline regions.

Figure 4.3 also illustrates structural characteristics of NOC in relation to the situation of OH groups explained in the following: When NOC is prepared by uniaxial stretching of WSC, the cellulose molecular chains tend to be oriented toward the stretching axis, as already described. Further, the hydroxymethyl groups at the C-6 position of the anhydroglucose unit are vertically standing up against the surface, which indicates that the neighboring anhydroglucose ring planes are facing each other. Simultaneously the standing-up OH groups in the individual molecular chains are also aligned like tracks along the stretching axis. On the contrary, the lateral order of the OH groups among the neighboring chains is not well coordinated because the molecular chains are slipping against each other. Therefore, the hydrophilic and polarized OH groups are completely oriented as molecular tracks only in the stretching direction across the entire NOC surface. Between the hydrophilic molecular tracks, the hydrophobic phase due to the anhydroglucose plane also appeared alternately, resulting in both hydrophilic and hydrophobic tracks next to each other

across the NOC surface. The amphiphilic molecular tracks enhance the unique surface properties of NOC as described later.

The NOC structure was basically indicated by the high-resolution TEM image (see Figure 4.4). The cross-section image of the NOC template with molecular ordering is also shown in Figure 4.4 [1–3]. The high-resolution TEM image shows a preferentially oriented direction on the surface and suggests tilting of the glucose planes of a cellulose molecule with an angle of 29.3° to the vertical axis against the surface of NOC. It should be noted that the static sessile contact angle of a drop of water on the NOC surface is ~72°, indicating it is fairly hydrophobic [11]. The surface condition is totally altered by stretching to provide tilting of the glucose planes to expose the specific hydrophobic site. Namely, the hydrophobic phases due to the anhydroglucose plane appear alternately next to the hydrophilic OH tracks, resulting in unique amphiphilic molecular tracks.

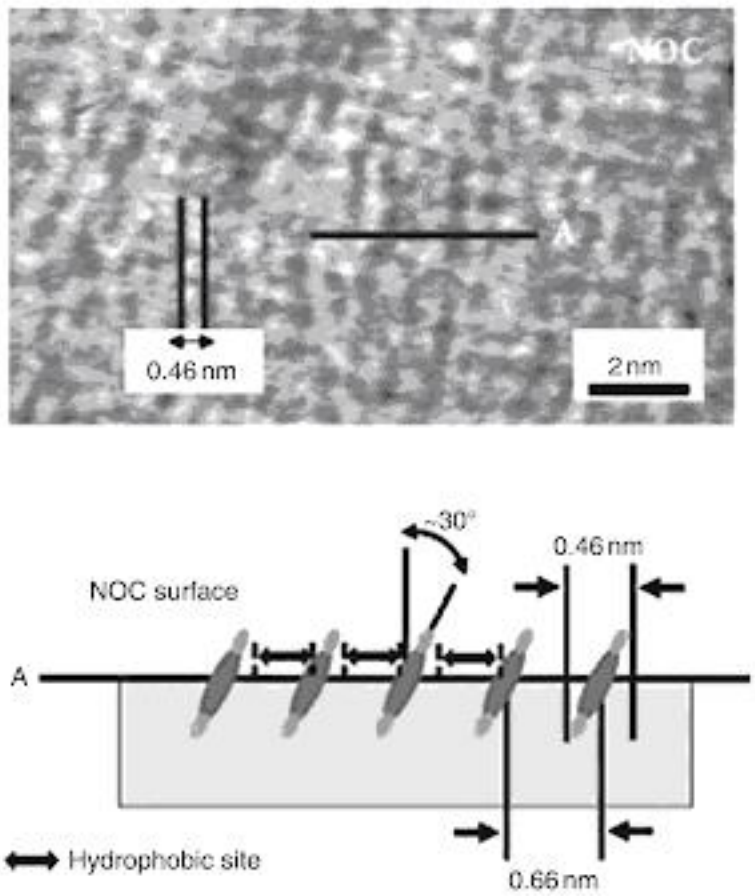

Figure 4.4 High-resolution TEM image of NOC, the molecular ordering template, together with the schematic cross-section image along the perpendicular A (= lateral direction) to the stretching direction indicating the tilted arrangement of the glucan chains. The film was negatively stained by uranyl acetate and spans a region of the copper support grid. Note the individual glucan chains that are separated by an average distance of 0.66 nm (arrows). The arrangement of glucan chains is clearly resolved with 0.46 nm in width.

The orientation parameter calculated from wide angle X-ray diffraction (WAXD) photographs was 0.88, which indicated a high degree of orientation. However, the crystallinity did not significantly follow the increase of the orientation by the stretching [1]. The crystallinity was ca. 14.8% and 16.8% before and after stretching, respectively [1, 13]. IR spectra of deuterated samples also supported the low crystallinity of the film, based on the ratio of the remaining hydroxyl groups in the drawn films that corresponds to the crystallinity index [14, 15]. Thus, we should consider the states of the structure for NOC to be ordered states that are neither crystalline nor amorphous.

The structural stability of NOC in water was examined, and it was found that the noncrystalline character based on the specific chain orientation of NOC was retained after the treatment in water even at 50 °C for long periods [16].

4.2.2 Various Nematic Ordered Templates and Modified Nematic Ordered Cellulose

4.2.2.1 Nematic Ordered Chitin and Chitin/Cellulose Blends

The chitin template prepared in the same way as the NOC template also has apparent orientation of molecular chains [17]. The distance between individual chains (1.6 nm for TEM, 0.54 nm for AFM) is greater than the crystalline lattice constant of the a axis of α-chitin (a: 0.474 nm, b: 1.886 nm, c: 1.032 nm, $\alpha = \beta = \gamma = 90$ degrees) [18]. Similar to NOC, in which the glucan chain dimensions are 0.4–0.5 nm viewed from its narrow axis, AFM images with the chain width of 0.45 nm clearly exhibit single molecular chains in the narrow axis on the surface of the chitin template. This means that nematic ordered chitin was achieved, similar to our previous work with cellulose [1]. High-resolution TEM images of the molecular assembly in the stretched samples of chitin/cellulose blend with a composition of 75/25, which was prepared in the same way as NOC, also exhibit the occurrence of the orientation of molecular aggregation, but are not resolved at the individual molecular chain scale [17]. By image analyses of the TEM photograph, the average width and distance between two parallel lines were found to be 1.38 ± 0.18 nm and 1.65 ± 0.27 nm, respectively. The average line width is narrower than that (1.51 ± 0.27 nm) from the TEM image of the nematic ordered pure chitin, indicating that the intermolecular interaction between cellulose and chitin may be engaged. Possibly each molecular chain is facing each other against the surface through a hydrophobic interaction such as a van der Waals force. On the other hand, the average distance between two parallel lines was not significantly different between the two stretched films in the pure chitin (1.62 nm ± 0.21)

and the cellulose/chitin blend (1.65 ± 0.27 nm). Therefore, it is considered that the cellulose/chitin molecular aggregates in the stretched film are aligned similarly to the nematic ordered pure chitin. In addition, these results indicate the presence of another nematic ordered state with a different scale, for example, nano/micro hierarchical structures, in chitin and the blends with cellulose. (See the more detailed study using WAXD on the nematic ordered pure chitin and the blends with cellulose in [6] and [17].)

4.2.2.2 Modified Nematic Ordered Cellulose

Other types of templates have been explored and the first successful fabrication of cellulose and cellulose acetate films with honeycomb-patterned pores was reported [9]. These were produced by casting water-in-oil emulsions on glass substrates in a saturated water vapor atmosphere. Micropatterned honeycomb films are formed more easily using this technique than by using lithographic techniques such as photolithography. In the film preparation, a honeycomb-patterned cellulose acetate was fabricated and then deacetylated to yield a cellulose film, without deformation of the honeycomb pores; the micropore sizes ranged from 1–100 μm, depending on the preparation conditions. As the volatile solvent in the polymer solution evaporated, the polymer precipitated to form a film, which simultaneously caused stretching by natural drying. The honeycomb-patterned frames are therefore expected to have specific arrangements of β-glucan chains, based on the NOC, which functions as a template.

A novel type of biomineralization process was proposed by developing a bi-functional cellulose template [5]. Namely, the NOC template was modified into a bi-functional template having a pair of the functions required for biomineralization, resulting in inducing oriented deposition of the biominerals as well as supplying anions in the synthesis. In this case, the new NOC template that is prepared to contain phosphate anions (termed p-NOC) is expected to mediate a unique order patterned deposition of calcium phosphates on the surface by reaction with calcium cations during immersion in a buffer solution.

The modification of NOC is performed as follows: A transparent water-swollen fixed gel of cellulose (WSC) is followed by the procedure using DMAc/LiCl solvent system as described in Section 4.2.1 [1, 13]. The WSC is immersed in phosphate buffered saline (PBS, Sigma-Aldrich co., Ltd.) for one week to prepare a water-swollen cellulose gel containing phosphate anions. Starting with the gel-like films containing phosphate anions thus prepared, p-NOC is obtained by uniaxial elongation at a draw ratio more than 2.0 at room temperature. In the drawing process, the specimen is kept in a wet state by pouring the PBS on the surface of the film. The specimen is then air-dried for 24 hours before being vacuum-dried at 25 °C for more than 48 hours. The AFM images of the p-NOC surface containing phosphate anions together with the original NOC substrate are shown in Figure 4.5. As a reference, a non-ordered cellulose template containing phosphate anions is also shown in Figure 4.5 [10].

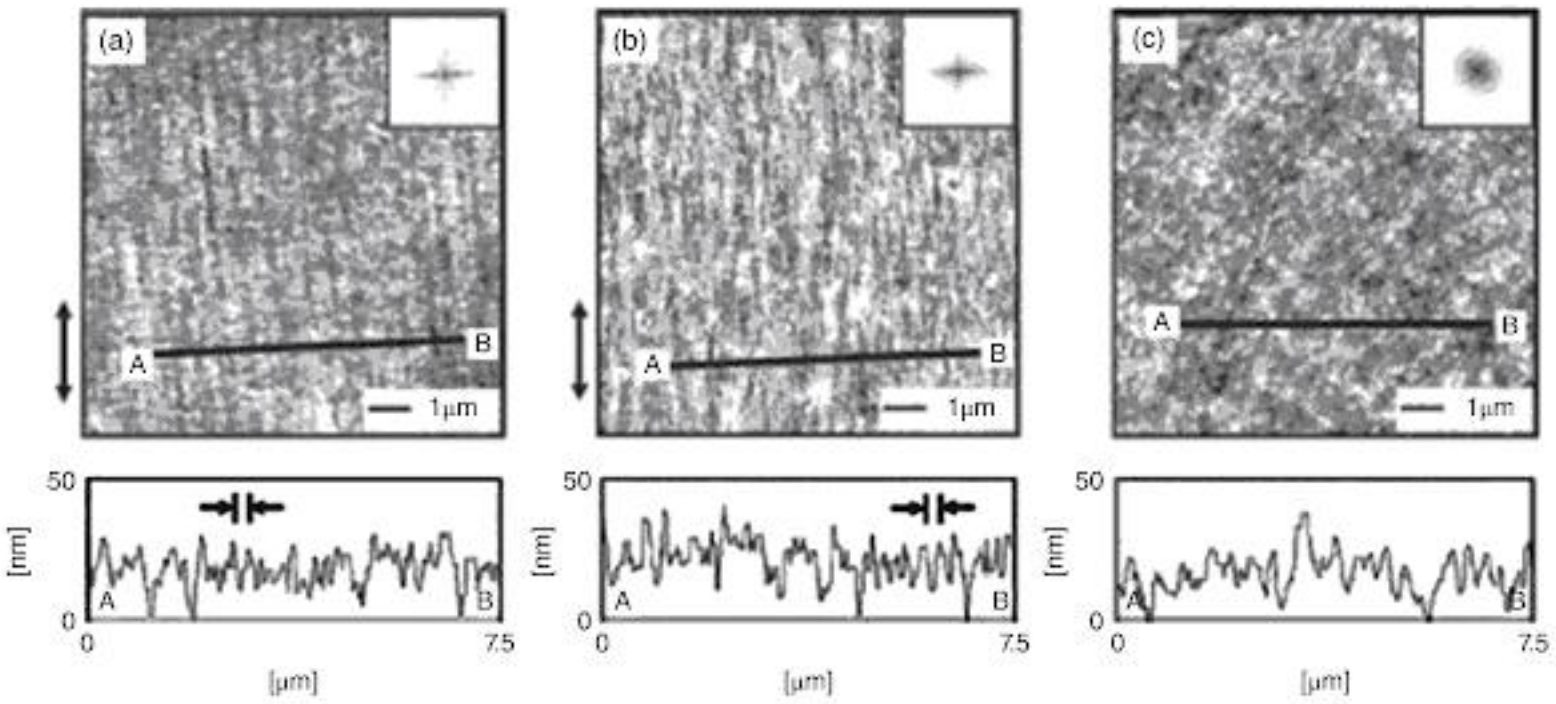

Figure 4.5 AFM images of (a) the NOC template, (b) the p-NOC template and (c) the non-ordered cellulose template as a reference for the p-NOC before the reaction with calcium cations. Insets in the upper right indicate the fast Fourier transformed images. The cross-section profiles along the perpendicular A–B are shown in the bottom of each figure. In figures (a) and (b), the average distances between two parallel lines were (a) ca. 0.17 μm and (b) ca. 0.14 μm. The double arrows indicate the stretching direction.

Comparing Figure 4.5a and Figure 4.5b, the AFM images of height mode demonstrate that the p-NOC containing the phosphate anions possessed a well-ordered surface morphology along the stretching direction similar to the original NOC substrate. Furthermore, the polarized distribution of spots in the two-dimensional fast Fourier transformed (2D-FFT) image inserted in Figure 4.5b confirms a high degree of uniaxial orientation on the surface of the p-NOC. The average line width was calculated from the cross-section analyses of the height along the A–B line perpendicular to the stretching direction (see the bottom figures in Figure 4.5). The average distance between the two parallel cellulose chains was $0.14 \pm 0.03\,\mu m$ in the p-NOC template surface (Figure 4.5b). The line width was similar to that of the original NOC template $0.17 \pm 0.06\,\mu m$ as shown in Figure 4.5a, indicating that the physical association of cellulose chains is not upset even if there are phosphate anions in the p-NOC template. In addition, the negatively polarized surface due to the tracks of OH groups along the molecular orientation is supposed to appear to some extent on the surface of the original NOC [1–4]. Thus, if phosphate anions are contained in NOC templates, then they are likely to be immobilized on the glucose planes only between the OH tracks in the surface that is negatively charged. This means that anions with negative charges could be introduced as the second minus charge into the initially negative-charged film surface. Accordingly, the phosphate anions are also supposed to be aligned along the molecular tracks in the newly prepared p-NOC template.

Without stretching the gel containing the phosphate anions, a non-ordered structure was observed on the surface, which is confirmed by the 2D-FFT image as shown in Figure 4.5c. By uniaxial stretching of the cellulose gel, it is shown that the p-NOC has the unique surface morphology similar to NOC that is totally different from the non-ordered cellulose template containing the phosphate anions. The root-mean-square (RMS) volumes were calculated from the obtained AFM height images to compare the surface roughness of each template. The RMS values for p-NOC and the non-stretched cellulose corresponded to 8.3 nm and 6.2 nm, respectively. Namely, p-NOC exhibited a rougher surface than cellulose without stretching.

4.3 Exclusive Surface Properties of NOC and Its Unique Applications

4.3.1 Bio-Directed Epitaxial Nano-Deposition on Molecular Tracks of the NOC Template

As already described, NOC exhibits several unique properties as a template having the exclusive surface of a certain nano/micro structure. Namely, the OH groups tend to be oriented as molecular tracks only in one direction across the entire NOC surface. In addition, as shown in Figure 4.4, the hydrophobic sites appear alternately next to the OH tracks, resulting in amphiphilic tracks in one direction.

The ordering amphiphilic tracks of hydrophilic OH groups and the hydrophobic polarity in NOC can induce an epitaxial deposition of biosynthesized cellulose nanofibers secreted from the gram-negative bacterium, *Gluconacetobacter xylinus* (= formerly *Acetobacter xylinum*), along the same axis of the tracks in NOC [2–4]. When active *Gluconacetobacter xylinus* cells are transferred to the oriented surface, they synthesize cellulose ribbons parallel to the molecular orientation of the substrate. This is evidenced by direct video imaging of the motion of the bacteria as they synthesize the cellulose ribbon. The movement of *Gluconacetobacter xylinus* in relation to cellulose biosynthesis was reported in 1976 [19]. The cell movement (at a constant rate of 4.5 μm/min at 24 °C) is the result of an inverse force imposed by the directed polymerization and crystallization of the cellulose. It is also well known that the bacterium rotates on its own axis. The bio-directed epitaxial nano-deposition of secreted fibers was studied over time and under varied conditions, including different substrates. Basically, the cells on the NOC template move straight along the molecular tracks. Midway through this series, the cell "jumps off" of the oriented substrate, and continues to secrete its cellulose ribbon, but now in the form of a spiral or tunnel structure that is the normal pattern of formation when not in contact with any organized substrate [20]. When the interaction between the bacterium and the surface of NOC is strong enough, the bacterium follows the track of the molecular template. As the polymer orientation of the NOC is not necessarily perfect, the bacterium may jump off the track at a structural defect. After the bacterium leaves the track, two forces, the inverse force of the secretion and the close interaction of adjacent microfibrils, affect the bacterium, possibly resulting in the synthesis of a spiral ribbon of microfibrils. In addition, the bacterium begins to rotate on its own axis. This rotation is the visible result of ribbon twisting which occurs to relieve strain induced by the absence of interaction with the substrate. When the ribbon is assembled in direct contact with the oriented molecular NOC substrate, ribbon twisting is prevented, thus suggesting a control of this oriented solid surface over the final physical interaction of polymer chains immediately after synthesis and during the early stages of crystallization.

Ribbon interaction is more clearly shown by field emission scanning electron microscopy (FE-SEM) in Figures 4.6a and b. In this experiment, the motion of the same sample is observed using light microscopy and

You have either reached a page that is unavailable for viewing or reached your viewing limit for this book.

hydrophobic tracks described in Section 4.2.1. Namely, the important factor in controlling bacterial movements may be close contact and strong interaction between the molecular tracks on NOC and the newly synthesized cellulose microfibrils. Figure 4.8 explains this concept. Normally, *Gluconacetobacter xylinus* secretes a cellulose nanofiber that comprises a microfibril of ca. 3.5 nm in width, as shown in Figure 4.8 left. The microfibrils from the subunit of terminal complexes are assembled by interfacial interactions including hydrogen bonding and van der Waals force between the component molecules, resulting in forming a ribbon-like cellulose nanofiber of ca. 50 nm in width and 10 nm in thickness, respectively [21]. On the other hand, a cellulose microfibril is synthesized along the molecular track on the NOC by the strong adhesive effect (Figure 4.8 right). This epitaxial deposition is clearly confirmed by the FE-SEM image of the width of the NOC-altered cellulose ribbons having 500 nm with splayed microfibrils 7–8 nm apart (see also Figures 4.6A and 4.6B [2–4]).

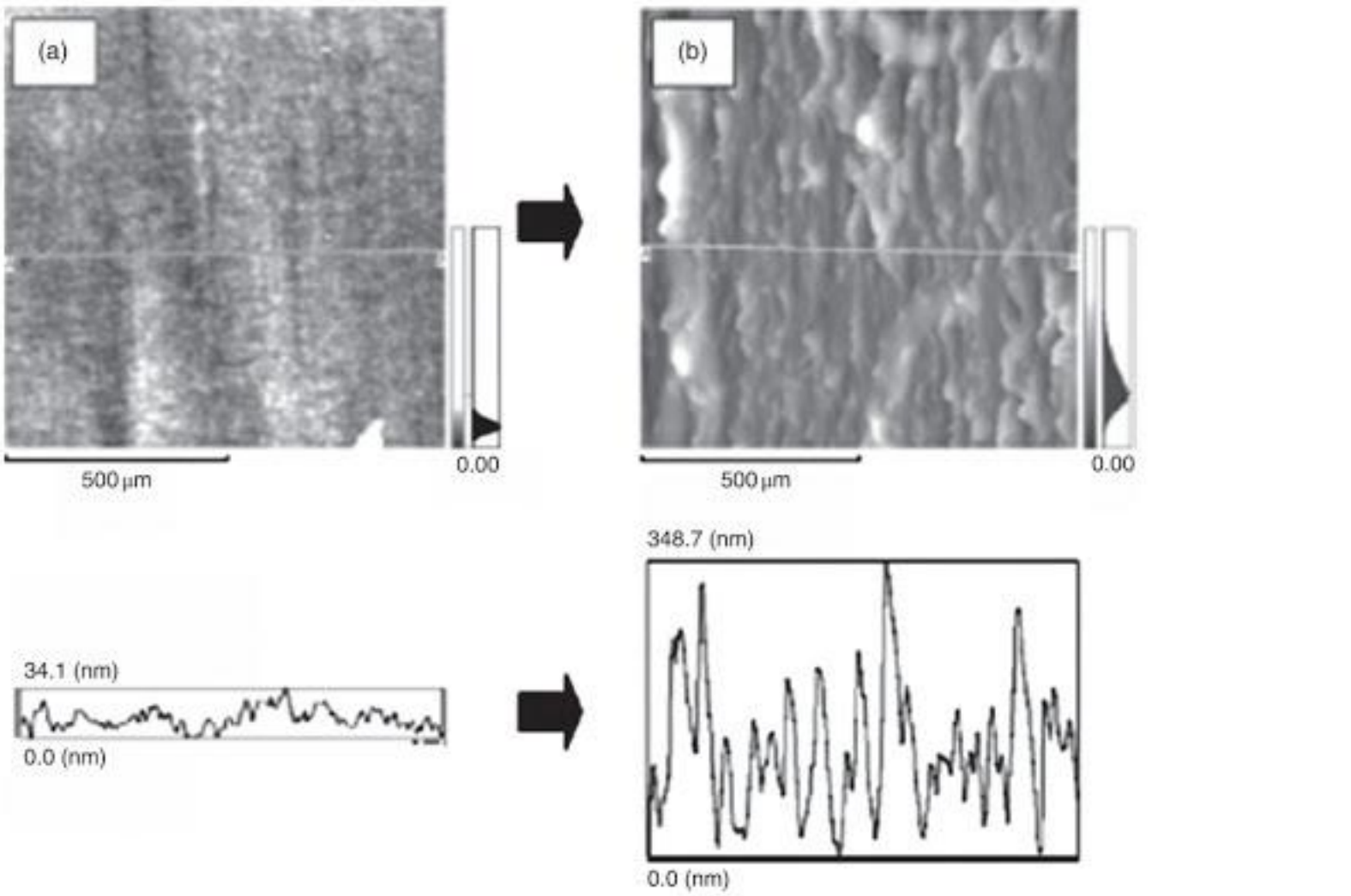

Figure 4.7 AFM images before (a) and after (b) incubation of *Gluconacetobacter xylinus* on NOC for 10 hours in SH media.

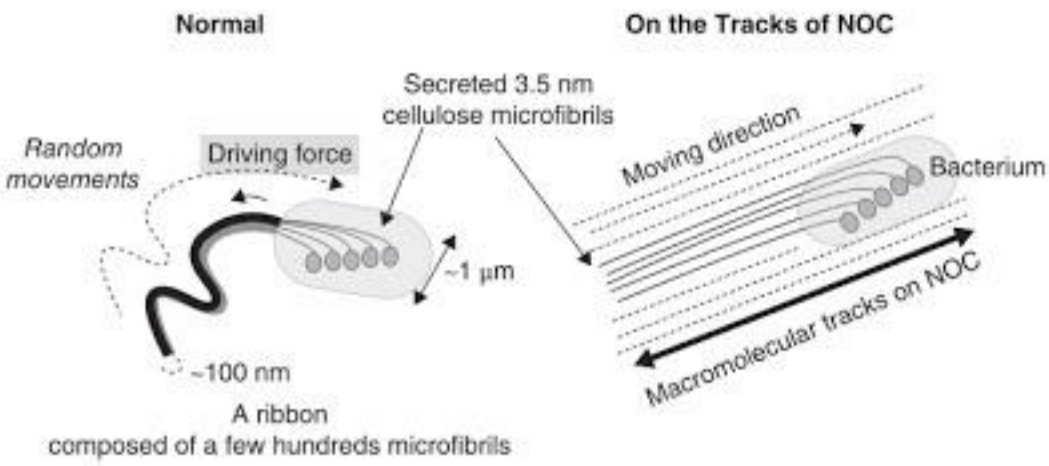

Figure 4.8 Schematic figures of self-assembly of cellulose microfibrils secreted from *G. xylinus* in normal fashion (left) and on the tracks of NOC templates (right). The circles indicate cellulose-synthesizing enzyme subunits linearly arranged across the cell body.

You have either reached a page that is unavailable for viewing or reached your viewing limit for this book.

4.3.3 Regulated Patterns of Bacterial Movements Based on Their Secreted Cellulose Nanofibers Interacting Interfacially with Ordered Chitin and Honeycomb Cellulose Templates

4.3.3.1 On Ordered Chitin Template

When active *Gluconacetobacter xylinus* cells are transferred to the nematic ordered chitin surface, they synthesize cellulose nanofibers (= cellulose ribbons) that are not parallel to the molecular orientation of the substrate, unlike the secreted fibers deposited on NOC templates. Instead, the bacteria begin to follow the molecular tracks, but soon they "jump off" the track, are diverted and then synthesize their cellulose parallel to neighboring tracks, once again soon jumping off. This "wavy" pattern was repeated across the template, as evidenced by direct video imaging of the motion of the bacteria as they secrete the cellulose nanofiber, as shown in Figure 4.9. Figure 4.9 shows the time course (120 s between each frame) of the wavy pattern of movement for a *G. xylinus* cell having 1 μm in width and 10 μm in length, respectively, together with the deposited fiber in the same waving pattern. The time lapse observation also proved that the cell movement was at a constant rate of 2.05 μm (standard deviation (SD) = ± 0.14 μm)/min at 24 °C, which is considered the result of an inverse force imposed by the directed polymerization and crystallization of the cellulose in the bacterium. The amplitude and periodicity of the waving movement as indicated in Figure 4.9 were 6.11 ± 0.53 μm and 17.85 ± 0.04 μm, respectively. As seen in the minimum standard deviation in the periodicity of the wavy pattern, the movement of the bacterium is fairly periodical and regularized. However, the rate of motion on the nematic ordered chitin template was the same as that for cell movements without templates. Furthermore, there was no difference in the rate between movement on the track and off the track, indicating that the interaction of the nascent cellulose with the nematic ordered chitin template was not as strong as that with the NOC template [2–4]. In nematic ordered chitin

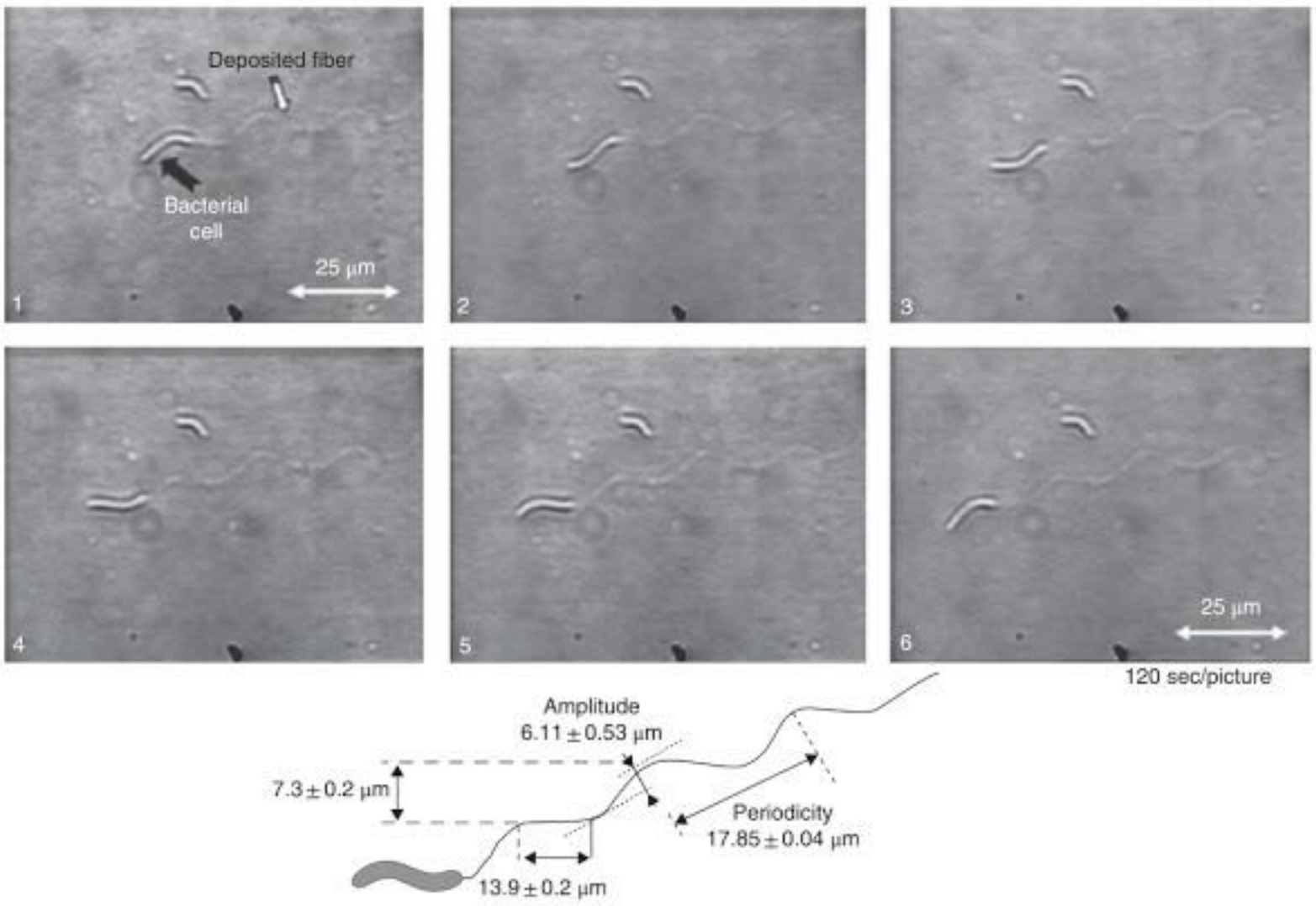

Figure 4.9 Successive images showing the motion using real-time video analysis of a bacterium as it secretes a cellulose nanofiber on the nematic ordered chitin template. The bacterium is attached, and thereafter synthesizing the fiber on the molecular tracks in the template to show a "wavy" moving pattern.

templates, hydrophilic hydroxyl groups at the C-6 position of the glucopyranose ring and the relatively hydrophobic acetamide groups at the C-2 position appeared alternately on the surface because of the 2_1 screw axis of the molecular chain, whereas the NOC template provides only hydroxyl groups at the C-6 position on the surface. The balance of the presence of the two substituents strongly affects the strength of the interaction between the surface and the secreted cellulose microfibrils. When the contact with the chitin template is not as strong as that for NOC, the biosynthesized individual sub-elementary fibrils (of a few nm in width) usually tend to self-assemble to form a ribbon-type nanofiber of 40–60 nm in width. The situation when the bacteria secrete cellulose nanofibers cannot be changed without such a strong interaction between the interfaces. Accordingly, the rate of the deposition of the fibrils on the nematic ordered chitin template that corresponds to the rate of the bacterial movement did not change from the initial rate without the template (both the moving rates were 2.05 μm ± 5% at 24 °C). On the contrary, when the interaction was strong enough as in the case for NOC, the rate of movement on NOC was much higher when compared with movements on the templates composed of 100/0 (pure chitin) and 0/100 (pure cellulose). One explanation for this phenomenon is to determine the rate-determining step for both production of fibers and the bacterial movements. It is assumed to be the self-assembly process of biosynthesized sub-elementary fibrils in forming a cellulose nanofiber [26]. Namely, in this case, the strong interfacial contact with the template prevented the assembly of the individual sub-elementary fibrils soon after the biosynthesis, resulting in inducing an increase in the rate, and also could cause the release of stress for the enzymatic synthesis of cellulose. As the result, the production of fibers on the NOC template increases so to match the rate of bacterial movement (see the details in [6]). These results suggest that the magnitude of the interfacial interaction can regulate the wavy pattern of bacterial movements and the deposition of nanofibers, which leads to the autonomous fabrication of 3D structures with a unique pattern and a controlled growth direction of the product.

With the addition of cellulose as a component for nematic ordered chitin template, the molecular ordering was altered, as described previously in Section 4.2.2.1. It was found that application of the preparative method for NOC to chitin and cellulose/chitin blends did not permit the formation of nematic ordered states like NOC on the molecular scale, but instead, induced a variety of hierarchical nematic ordered states on various scales [17]. It was expected to alter the magnitude of the interfacial interactions that occurred with the microfibrils by the addition of cellulose as a component. In the two templates of nematic ordered chitin/cellulose blends of 50/50 and 25/75, the moving patterns were still "wavy". However, a remarkable difference appeared depending on the cellulose component ratio. The more cellulose was added, the less the amplitude became, namely, getting close to a linear pattern [6]. This is interpreted that more cellulose that is contained, the more the moving amplitudes into a straight manner are reduced. The moving rate for the individual blend ratios seemed to be within a non-significant range.

4.3.3.2 On Honeycomb Cellulose Template

A honeycomb-patterned cellulose film was used as a scaffold for the culture of *G. xylinus* [10]. When the molecular orientation on the film surface exhibits amphiphilic molecular tracks similar to those on NOC, the bacterial cells autonomously fabricate 3D honeycomb structures by the deposition of secreted cellulose nanofibers on templates [2–4, 6, 8]. According to the detailed examination of NOC (see Section 4.2.1), the hydrophobic phases due to the anhydroglucose plane appear alternately next to the hydrophilic OH tracks, resulting in unique amphiphilic molecular tracks. This molecular order on the surface of the honeycomb frames appeared to have a similar ordering to NOC, including the molecular orientation along the honeycomb frame and the tilted angle of the glucose plane [1–4, 6].

The first step is to induce the bacteria to selectively secrete nanofibers onto the honeycomb frame surfaces. The bacteria were therefore incubated under slow rotation to enable the bacteria to secrete and deposit cellulose nanofibers on the surfaces of the honeycomb frames. This means that once bacteria apparently attach to the honeycomb frame surface, they keep secreting or producing nanocellulose onto the same honeycomb frame surface. In this critical rotation culture, bacteria were naturally selected to deposit the nanofiber onto honeycomb frames in the entire template. As a result of this selective attachment of bacterial nanofibers, which does not indicate bacterial attachment, during incubation, the cultured bacteria continuously deposit cellulose nanofibers along the honeycomb frame surfaces. Then the selective deposition was found by the real-time video observation to occur in the entire areas of honeycomb frame surfaces. Namely, this rotational culturing of the bacteria successfully achieved a preferential location on the entire honeycomb frame surface, presumably by anchoring as a result of selective interactions between the secreted nanofibers and the surfaces, as shown in Figure 4.10. It should be added that before anchoring, the bacterial cells were just floating and not observable in the same frame as in Figure 4.10.

After the attached movement of *G. xylinus* along the honeycomb frame surfaces, the bacterial cells began to synthesize cellulose nanofibers, enabling further selective

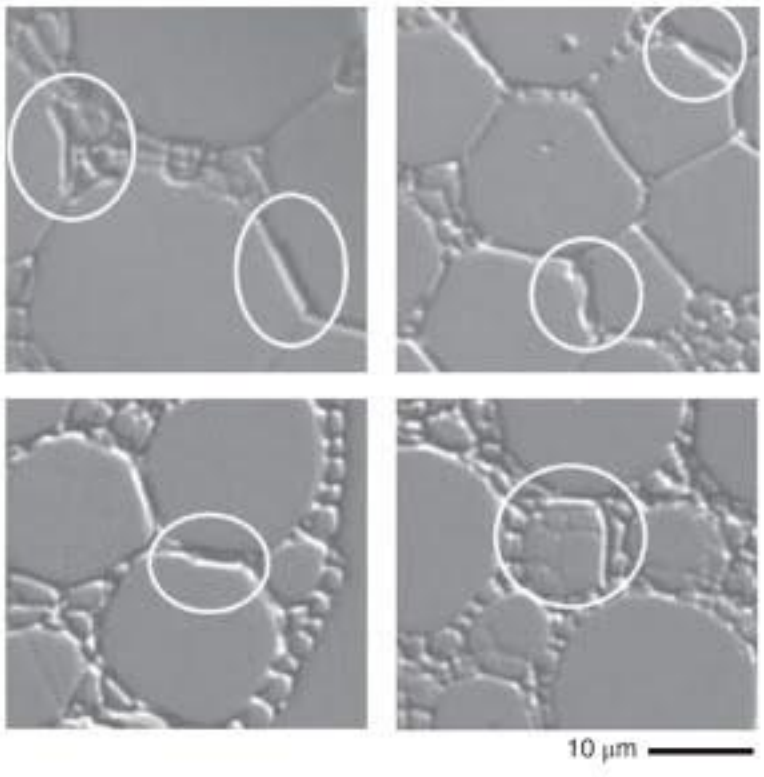

Figure 4.10 Differential interference light microscopic images of selective attachment of bacteria (inside circles) on surfaces of honeycomb frames under slow rotation during culture.

movements along the honeycomb frames of the substrate, as shown in Figure 4.11. In contrast, there were no cellulose fibers inside the pore spaces. The bacterial movement can therefore only be regulated on the surfaces of the honeycomb frames across the entire template, as shown by direct video imaging of the motion of a bacterium as it secreted the cellulose nanofibers. Presumably, the rest of the bacteria, which are not attached to the honeycomb frame, are floating in the media, and not capable of fixing themselves onto any scaffold.

Another method of fabricating 3D honeycomb cellulose structures was reported by Uraki et al. [27, 28]. The honeycomb film was prepared by a transcription method [26], for use as a honeycomb groove for *G. xylinus* movement to give a 3D architecture. This method was based on physical mechanical control of the bacterial movements; this is totally different from the present study, which was based on physicochemical interfacial interactions between cellulose nanofibers and templates.

As described above [2–4], the bacteria followed the orientation direction of the NOC and moved at 4.5 μm/min at 24 °C. In the present study, the cells moved at a

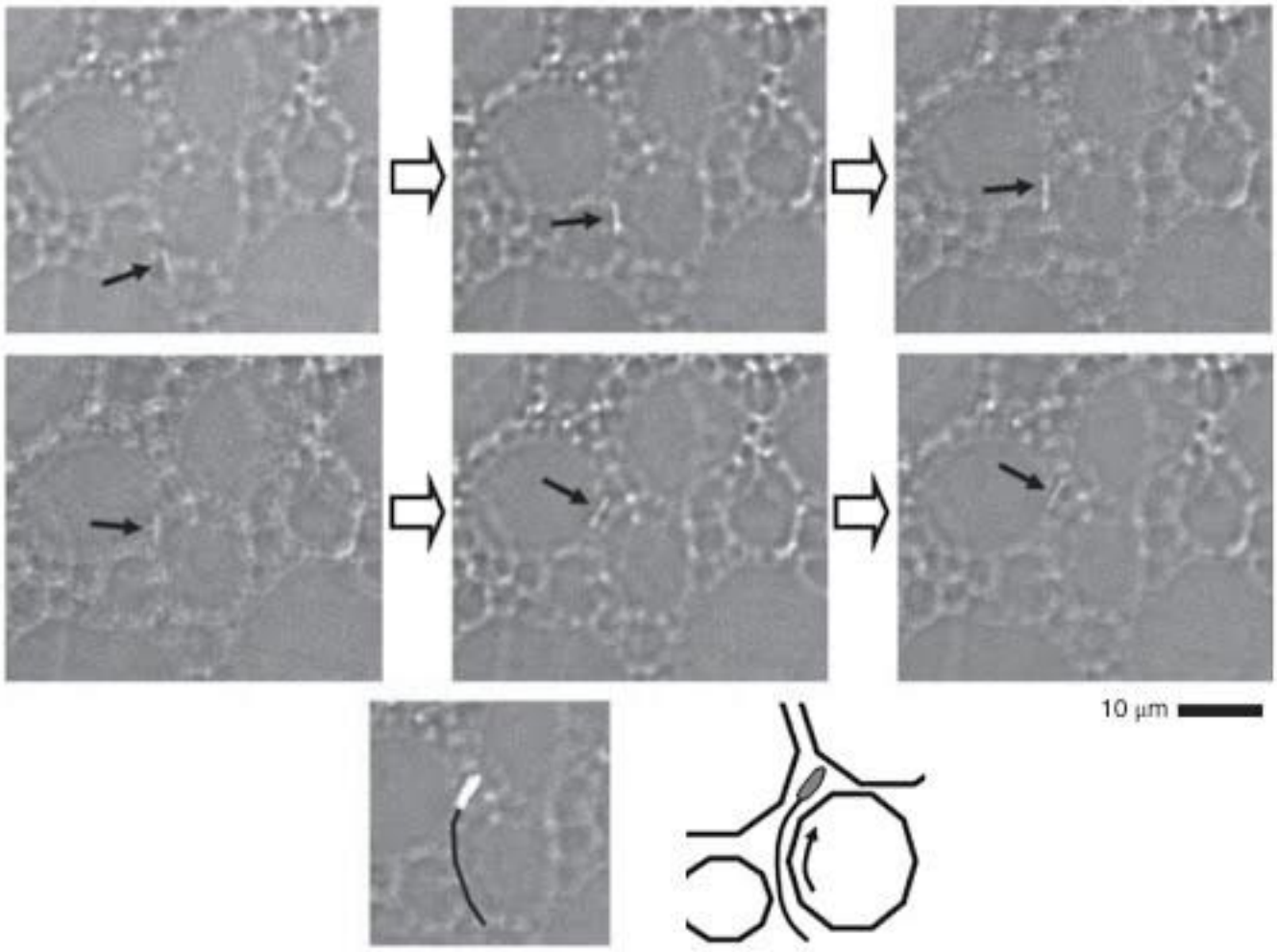

Figure 4.11 Successive images showing motion of a bacterium as it secretes a cellulose nanofiber, using real-time video analysis. The bacterium was selectively attached to the honeycomb frame and synthesized its cellulose fiber on the molecular tracks on the honeycomb frame. The interval of each image was set to be 1 min.

constant rate of 2.79 ± 0.46 μm/min at 24 °C when forming the first layer on the top of the honeycomb frame. This was considered to be the result of interactive forces between the surface of the honeycomb film and the secreted microbial cellulose fibers. For the second and subsequent layers, interactions between the cellulose nanofibers contributed to the movement rate; it became 2.92 ± 0.26 μm/min at 24 °C, which was faster than that for the first layer. The experimental results could be achieved by keeping observation of bacterial deposition all through the beginning to the end under an optical microscope using real-time video system (3 frames/min). Furthermore, both rates are faster than that of 2.0 μm/min at 25 °C [19] for cell movement without templates. The increase in the movement rate for NOC and the honeycomb templates may be caused by the inhibition of the self-assembly of the nascent cellulose microfibrils by the strong interactions between the biosynthesized fibers and the template [26]. The increase in the number of contact points on the microfibrils then causes strong interactions with the scaffold surface. This phenomenon is the rate-determining step for both production of fibers and bacterial movement [2, 3, 6, 25]. In this case, the strong interfacial contact with the template prevented the assembly of individual cellulose microfibrils of width 3.5 nm soon after biosynthesis, resulting in an increase in the rate, and could also cause stress release in the enzymatic synthesis of cellulose [3, 6]. As a result, the production rate of fibers on the surface of an NOC-like template increases with the increasing rate of bacterial movement.

The two-dimensional (2D) microscopic images of the honeycomb frames before and after the incubation of the bacteria showed no change in the 2D honeycomb pattern after culture. However, AFM observations revealed the phenomenon shown in Figure 4.12. In this study, an AFM with a voice coil motor was used to obtain topographic images with very rough surfaces. Normal AFM instruments equipped with a piezoelectric scanner could not be used to observe such rough honeycomb frames, because the piezo element cannot scan the large height changes. The changes in the heights in the surface topographic images of a honeycomb-patterned cellulose film are shown in Figure 4.12. Before and after incubation, microscopic observations with a light microscope and AFM were performed for the same sample, the same position, and the same measurement spot. It should be noted that great skill was needed to perform the experiments. This method was used to prove the 2D deformation of the honeycomb pattern. However, the cross-sectional AFM

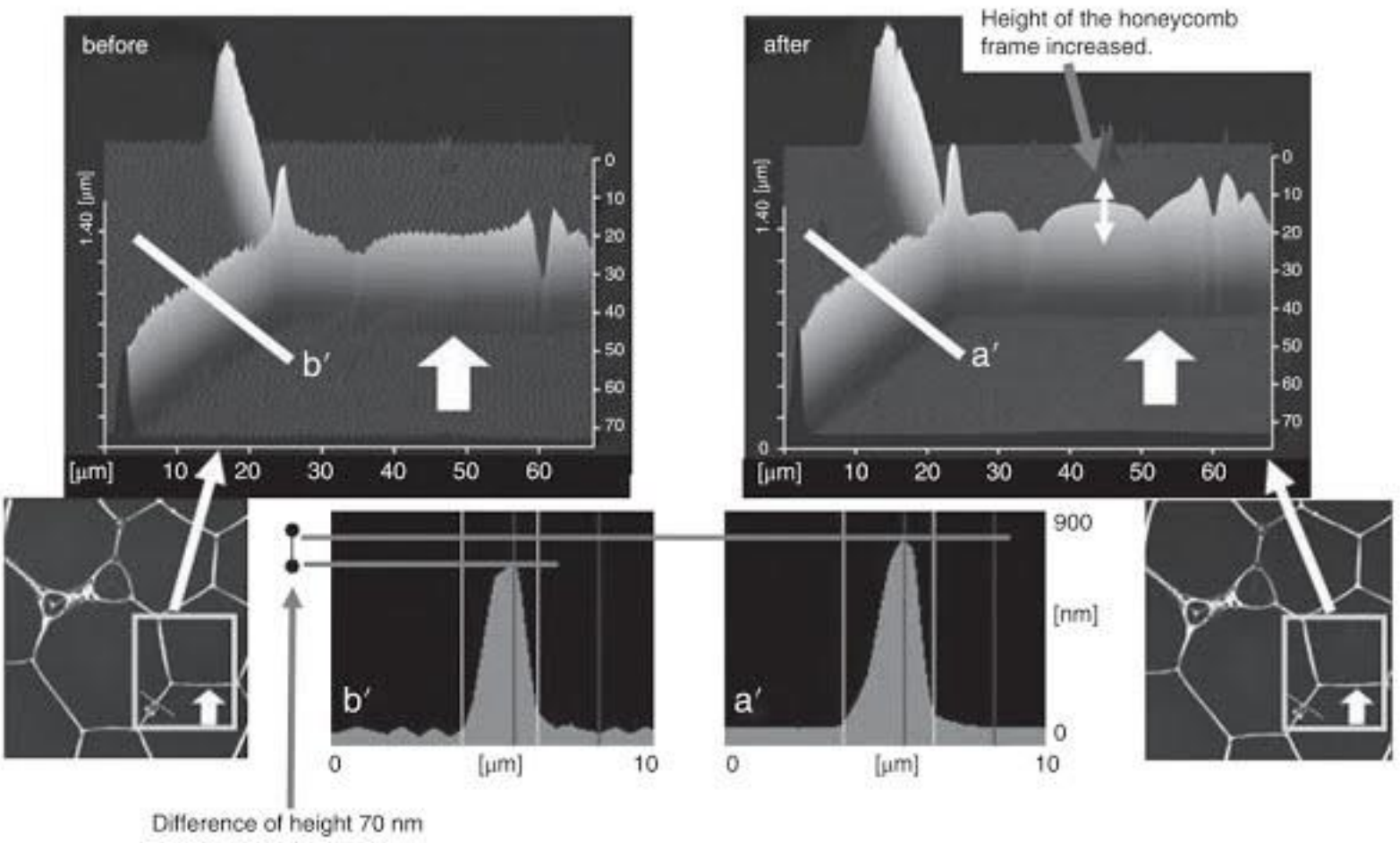

Figure 4.12 Morphological changes in the honeycomb frame on film, observed using atomic force microscopy, after culture. The square areas were focused and cross-sectioned, and show the 3D images before and after culture. Twenty layers of bacterial cellulose nanofibers were accumulated in 10 h (one layer = 3.5 nm).

You have either reached a page that is unavailable for viewing or reached your viewing limit for this book.

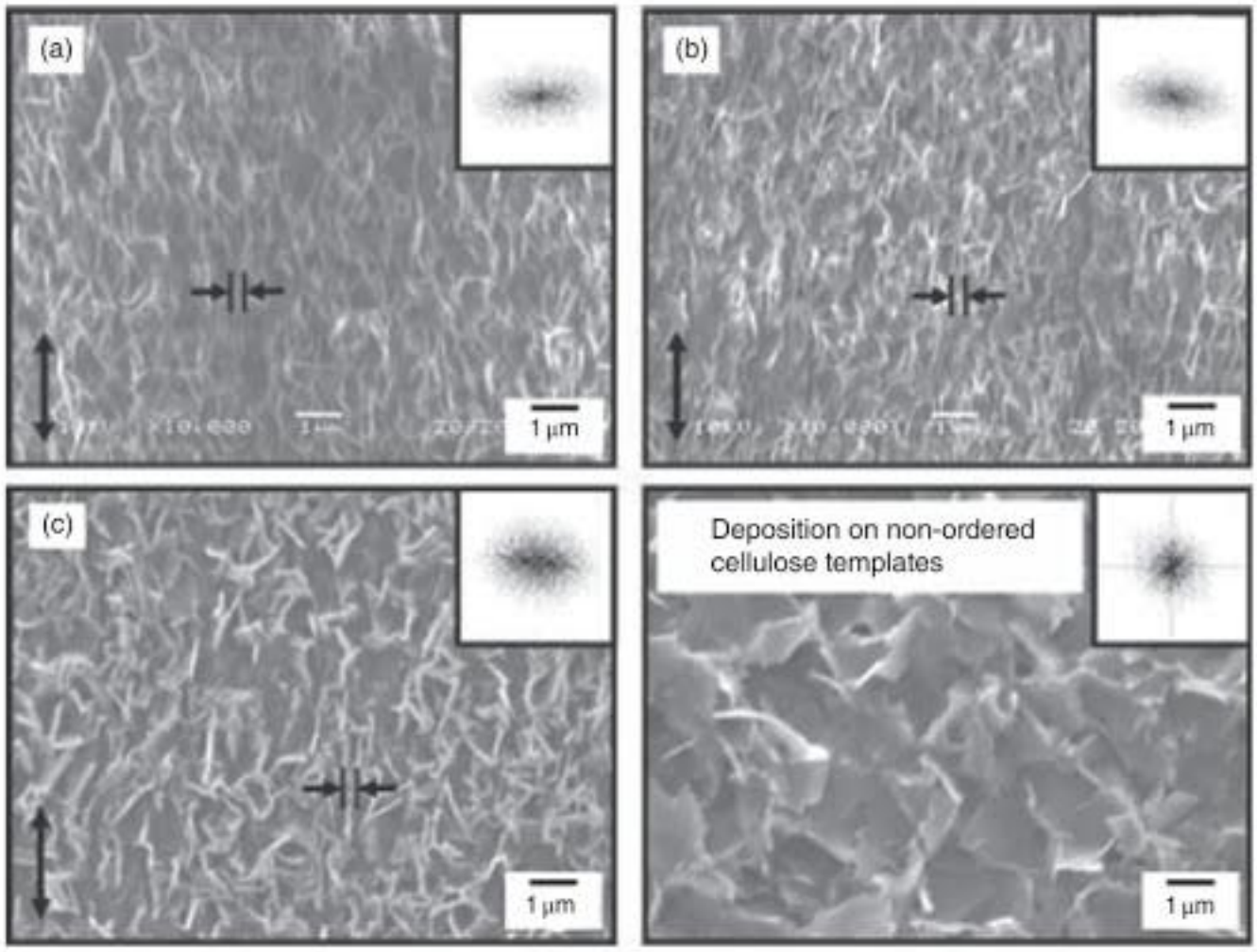

Figure 4.13 SEM images of the surface of p-NOC templates after reactions with calcium cations for (a) 0.5, (b) 5.0 and (c) 10 min with the fast Fourier transformed images as insets on the right. The morphology of calcium phosphate deposition on the non-ordered cellulose template after the same reaction for 10 min is also displayed as a reference for the p-NOC template. In (a)–(c), the line widths of calcium phosphates were 0.23 ± 0.07 μm, 0.19 ± 0.04 μm and 0.30 ± 0.08 μm, respectively. The double arrows indicate the stretching direction.

p-NOC template is expected as a bio-mimic template in terms of inducing the orientation of calcium phosphates, as well as the phosphate anion supplier [10].

4.3.5 Three-Dimensional Culture of Epidermal Cells on NOC Scaffolds

As so far described, amphiphilic molecular tracks of both hydrophilic and hydrophobic tracks next to each other alternating across the NOC surface are capable of enhancing the unique surface properties, which include serving as a template or scaffold for ordered deposition of various substances, such as nanofibers or inorganics [2–4, 6, 8, 10, 11].

The interfacial affinity between cells and culture plates is in general affected by differences in the plate surface properties, because a relatively hydrophobic culture plate is believed to induce the proliferation of cells following cell adhesion and subsequent settlement [31]. Recently, some scaffolds for cell culture have been proposed to establish a technique for regeneration medicine. Among available scaffolds, collagen [32–36], hyaluronic acid [37–39], chitosan [40], silk fibroin, and spider silk [41, 42] are major biopolymers playing a bioactive role in such medical purposes. Although cotton cellulose has not been thought to be biocompatible, it was recently clarified that bacterial cellulose pellicle produced from *Gluconacetobacter xylinus* has biocompatibility [43] and could be used for medical materials and tissue engineering [43, 44]. The latest research reported that cell divisions were induced toward the direction of cellulose nanofiber as the scaffold [45, 46]. Here, the authors succeeded in culturing epidermal cells on the noncrystalline cellulose template (NOC) with ordered cellulose molecules, instead of crystalline cellulose nanofibrils.

Initially, surface characterization of NOC templates was carried out by contact angle measurements and atomic force microscopy (AFM) analyses. Then, cell behaviors when cultured on NOC templates were observed using inversed phase contrast microscopy, followed by attempts to produce a three-dimensional culture of epidermal keratinocytes on a newly modified NOC system proposed.

You have either reached a page that is unavailable for viewing or reached your viewing limit for this book.

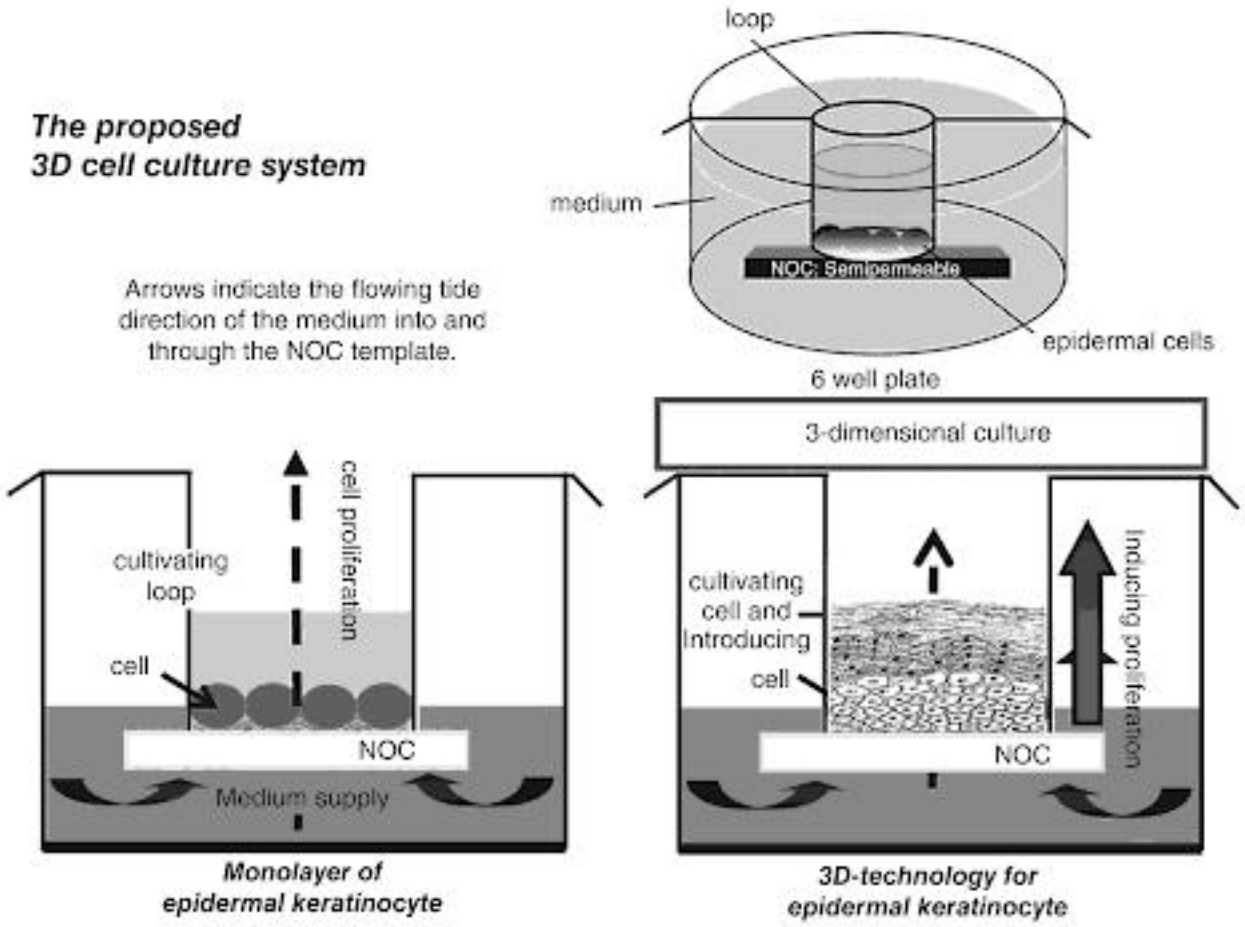

Figure 4.15 Schematic image of three-dimensional cultivation on the semipermeable NOC template. Broken arrow indicates possible proliferation direction of epidermal cells and arrows indicate the flowing tide direction of the medium into and through NOC template.

template surface (Figure 4.16). Furthermore, after 5 days of cultures, some colonies with 36 μm differences in height were observed on top of the previously formed cell layer. This indicated that cell division was induced upward, perpendicular to the NOC template bottom. Specifically, this effect indicated that the film played a role as a semipermeable membrane in providing and maintaining fresh culture conditions (Figure 4.15). To support the 3-D features mentioned above, the height of a single cell was measured by AFM in a cultivation that was allowed to build only a single cell layer on the NOC surface in the loop bottom. The cross-sectional image was assumed to indicate the height of a single fixed cell, at 1.42 ± 0.13 μm. Although measurement of the height of some layered cells, as a colony, was attempted, it was too high to detect by AFM. Alternatively, the height of these layers was measured at ~36 μm via a through-focus series of images using light microscopy. The colony was concluded to consist of ~30 layered cells. These results also suggested that the very bottom layer of cells did not detach from the NOC template during culture; therefore, the formerly established layered cells were considered to fulfill the role of a scaffold for the next newly-formed cell layer.

This study served to establish that NOC, as a cellulose film having a unique surface structure and properties, could be employed as a 3-D culture template for epidermal cells. Initial light microscopic observations of cell attachment and growth (or proliferation) on NOC templates indicated that the template was suitable as a cultivating scaffold for animal cells. It also indicated that the template was suitable for inducing construction processes leading to the formation of a three-dimensional cell accumulation because the NOC structure played a role as both a scaffold and a semipermeable membrane. The functions of the scaffold in supporting cell adherence and proliferation were enhanced by the amphiphilic molecular tracks on the unique NOC surface. However, the semipermeable membrane function was attributed to the dominant noncrystalline domains of the NOC film, providing fresh nutrient for the cells from the bottom to the top, similar to the process of human skin formation.

4.4 Conclusion

In biological systems, skeletal materials such as cell walls, bones, and shells are made primarily of a nano-scale building block of polysaccharides, proteins, and inorganic salts. The assembly of these building blocks facilitates the production of a hierarchical framework

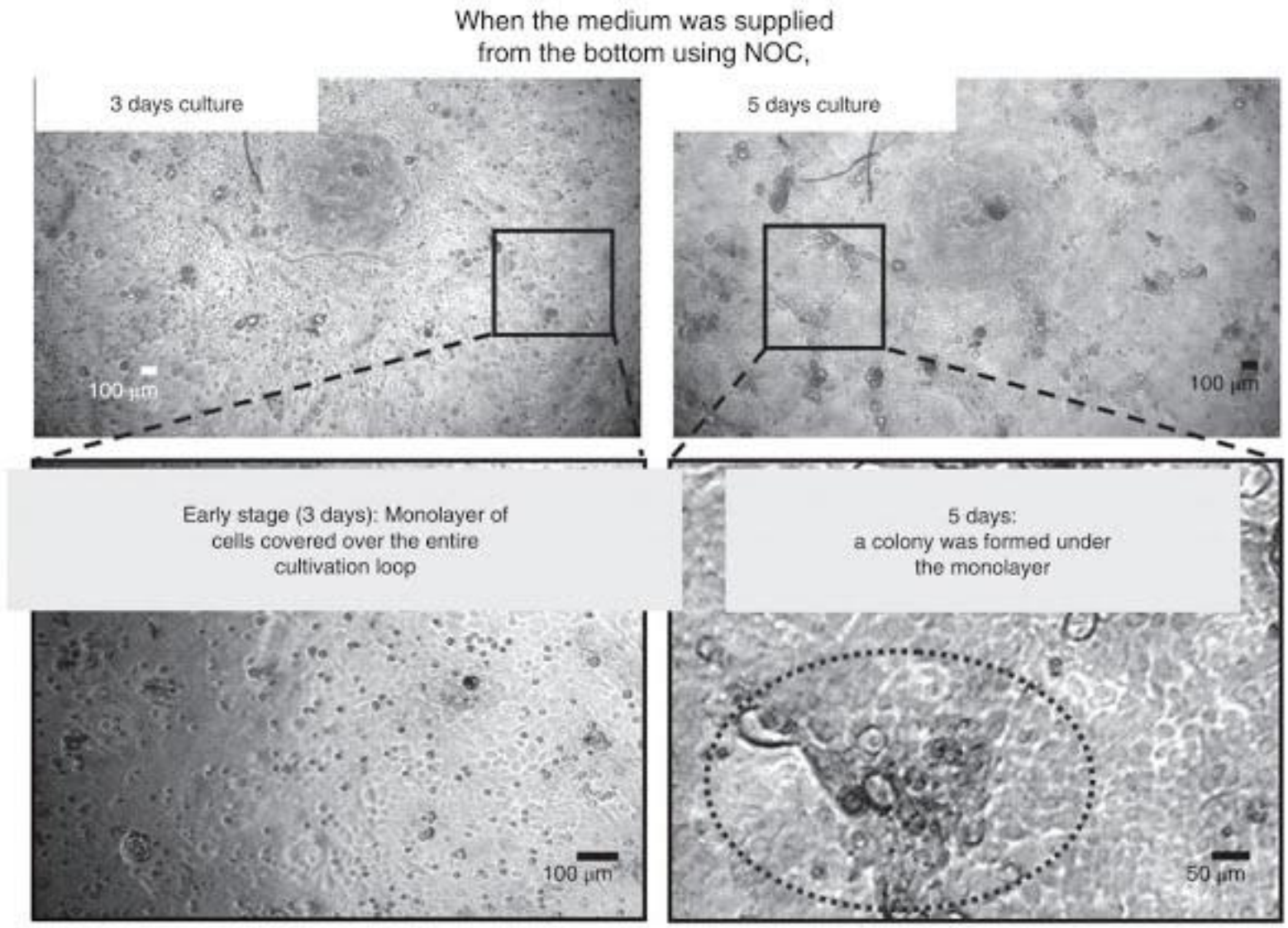

Figure 4.16 Cell proliferation on the provided medium of the NOC templates from the loop bottom to the top through the semipermeable NOC template. Culture times, (a, a') 3 days and (b, b') 5 days cultivation, and circle, colony. On NOC, the cells kept covering the surface after 5 days culture, indicating that the former layers could be a scaffold for the next generation coming from the bottom.

structure. The formation dynamics observed in this NOC could be applicable to the design of nano-scale controlled, hierarchically structured materials with specific properties. We have employed a biological system combined with a polymer platform with an NOC-like surface in order to directly fabricate hierarchically ordered materials from the nano level up to the micron level. Thus, if a nano/micro-patterned film with similar surface characteristics as NOC can be fabricated, the 3D-patterned materials will be built up by mediation of the cellulose or related scaffolds, and thereby widely appreciated and used.

References

1 Kondo T., Togawa E., Brown, Jr., R.M. (2001) *Biomacromolecules*, **2**, 1324–1330.
2 Kondo, T. (2007) In *Cellulose: Molecular and Structural Biology*, R.M. Brown, Jr., I.M. Saxena (eds.), Springer, Dordrecht, pp. 285–306.
3 Kondo, T. (2012) In *Bacterial Nano Cellulose: A Sophisticated Multifunctional Material*, M. Gama, P. Gatenholm, D. Klemm (eds.), CRC Press, Boca Raton, FL, pp. 113–142.
4 Kondo, T., Nojiri, M., Hishikawa, Y. et al. (2002) *Proc. Natl. Acad. Sci. U.S.A.*, **99**, 14008–14013.
5 Hesse, S., Kondo, T. (2005) *Carbohy. Polym.*, **60**, 457–465.
6 T. Kondo, W. Kasai, M. Nojiri, et al. (2012) *J. Biosci. Bioeng.*, **114**, 113–120.
7 Kondo, T., Kasai, W., Brown, Jr., R.M. (2004) *Cellulose*, **11**, 463–474.
8 Kondo, T., Kasai, W. (2014) *J. Biosci. Bioeng.*, **118**, 482–487.

9 Kasai, W., Kondo, T. (2004) *Macromol. Biosci.*, **4**, 17–21.
10 Higashi, K., Kondo, T. (2012) *Cellulose*, **19**, 81–91.
11 Seyama, T., Suh, E-Y., Kondo, T., (2013) *Biofabrication*, **5**, 025010.
12 Horii, F., Hirai, A., Kitamaru, R. (1983) *Polym. Bull.*, **10**, 357–361.
13 Togawa, E., Kondo, T. (1999) *J. Polym. Sci., B:Polym. Phys*, **37**, 451–459.
14 Hishikawa, Y., Togawa, E., Kataoka, Y., Kondo, T. (1999) *Polymer*, **40**, 7117–7124.
15 Hishikawa, Y., Togawa, E., Kondo, T. (2010) *Cellulose*, **17**, 539–545.
16 Togawa, E., Kondo, T. (2007) *J. Polym. Sci., B:Polym. Phys.*, **45**, 2850–2859.
17 Kondo, T., Kasai, W., Brown, Jr., R.M. (2004) *Cellulose*, **11**, 463–474.
18 Minke, R., Blackwell, J. (1978) *J. Mol. Biol.*, **120**, 167–181.
19 Brown, Jr., R.M., Willison, J.H.M., Richardson, C.L. (1976) *Proc. Nat. Acad. Sci. U.S.A.*, **73**, 4565–4569.
20 Thompson N.S., Kaustinen, H.M., Carlson, J.A. Uhlin, K.I. (1988) *Int. J. Biol. Macromol.*, **10**, 126–127.
21 Tokoh, C.K.M., Takabe, M., Fujita Saiki, H. (1998) *Cellulose*, **5**, 249–261.
22 Benziman, M., Haigler, C.H., Brown, Jr., R.M. et al. (1980) *Proc. Nat. Acad. Sci. U.S.A.*, **77**, 6678–6682.
23 Haigler, C.H., Brown, Jr., R.M., Benziman, M. (1980) *Science*, **210**, 903–906.
24 Haigler C.H., White A.R., Brown, Jr., R.M., Cooper, K.M. (1982) *J. Cell. Biol.*, **94**, 64–69.
25 Yamamoto H., Horii F., Hirai A. (1996) *Cellulose*, **3**, 229–242.
26 Tomita, Y., Kondo, T. (2009) *Carbohydr. Polym.*, **77**, 754–759.
27 Nemoto, J., Uraki, Y., Kishikoto, T. et al. (2005) *Biotech.*, **96**, 1955–1958.
28 Uraki Y., Nemoto J., Otsuka H. et al. (2007) *Carbohydr. Polym.*, **69**, 1–6.
29 Rho, J.Y. Kuhn-Spearing L., Zioupos, P. (1998) *Med. Engine. Phys.*, **20**, 92–102.
30 Kato, T., Sugawara, A., Hosoda, N. (2002) *Adv. Mater.*, **14**, 869–877.
31 Ikada, Y., Tamada Y. (1986) In *Polymers in Medicine II*, E. Chiellini, P. Giusti, C. Migliaresi, L. Nicolais (eds.), Plenum, New York, pp. 101–115.
32 Doillon, C.J. (1992) *Clin. Mater.*, **9**, 189–193.
33 Hutmacher, D.W., Vanscheidt, W. (2002) *Drugs of Today*, **38**, 113–133.
34 Brännvall, K., Bergman, K., Wallenquist, U. et al. (2007) *J. Neurosci., Res.*, **85**, 2138–2146.
35 Uchino, T., Takezawa, T., Ikarashi, Y. (2009) *Toxicology in Vitro*, **23**, 333–337.
36 Zhong, S.P., Zhang, Y.Z., Lim, C.T. (2010) *WIREs Nanomed. Nanobiotech.*, **2**, 510–525.
37 Price, R.D., Berry, M.G., Navsaria, H.A. (2007) *J. Plast. Reconstr. Aesthet. Surg.*, **60**, 1110–1119.
38 Tezel, A., Fredridkson, G.H. (2008) *J. Cosmet. Laser Ther.*, **10**, 35–42.
39 Scuderi, N., Anniboletti, T., Carlesimo, B., Onesti, M.G. (2009) *Our Experience In Vivo*, **23**, 991–1004.
40 Tchemtchoua, V.T. et al. (2011) *Biomacromolecules*, **12**, 3194–3204.
41 Okabayashi, R., Nakamura, M., Okabayashi, T. et al. (2009) *J. Biomed. Mater. Res. B. Appl. Biomat.*, **90B**, 641–646.
42 Wendt, H., Hillmer, A., Reimers, K. et al. (2011) *PLoS ONE*, **6**, e21833.
43 Klemm, D, Heublein, B., Fink, H.P., Bohn, A. (2005) *Angew. Chem. Int. Ed.*, **44**, 3358–3393.
44 Helenius, G., Bäckdahl, H., Bodin, A. et al., (2006) *J. Biomed. Mater. Res.*, **76A**, 431–438.
45 Dugan J.M., Collins R.F., Gough J.E., Eichhorn, S.J. (2013) *Acta Biomater.*, **9**, 4707–4715.
46 Dugan J.M., Gough J.E., Eichhorn, S.J. (2010) *Biomacromolecules*, **11**, 2498–2504.

5

Preparation and Application of Biomimetic Materials Inspired by Mussel Adhesive Proteins

*Heng Shen, Zhenchao Qian, Ning Zhao, and Jian Xu**

Beijing National Laboratory for Molecular Sciences, Chinese Academy of Sciences, Beijing, China

5.1 Introduction

Mussels are a kind of common marine organisms. They exhibit strong adhesive ability and can attach themselves to the surface of boats, rocks, and other organisms, bearing the impact of storm and waves. Surprisingly, mussels can adhere to almost all kinds of substrates, even including the surface of Teflon which is considered a non-sticky surface due to its low surface energy. Their versatile, strong, and long-term adhesion in a wet environment attracts a lot of research attention.

It is found that the mussels adhere to the solid surface through byssus in a radial pattern, and every byssus forms an adhesive disk of several square millimeters with substrate. Allen and Wilker [1, 2] measured the adhesion strength of a single adhesive disk of different mussels to the rock surface and found it was between 0.3–6 MPa. There are 25–30 kinds of proteins in byssus, and 7 or 8 proteins exist in the area of the adhesive disk. These specific proteins are called mussel foot proteins (mfp) by Waite and co-workers [3]. Among these mfps, mfp-1 [4, 5] is mainly distributed in the cuticle and it is related to the high strength and high toughness of the byssus but is not involved in the interface adhesion. Mfp-2 [6, 7] and mfp-4 [8] are mainly distributed in the interior of the adhesive disk and they are related to the cross-linking and solidification, which increase the cohesive energy. Mfp-3 [9] and mfp-5 10] are the major proteins distributed on the interface of the byssus and the substrate. Although mfp-6 [11] is also distributed on the interface, it is responsible for connecting proteins on the interface and the interior. After analyzing the amino acid sequence of mfp, the fact that all of these mfps contain a kind of amino acid called 3, 4-dihydroxyphenyl-L-alanine (Dopa) is revealed. Especially in mfp-3 and mfp-5, the content of Dopa is as high as 20% and 28%, respectively.

Figure 5.1 shows the possible interactions between Dopa and various substrates, including metal ions, metal oxides and organic groups [12]. The extensive reactivity of mussels is responsible for their versatile adhesion. In the 1980s, Koide et al. found that the byssus of mussel could enrich metal ions from waste water [13] and the content of the inorganic component (Fe, Mn, Cu, Zn, V, Al and Ti) was up to 2 wt% [14]. Taylor et al. [15, 16] studied the coordination interaction between peptide containing Dopa and Fe^{3+} using Raman spectra. This revealed that the bis- or tris-coordination complex was formed by changing the ratio of Dopa and Fe^{3+}. When the mole ratio of Dopa to Fe^{3+} was 3:1, the stability constant of the formed tris-coordination catechol/Fe complex in a neutral solution with 0.1 M NaCl exceeded 10^{40}. Further research found that the association constants of catechol group with other metal ions were also very high [17]. The stability constants of Dopa with solid metals or metal oxides are high as well. Dalsin et al. [18] detected that charge transfer complexes were formed when a model compound containing Dopa made contact with the surface of titanic oxide and iron oxide by different detection methods. The coordination bond between Dopa and the metal oxides which can replace the hydration on the interface is the key factor in adhesion for the mussel adhesive proteins. For organic substrates, the high combining capacity of Dopa with substrates is due to the high reactivity of oxidized dopaquinone. The dopaquinone can react with Dopa to form free radicals and couple to form di-Dopa structure [19, 20]. It also can react with amino, thiol and imidazole via Michael-addition or Schiff base reaction to form covalent bonds [21, 22]. These reactions not only enhance the interactions between mfps and organic substrates but also lead to the cross-linking of mfps, resulting in the enhancement of the cohesive strength. In addition, the catechol of Dopa

* Email: jxu@iccas.ac.cn

Bioinspired Materials Science and Engineering, First Edition. Edited by Guang Yang, Lin Xiao, and Lallepak Lamboni.

You have either reached a page that is unavailable for viewing or reached your viewing limit for this book.

residue of adhesive on the surface due to the strong interaction between Dopa and the contacted surface. In addition, the addition of oxidants reduced the adhesion for TiO_2 while it enhanced that for tissue. It was speculated that after Dopa was oxidized from catechol to quinone, the non-covalent bond with TiO_2 reduced while the covalent bond formed with tissue.

Wilker and et al. [28–30] synthesized a series of poly[(3,4-dihydroxystyrene)-co-styrene] and studied the adhesive properties under different modes of cross-linking. By adjusting the component of the monomer, the molecular weight of the polymer and the cross-linking condition, the highest shear adhesive strength on aluminum reached 7 MPa, which was comparable with cyanoacrylate. The authors added the cationic styrene monomer to synthesize the terpolymer in order to investigate the effect of the electrostatic interaction on the adhesion, and it revealed that the wet adhesion was preferable to the commercial adhesive. The optimal content of the cationic styrene monomer was 7%.

Lee et al. [31] combined the properties of physical dry adhesion of geckos resulting from the micro- and nano-structure and the chemical wet adhesion of mussels resulting from the Dopa to fabricate a hybrid adhesive. They employed arrays of gecko-mimetic nanoscale pillars coated with a thin mussel-mimetic polymer film, which was composed of poly(dopamine methacrylamide-co-methoxyethyl acrylate) (p(DMA-co-MEA)) (Figure 5.2a). The wet adhesion of the hybrid adhesive was enhanced 15-fold compared with that without the mussel-mimetic polymer coating, and the property had only slightly decreased after over 1000 adhesion cycles (Figure 5.2b, c).

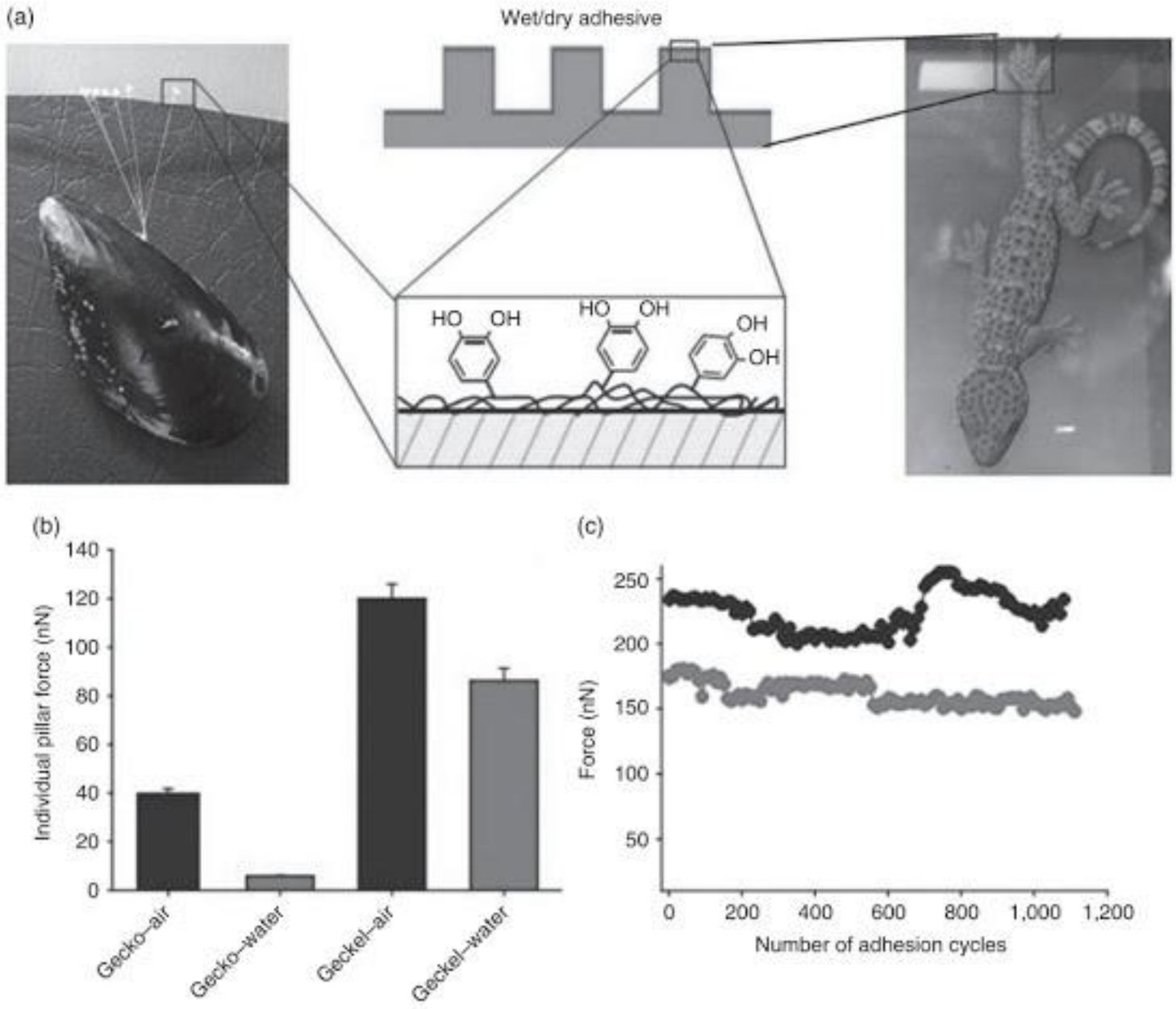

Figure 5.2 (a) Scheme of the gecko- and mussel-inspired wet/dry adhesive. (b) Adhesion forces of the adhesive with and without mussel-mimetic polymer in wet and dry condition. (c) Performance of geckel adhesive during multiple contact cycles in water (red) and air (black) [31].

You have either reached a page that is unavailable for viewing or reached your viewing limit for this book.

Glass et al. [32, 33] further increased the wet adhesion by optimizing the size of the pillars, the thickness of the mussel-mimetic polymer coating, and the degree of cross-linking.

Special prepared mussel-mimetic polymers are qualified to be medical adhesives. In this field, they usually must meet several special demands: (1) be soluble in biological fluids; (2) offer sufficient wet adhesion; (3) have controllable rapid gelation in seconds; (4) have adjustable viscoelasticity; and (5) have excellent biocompatibility.

Messersmith et al. [34, 35] designed various adhesive hydrogels with line, star and branching PEGs which were modified with Dopa. The effects of the cross-linking condition, the molecular weight of PEGs and the topological structure of the polymer chain on the gelation time and gel structure were investigated. They also synthesized the adhesive hydrogel via light-induced polymerization. This strategy, without extra oxidants, was efficient enough to avoid the decrease of the adhesion caused by oxidization, and the elastic modulus of the gel was controllable by adjusting the dosage of the cross-linking agent to match that of biological tissue [36]. They applied these kinds of bio-mimetic adhesives to the application of living organism. For instance, they synthesized a kind of adhesive precursor polymer consisting of a four-armed poly(ethylene glycol) (PEG) core, whose end groups were derived from catechol, and the *in vivo* performance was assessed in a murine model of extrahepatic syngeneic islet transplantation. It was found that the catechol-derived PEG (cPEG) solutions gelled in 30 seconds under oxidation conditions and no obvious inflammatory reaction was elicited in one year [37]. This adhesive polymer was also successfully used for the closure of iatrogenic membrane defects [38]. They also synthesized a series of adhesive polymers composed of Dopa, PEG and polycaprolactone (PCL). These polymers were cast onto the bovine pericardium and used in hernia repair. It was revealed that the adhesive strength was significantly higher than fibrin glue and the mechanical strength, swelling degree, or degradation rate could be tailored by the composition of the PCL [39].

Metal ions play another critical role in mussel adhesion. Taking advantage of the strong and reversible coordination interaction of Dopa with Fe^{3+}, various self-healing hydrogels have been developed. Waite et al. [40] developed a simple strategy to control catechol-Fe^{3+} interpolymer cross-linking via pH (Figure 5.3). They prepared the self-healing hydrogel by mixing synthetic four-armed PEG-$Dopa_4$ with Fe^{3+}. With the increase of the pH from 5 to 12, the complex turned to tris-complex from mono-complex, gradually leading to the increase of the cross-linking degree. The mechanical strength was comparable to that of the hydrogel formed by covalent cross-linking. Similar self-healing hydrogels with different macromolecules as a skeleton, such as chitosan [41], gelatin [42], polyallylamine [43], and polyacrylamide [44], were also reported. Campo et al. [45] synthesized PEG-ND_4 using nitrodopamine (ND) instead of Dopa, and fabricated self-healing hydrogel by cross-linking with Fe^{3+} as well. At the same time, the nitrodopamine was cleaved under ultraviolet irradiation, resulting in the degradation of the hydrogel. This evidenced underwater bonding and unbonding on demand and had potential applications in multiple cell and medical fields. Kohane et al. [46] synthesized PEG4-dopmanine with low molecular weight of four-armed PEG (2000 Da). This liquid polymer changed to an elastic solid with good biocompatibility and biodegradation after being mixed with a small amount of Fe^{3+} solution and the elastic property could be tailored by adjusting the Fe^{3+} concentration. Both hydrophilic and hydrophobic drugs could be incorporated into the elastomer and released slowly, indicating its potential application in drug delivery and other biomedical fields.

Besides the reversible interaction between catechol and Fe^{3+}, boric acid can be used as the reversible cross-linker with the catechol group as well. Messersmith et al. [47] fabricated pH-responsive and self-healing hydrogels based on a boronate-catechol complexation (Figure 5.4a). When 1,3-benzenediboronic acid was added, the liquid synthetic cPEG catechol transformed into hydrogel under basic aqueous conditions due to the cross-linking by forming a tetrahedral borate ester with the catechol end groups, and this cross-linking network could be dissociated in and acidic condition. Stadler et al. [48] found that covalent gels could be formed by adding $NaBH_4$ to a copolymer containing catechol groups in DMF (Figure 5.4b). The gels could adsorb humidity and the $NaBH_4$ would be hydrolyzed to H_3BO_3, which made the covalent bonds from irreversible to reversible. They proved that water played a key role in reversible cross-linking between boric acid and catechol.

Recently, Waite et al. [49] developed a new strategy to fabricate self-healing polymers through a surface-initiated hydrogen bond between interfacial catechol groups without the assistance of Fe^{3+} or boric acid (Figure 5.5). The polymer was synthesized from triethylsilane-blocked catecholacrylate. The polymer rod was cut into two parts, and after being immersed in the low pH buffer, the silyl-blocked catechol was hydrolyzed and the catechol groups at the interface were exposed. Complete healing was realized after rejoining the cut rods in water due to the interfacial hydrogen bonding from the exposed catechol groups. These self-healing polymeric materials without additional additives, such as metal ions or boric acid under wet conditions, show significant promise in biomedical and environmental applications.

Metal oxides nanoparticles have been widely used in various fields, including materials, energy, catalysts, and

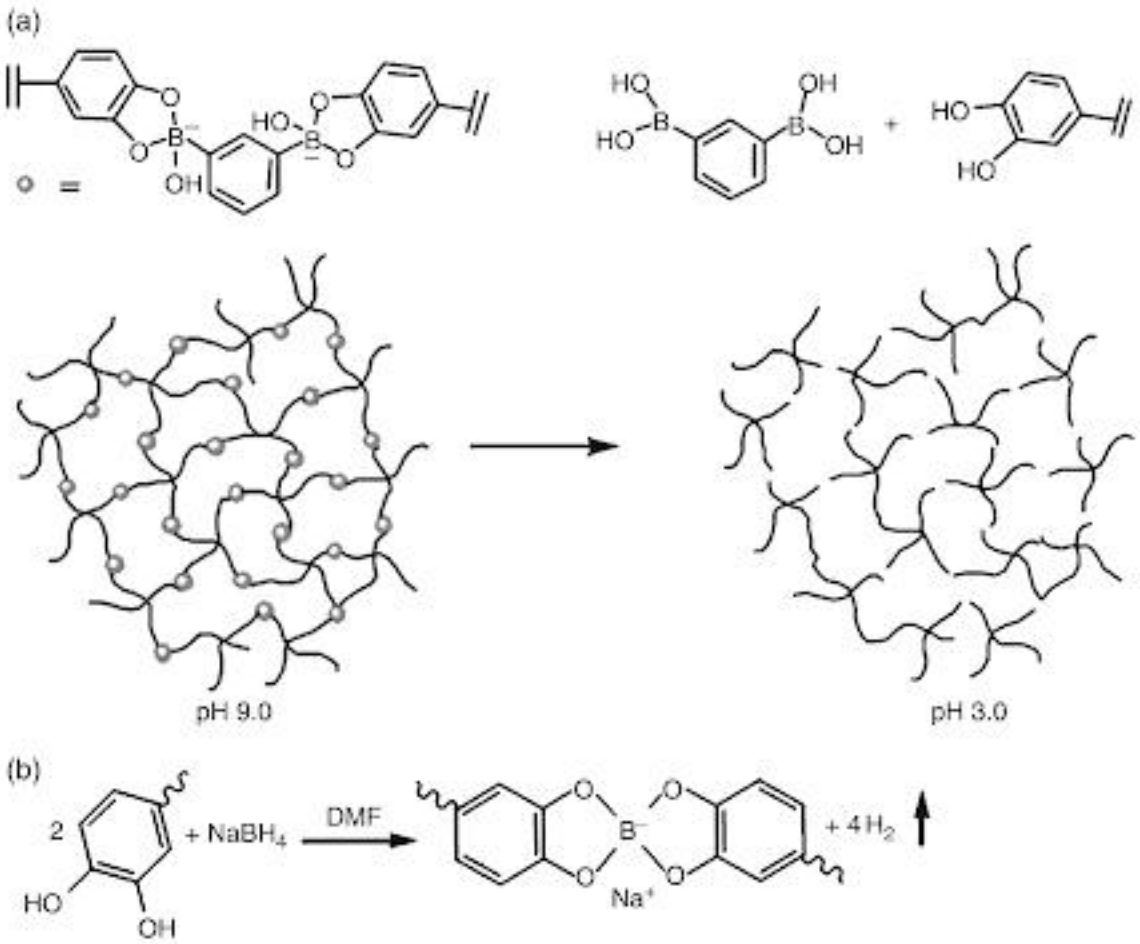

Figure 5.4 (a) pH-responsive hydrogel based on cPEG and 1,3-benzenediboronic acid [47]. (b) gel structure in DMF [48].

biomedicine. However, nanoparticles tend to aggregate as a result of their small size and high surface energy. This disadvantage usually limits their applications, thus surface modification of nanoparticles is essential not only to avoid aggregation but also to introduce the unique properties of the modifying agent. Catechol derivatives are efficient for bidentate coordination with metal ions, especially with ferric ions. Various stabilizers with bioactive molecules and catecholic anchors that modified NPs have been explored. Their long-lasting stability in a physiological environment and their biocompatibility make the NPs potentially useful in biomedical applications such as MRI imaging [50–52] and cancer therapy [53, 54].

Of these successful research studies, Xu et al. are one of the first research groups to apply superparamagnetic nanoparticles for potential therapeutic work with catecholic anchors. The authors developed an easy method to fabricate a stable conjugate of porphyrin and magnetite nanoparticles with dopamine as a surface anchor. The modified nanoparticles could induce the cell apoptosis when exposed to yellow light after penetrating the cytoplasm of the cancer cell line HeLa cells [53]. Similarly, Park et al. immobilized hyaluronic acid (HA) with dopamine as the surface anchor onto the magnetite nanocrystals [54]. Bawendi et al. coated superparamagnetic Fe2O3 nanoparticles with a synthetic zwitterionic dopamine sulfonate (ZDS) ligand [51]. Mattoussiet et al. coated iron oxide nanocrystals with multidentate catechol-PEG anchors [52]. Schmalz et al. employed PDMAEMA chains as the coating of Fe2O3 via ATRP using a dopamine-functionalized initiator as an anchor [55]. Frey et al. coated MnO nanoparticles with synthetic PEG-catechol ligands through oxyanionic polymerization [56]. These hybrid nanoparticles were suitable for biomedical applications because of their long-term stability and biocompatibility.

Hyeon et al. [50] synthesized a new kind of multiple-interaction ligand (MIL), consisting of methoxypoly(ethylene glycol) (mPEG), hyperbranchedpolyethylenimine (bPEI) and poly(L-3,4-dihydroxyphenylalanine) (polyDOPA). Different nanoparticles, for instance, Fe_3O_4, MnO and Au, coated with one kind of MIL called MIL2 (the molar ratio of each segment PEG: PEI: DOPA = 8: 1: 15) were highly stable in harsh aqueous environments, such as highly acidic and basic media, a highly concentrated NaCl solution, and even boiling water. The authors suggested this ultra-stability resulted from the cooperative work of different binding

You have either reached a page that is unavailable for viewing or reached your viewing limit for this book.

You have either reached a page that is unavailable for viewing or reached your viewing limit for this book.

You have either reached a page that is unavailable for viewing or reached your viewing limit for this book.

You have either reached a page that is unavailable for viewing or reached your viewing limit for this book.

You have either reached a page that is unavailable for viewing or reached your viewing limit for this book.

You have either reached a page that is unavailable for viewing or reached your viewing limit for this book.

You have either reached a page that is unavailable for viewing or reached your viewing limit for this book.

You have either reached a page that is unavailable for viewing or reached your viewing limit for this book.

You have either reached a page that is unavailable for viewing or reached your viewing limit for this book.

You have either reached a page that is unavailable for viewing or reached your viewing limit for this book.

You have either reached a page that is unavailable for viewing or reached your viewing limit for this book.

You have either reached a page that is unavailable for viewing or reached your viewing limit for this book.

You have either reached a page that is unavailable for viewing or reached your viewing limit for this book.

You have either reached a page that is unavailable for viewing or reached your viewing limit for this book.

You have either reached a page that is unavailable for viewing or reached your viewing limit for this book.

You have either reached a page that is unavailable for viewing or reached your viewing limit for this book.

You have either reached a page that is unavailable for viewing or reached your viewing limit for this book.

You have either reached a page that is unavailable for viewing or reached your viewing limit for this book.

You have either reached a page that is unavailable for viewing or reached your viewing limit for this book.

You have either reached a page that is unavailable for viewing or reached your viewing limit for this book.

You have either reached a page that is unavailable for viewing or reached your viewing limit for this book.

You have either reached a page that is unavailable for viewing or reached your viewing limit for this book.

You have either reached a page that is unavailable for viewing or reached your viewing limit for this book.

You have either reached a page that is unavailable for viewing or reached your viewing limit for this book.

You have either reached a page that is unavailable for viewing or reached your viewing limit for this book.

You have either reached a page that is unavailable for viewing or reached your viewing limit for this book.

You have either reached a page that is unavailable for viewing or reached your viewing limit for this book.

You have either reached a page that is unavailable for viewing or reached your viewing limit for this book.

You have either reached a page that is unavailable for viewing or reached your viewing limit for this book.

You have either reached a page that is unavailable for viewing or reached your viewing limit for this book.

You have either reached a page that is unavailable for viewing or reached your viewing limit for this book.

You have either reached a page that is unavailable for viewing or reached your viewing limit for this book.

You have either reached a page that is unavailable for viewing or reached your viewing limit for this book.

You have either reached a page that is unavailable for viewing or reached your viewing limit for this book.

You have either reached a page that is unavailable for viewing or reached your viewing limit for this book.

You have either reached a page that is unavailable for viewing or reached your viewing limit for this book.

You have either reached a page that is unavailable for viewing or reached your viewing limit for this book.

You have either reached a page that is unavailable for viewing or reached your viewing limit for this book.

You have either reached a page that is unavailable for viewing or reached your viewing limit for this book.

You have either reached a page that is unavailable for viewing or reached your viewing limit for this book.

You have either reached a page that is unavailable for viewing or reached your viewing limit for this book.

You have either reached a page that is unavailable for viewing or reached your viewing limit for this book.

You have either reached a page that is unavailable for viewing or reached your viewing limit for this book.

You have either reached a page that is unavailable for viewing or reached your viewing limit for this book.

You have either reached a page that is unavailable for viewing or reached your viewing limit for this book.

You have either reached a page that is unavailable for viewing or reached your viewing limit for this book.

You have either reached a page that is unavailable for viewing or reached your viewing limit for this book.

You have either reached a page that is unavailable for viewing or reached your viewing limit for this book.

You have either reached a page that is unavailable for viewing or reached your viewing limit for this book.

You have either reached a page that is unavailable for viewing or reached your viewing limit for this book.

You have either reached a page that is unavailable for viewing or reached your viewing limit for this book.

You have either reached a page that is unavailable for viewing or reached your viewing limit for this book.

You have either reached a page that is unavailable for viewing or reached your viewing limit for this book.

You have either reached a page that is unavailable for viewing or reached your viewing limit for this book.

You have either reached a page that is unavailable for viewing or reached your viewing limit for this book.

You have either reached a page that is unavailable for viewing or reached your viewing limit for this book.

You have either reached a page that is unavailable for viewing or reached your viewing limit for this book.

You have either reached a page that is unavailable for viewing or reached your viewing limit for this book.

You have either reached a page that is unavailable for viewing or reached your viewing limit for this book.

You have either reached a page that is unavailable for viewing or reached your viewing limit for this book.

You have either reached a page that is unavailable for viewing or reached your viewing limit for this book.

You have either reached a page that is unavailable for viewing or reached your viewing limit for this book.

You have either reached a page that is unavailable for viewing or reached your viewing limit for this book.

You have either reached a page that is unavailable for viewing or reached your viewing limit for this book.

You have either reached a page that is unavailable for viewing or reached your viewing limit for this book.

You have either reached a page that is unavailable for viewing or reached your viewing limit for this book.

You have either reached a page that is unavailable for viewing or reached your viewing limit for this book.

You have either reached a page that is unavailable for viewing or reached your viewing limit for this book.

You have either reached a page that is unavailable for viewing or reached your viewing limit for this book.

You have either reached a page that is unavailable for viewing or reached your viewing limit for this book.

You have either reached a page that is unavailable for viewing or reached your viewing limit for this book.

You have either reached a page that is unavailable for viewing or reached your viewing limit for this book.

You have either reached a page that is unavailable for viewing or reached your viewing limit for this book.

You have either reached a page that is unavailable for viewing or reached your viewing limit for this book.

You have either reached a page that is unavailable for viewing or reached your viewing limit for this book.

You have either reached a page that is unavailable for viewing or reached your viewing limit for this book.

You have either reached a page that is unavailable for viewing or reached your viewing limit for this book.

You have either reached a page that is unavailable for viewing or reached your viewing limit for this book.

You have either reached a page that is unavailable for viewing or reached your viewing limit for this book.

You have either reached a page that is unavailable for viewing or reached your viewing limit for this book.

You have either reached a page that is unavailable for viewing or reached your viewing limit for this book.

You have either reached a page that is unavailable for viewing or reached your viewing limit for this book.

You have either reached a page that is unavailable for viewing or reached your viewing limit for this book.

You have either reached a page that is unavailable for viewing or reached your viewing limit for this book.

You have either reached a page that is unavailable for viewing or reached your viewing limit for this book.

You have either reached a page that is unavailable for viewing or reached your viewing limit for this book.

You have either reached a page that is unavailable for viewing or reached your viewing limit for this book.

You have either reached a page that is unavailable for viewing or reached your viewing limit for this book.

You have either reached a page that is unavailable for viewing or reached your viewing limit for this book.

You have either reached a page that is unavailable for viewing or reached your viewing limit for this book.

You have either reached a page that is unavailable for viewing or reached your viewing limit for this book.

You have either reached a page that is unavailable for viewing or reached your viewing limit for this book.

You have either reached a page that is unavailable for viewing or reached your viewing limit for this book.

You have either reached a page that is unavailable for viewing or reached your viewing limit for this book.

You have either reached a page that is unavailable for viewing or reached your viewing limit for this book.

You have either reached a page that is unavailable for viewing or reached your viewing limit for this book.

You have either reached a page that is unavailable for viewing or reached your viewing limit for this book.

You have either reached a page that is unavailable for viewing or reached your viewing limit for this book.

You have either reached a page that is unavailable for viewing or reached your viewing limit for this book.

You have either reached a page that is unavailable for viewing or reached your viewing limit for this book.

You have either reached a page that is unavailable for viewing or reached your viewing limit for this book.

You have either reached a page that is unavailable for viewing or reached your viewing limit for this book.

You have either reached a page that is unavailable for viewing or reached your viewing limit for this book.

You have either reached a page that is unavailable for viewing or reached your viewing limit for this book.

You have either reached a page that is unavailable for viewing or reached your viewing limit for this book.

You have either reached a page that is unavailable for viewing or reached your viewing limit for this book.

You have either reached a page that is unavailable for viewing or reached your viewing limit for this book.

You have either reached a page that is unavailable for viewing or reached your viewing limit for this book.

You have either reached a page that is unavailable for viewing or reached your viewing limit for this book.

You have either reached a page that is unavailable for viewing or reached your viewing limit for this book.

You have either reached a page that is unavailable for viewing or reached your viewing limit for this book.

You have either reached a page that is unavailable for viewing or reached your viewing limit for this book.

You have either reached a page that is unavailable for viewing or reached your viewing limit for this book.

You have either reached a page that is unavailable for viewing or reached your viewing limit for this book.

You have either reached a page that is unavailable for viewing or reached your viewing limit for this book.

You have either reached a page that is unavailable for viewing or reached your viewing limit for this book.

You have either reached a page that is unavailable for viewing or reached your viewing limit for this book.

You have either reached a page that is unavailable for viewing or reached your viewing limit for this book.

You have either reached a page that is unavailable for viewing or reached your viewing limit for this book.

You have either reached a page that is unavailable for viewing or reached your viewing limit for this book.

You have either reached a page that is unavailable for viewing or reached your viewing limit for this book.

You have either reached a page that is unavailable for viewing or reached your viewing limit for this book.

You have either reached a page that is unavailable for viewing or reached your viewing limit for this book.

You have either reached a page that is unavailable for viewing or reached your viewing limit for this book.

You have either reached a page that is unavailable for viewing or reached your viewing limit for this book.

You have either reached a page that is unavailable for viewing or reached your viewing limit for this book.

You have either reached a page that is unavailable for viewing or reached your viewing limit for this book.

You have either reached a page that is unavailable for viewing or reached your viewing limit for this book.

You have either reached a page that is unavailable for viewing or reached your viewing limit for this book.

You have either reached a page that is unavailable for viewing or reached your viewing limit for this book.

You have either reached a page that is unavailable for viewing or reached your viewing limit for this book.

You have either reached a page that is unavailable for viewing or reached your viewing limit for this book.

You have either reached a page that is unavailable for viewing or reached your viewing limit for this book.

You have either reached a page that is unavailable for viewing or reached your viewing limit for this book.

You have either reached a page that is unavailable for viewing or reached your viewing limit for this book.

You have either reached a page that is unavailable for viewing or reached your viewing limit for this book.

You have either reached a page that is unavailable for viewing or reached your viewing limit for this book.

You have either reached a page that is unavailable for viewing or reached your viewing limit for this book.

You have either reached a page that is unavailable for viewing or reached your viewing limit for this book.

You have either reached a page that is unavailable for viewing or reached your viewing limit for this book.

You have either reached a page that is unavailable for viewing or reached your viewing limit for this book.

You have either reached a page that is unavailable for viewing or reached your viewing limit for this book.

You have either reached a page that is unavailable for viewing or reached your viewing limit for this book.

You have either reached a page that is unavailable for viewing or reached your viewing limit for this book.

You have either reached a page that is unavailable for viewing or reached your viewing limit for this book.

You have either reached a page that is unavailable for viewing or reached your viewing limit for this book.

You have either reached a page that is unavailable for viewing or reached your viewing limit for this book.

You have either reached a page that is unavailable for viewing or reached your viewing limit for this book.

You have either reached a page that is unavailable for viewing or reached your viewing limit for this book.

You have either reached a page that is unavailable for viewing or reached your viewing limit for this book.

You have either reached a page that is unavailable for viewing or reached your viewing limit for this book.

You have either reached a page that is unavailable for viewing or reached your viewing limit for this book.

You have either reached a page that is unavailable for viewing or reached your viewing limit for this book.

You have either reached a page that is unavailable for viewing or reached your viewing limit for this book.

You have either reached a page that is unavailable for viewing or reached your viewing limit for this book.

You have either reached a page that is unavailable for viewing or reached your viewing limit for this book.

You have either reached a page that is unavailable for viewing or reached your viewing limit for this book.

You have either reached a page that is unavailable for viewing or reached your viewing limit for this book.

You have either reached a page that is unavailable for viewing or reached your viewing limit for this book.

You have either reached a page that is unavailable for viewing or reached your viewing limit for this book.

You have either reached a page that is unavailable for viewing or reached your viewing limit for this book.

You have either reached a page that is unavailable for viewing or reached your viewing limit for this book.

You have either reached a page that is unavailable for viewing or reached your viewing limit for this book.

You have either reached a page that is unavailable for viewing or reached your viewing limit for this book.

You have either reached a page that is unavailable for viewing or reached your viewing limit for this book.

You have either reached a page that is unavailable for viewing or reached your viewing limit for this book.

You have either reached a page that is unavailable for viewing or reached your viewing limit for this book.

You have either reached a page that is unavailable for viewing or reached your viewing limit for this book.

You have either reached a page that is unavailable for viewing or reached your viewing limit for this book.

You have either reached a page that is unavailable for viewing or reached your viewing limit for this book.

You have either reached a page that is unavailable for viewing or reached your viewing limit for this book.

You have either reached a page that is unavailable for viewing or reached your viewing limit for this book.

You have either reached a page that is unavailable for viewing or reached your viewing limit for this book.

You have either reached a page that is unavailable for viewing or reached your viewing limit for this book.

You have either reached a page that is unavailable for viewing or reached your viewing limit for this book.

You have either reached a page that is unavailable for viewing or reached your viewing limit for this book.

You have either reached a page that is unavailable for viewing or reached your viewing limit for this book.

You have either reached a page that is unavailable for viewing or reached your viewing limit for this book.

You have either reached a page that is unavailable for viewing or reached your viewing limit for this book.

You have either reached a page that is unavailable for viewing or reached your viewing limit for this book.

You have either reached a page that is unavailable for viewing or reached your viewing limit for this book.

You have either reached a page that is unavailable for viewing or reached your viewing limit for this book.

You have either reached a page that is unavailable for viewing or reached your viewing limit for this book.

You have either reached a page that is unavailable for viewing or reached your viewing limit for this book.

You have either reached a page that is unavailable for viewing or reached your viewing limit for this book.

You have either reached a page that is unavailable for viewing or reached your viewing limit for this book.

You have either reached a page that is unavailable for viewing or reached your viewing limit for this book.

You have either reached a page that is unavailable for viewing or reached your viewing limit for this book.

You have either reached a page that is unavailable for viewing or reached your viewing limit for this book.

You have either reached a page that is unavailable for viewing or reached your viewing limit for this book.

You have either reached a page that is unavailable for viewing or reached your viewing limit for this book.

You have either reached a page that is unavailable for viewing or reached your viewing limit for this book.

You have either reached a page that is unavailable for viewing or reached your viewing limit for this book.

You have either reached a page that is unavailable for viewing or reached your viewing limit for this book.

You have either reached a page that is unavailable for viewing or reached your viewing limit for this book.

You have either reached a page that is unavailable for viewing or reached your viewing limit for this book.

You have either reached a page that is unavailable for viewing or reached your viewing limit for this book.

You have either reached a page that is unavailable for viewing or reached your viewing limit for this book.

You have either reached a page that is unavailable for viewing or reached your viewing limit for this book.

You have either reached a page that is unavailable for viewing or reached your viewing limit for this book.

You have either reached a page that is unavailable for viewing or reached your viewing limit for this book.

You have either reached a page that is unavailable for viewing or reached your viewing limit for this book.

You have either reached a page that is unavailable for viewing or reached your viewing limit for this book.

You have either reached a page that is unavailable for viewing or reached your viewing limit for this book.

You have either reached a page that is unavailable for viewing or reached your viewing limit for this book.

You have either reached a page that is unavailable for viewing or reached your viewing limit for this book.

You have either reached a page that is unavailable for viewing or reached your viewing limit for this book.

You have either reached a page that is unavailable for viewing or reached your viewing limit for this book.

You have either reached a page that is unavailable for viewing or reached your viewing limit for this book.

You have either reached a page that is unavailable for viewing or reached your viewing limit for this book.

You have either reached a page that is unavailable for viewing or reached your viewing limit for this book.

You have either reached a page that is unavailable for viewing or reached your viewing limit for this book.

You have either reached a page that is unavailable for viewing or reached your viewing limit for this book.

You have either reached a page that is unavailable for viewing or reached your viewing limit for this book.

You have either reached a page that is unavailable for viewing or reached your viewing limit for this book.

You have either reached a page that is unavailable for viewing or reached your viewing limit for this book.

You have either reached a page that is unavailable for viewing or reached your viewing limit for this book.

You have either reached a page that is unavailable for viewing or reached your viewing limit for this book.

You have either reached a page that is unavailable for viewing or reached your viewing limit for this book.